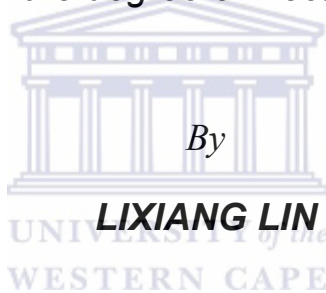




UNIVERSITY *of the*
WESTERN CAPE

HYDRAULIC PROPERTIES OF THE TABLE MOUNTAIN GROUP (TMG) AQUIFERS

*Dissertation submitted to the University of the Western Cape in the
fulfillment of the degree of Doctor of Philosophy*



LIXIANG LIN

Department of Earth Sciences
Faculty of Natural Sciences, University of the Western Cape

Supervisor
Professor YONGXIN XU

Co-supervisor
Dr. RIAN TITUS

November 2007
Cape Town, South Africa

DECLARATION

I declare that **HYDRAULIC PROPERTIES OF THE TABLE MOUNTAIN GROUP (TMG) AQUIFERS** is my own work, that it has not been submitted for any degree or examination in any other university, and that all the sources I have used or quoted have been indicated and acknowledge by complete references.

Full name: Lixiang Lin

Date: Nov. 2007

Signed.....



ABSTRACT

Hydraulic Properties of the Table Mountain Group (TMG) Aquifers

Lixiang Lin
PhD Thesis
Department of Earth Sciences
University of the Western Cape, South Africa

Keywords: Fractured Rocks, hydraulic properties, porosity, hydraulic conductivity, storativity, hydraulic tensor, hydraulic test, conceptual model, numerical model, Table Mountain Group

The Table Mountain Group (TMG), located at the southmost cape of African Continent, is one out of three major regional aquifer systems in South Africa, which has a potential of bulk water supply to meet the requirements of irrigation and local municipalities in the Western and Eastern Cape provinces. The TMG aquifers comprising a thick sequence of hard sedimentary rocks dominated by fractured sandstones have the outcrop area of 37000 km², the deposit area of 248000 km² and the thickness ranging from 900m to 4000m. Large-scale distribution of the TMG over various geological structures leads to a big diversity in its hydrogeological properties, especially the hydraulic properties which are critical in determining the aquifers' abstraction potential and sustainable yield. A proper estimation of hydraulic properties, with focus on the investigation of aquifer porosity, permeability and storativity, is important for the sound evaluation and sustainable utilization of the groundwater resource in the TMG area.

Data from previous studies and current research have been collated and analyzed to help establish conceptual models of the TMG aquifers and to quantify the intrinsic aquifer properties – hydraulic properties. Based on the study of hydrogeological settings and aquifer types, combined with the interpretation of aquifer hydraulic tests, it is realized that the hydraulic properties of the TMG rocks are strongly controlled by fractures regarding the groundwater flow path within the TMG rocks. Media study on the nature of the fractures or fracture networks therefore is conducted in detail. Subsequently, the establishment of the fractured-media conceptual models on the basis of stochastic analyses is helpful for the better understanding of groundwater behaviors in the TMG aquifers. With the data derived from field measurements and interpretation of remote sensing data, the fractured rock hydraulic

conductivities are estimated by using a hydraulic conductivity tensor approach. Considering the influential factors such as aperture, roughness, stress condition, and most importantly the connectivity of fractures, the tensor model is accordingly modified to meet different boundary conditions for the estimation of the hydraulic conductivities on the surface and at depth. As a result, the estimated hydraulic conductivities at most sites fall in the range of 10^{-2} ~ 10^{-3} m/d that is roughly consistent with site pumping test results. However, it decreases with depth following a negative power law, which implies that the majority of fractures tend to be closed at depth. Site hydraulic tests also show the similar tendency of vertically spatial variation of the hydraulic conductivities.

The study of fracture connectivity shows another hydrogeological significance. Fracture networks on the measurement scale present the feature of various fracture blocks in the system rather than they are well connected. The 3-D model demonstrates that very few fractures in the TMG sandstones are competent for groundwater flow. With this regard the computation of hydraulic conductivities is hence calibrated.

Multiple approaches are employed to estimate porosity and associated aquifer storativity. Results show that porosity of the TMG sandstones is strongly scale-dependent, of which the value of core sample laboratory tests yield an upper limit of 1.0%~3.6%. The porosity of pumping tests and in-situ fracture measurements fall in the middle range of 0.05%~0.6%, whilst the application of lineament interpretation from remote sensing data produce its lower limit of 1.2×10^{-8} . Assuming the TMG rocks are homogeneous media, the storativity value should have the same trend at various scales. These results indicate that the TMG groundwater resource at a larger scale may be overestimated if use the aquifer parameters derived from a smaller-scale study.

Research findings in current study provide a new insight into the fractured rock aquifers in the TMG area. Some of the results will have wide implications on the groundwater management and forms a solid basis for the further study of the TMG aquifers.

ACKNOWLEDGEMENTS

This thesis would not have been possible without the assistance and cooperation of many individuals and institutions. I would like to acknowledge my debt and wish to record my sincere thanks to the following:

- My supervisor Professor Yongxin Xu from Earth Sciences Department, University of the Western Cape for his thorough and thoughtful coaching.
- My wife and old colleague, Dr Haili Jia from Department of geology, University of Fort Hare, for her assistance, support and understanding during the study and research in South Africa.
- The Department of Water Affairs and Forestry in Bellville, in particular Mr. Mike Smart for their kind help with collecting data and arrangement of the field exploration.
- The Council for Geosciences, Western Cape, especially Dr. Luc Chavelley for their kind assistance during the research in many fields of hydrogeology.
- Dr Shafick Adams from Water Research Commission, for all his suggestion, support and assistance during the study.
- Prof. Abraham Thomas, Mr. Reginald Domoney, Mr. Peter Meyer and Mr. Braun Lawrence, for their assistance and cooperation during research in South Africa.
- The postgraduate students: Segun M Adelana, Jaco Nel, Anthony Duah, Humberto Antonio Saeze (PhD students), Mfundu Biyela and Henok Solomon (MSc students) in Groundwater Group at UWC are thanked for their friendship and assistance.
- Specially, Mrs. Caroline Barnard for all her hard work and patience for assisting the author to complete this thesis.

TABLE OF CONTENTS

ABSTRACT	I
ACKNOWLEDGEMENTS	IV
CHAPTER 1 INTRODUCTION.....	1
1.1 BACKGROUND	1
1.2 RESEARCH OBJECTIVES	3
1.3 LAYOUT OF THIS STUDY	4
CHAPTER 2 HYDROGEOLOGICAL BACKGROUND AND LITERATURE REVIEW	6
2.1 INTRODUCTION.....	6
2.2 GEOLOGICAL BACKGROUND	7
2.2.1 Geomorphology.....	7
2.2.2 Stratigraphy	8
2.2.3 Geological structure	10
2.2.4 Neotectonics.....	12
2.3 REGIONAL HYDROGEOLOGICAL SETTING.....	16
2.3.1 Delineation of the TMG Aquifer	16
2.3.2 Division of hydrogeological unit.....	18
2.4 TYPE OF AQUIFERS	21
2.5 CURRENT GROUNDWATER USE.....	24
2.6 WELLFIELD AND STUDY AREA IN THE TMG	25
2.7 SUMMARY	27
CHAPTER 3 AQUIFER MEDIA	29
3.1 INTRODUCTION.....	29
3.2 FAULT.....	30
3.3 CLASSIFICATION OF FRACTURES	32
3.4 CORE SAMPLE STUDY – A CASE AT RIEFONTEIN DEEP BOREHOLE	33
3.4.1 Introduction to site hydrogeology	33
3.4.2 Fracture geometry	35
3.4.2.1 Fractures from surface measurement.....	35
3.4.2.2 Fracture from core logging	36
3.4.2.3 Fracture density at depth	37
3.4.3 Hydraulically active fracture	38
3.4.4 Implication of the hydraulically active fractures	42
3.5 APPLICATION OF REMOTE SENSING DATA	42
3.5.1 Lineament mapping.....	43
3.5.2 Lineament analysis.....	45
3.6 FRACTURE CHARACTERIZATION WITH DATA FROM FIELD MEASUREMENTS.....	48
3.6.1 Fracture field measurement and data statistics	48
3.6.2 Stochastic realization and connectivity of natural fractures.....	51
3.6.2.1 An approach to fracture realization	51
3.6.2.2 Application to field data	53
3.6.2.3 Connectivity pattern of fractures	55
3.7 SUMMARY	61
CHAPTER 4 HYDRAULIC PROPERTIES	63
4.1 INTRODUCTION.....	63
4.2 POROSITY AND STORATIVITY	65
4.2.1 Relationship between porosity and storativity	65
4.2.2 Porosity.....	66
4.2.3 Storativity.....	70

4.3 TRANSMISSIVITY OF THE TMG	72
4.3.1 Solution to hydraulic test	72
4.3.2 Result from hydraulic test	74
4.3.3 Discussion on hydraulic test	75
4.4 HYDRAULIC CONDUCTIVITY STUDY FOR THE TMG AQUIFERS	77
4.4.1 Problem and objective	77
4.4.2 Methodology	79
4.4.2.1 Adaptation of hydraulic conductivity tensor approach	79
4.4.2.2 Calibration of hydraulic conductivity tensor approach	82
4.4.3 Application to the field data	87
4.4.3.1 Hydraulic conductivity at borehole site	88
4.4.3.2 Hydraulic conductivity at depth	89
4.5 SUMMARY	91
CHAPTER 5 A SITE-SPECIFIC STUDY OF HYDRAULIC PROPERTIES	93
5.1 INTRODUCTION	93
5.2 SITE HYDROGEOLOGY	93
5.3 CHARACTERIZATION OF FRACTURED AQUIFER	96
5.3.1 Field logs	97
5.3.1.1 Core log	97
5.3.1.2 Surface geophysical log	100
5.3.1.3 Fracture measurement on the surface	102
5.3.2 Fracture network	102
5.4 HYDRAULIC PROPERTIES	103
5.4.1 Well bore hydraulic tests	103
5.4.1.1 Packer test	104
5.4.1.2 Pumping test	105
5.4.2 Fracture network model (FNM)	107
5.5 DISCUSSION AND SUMMARY	109
CHAPTER 6 SUMMARY AND RECOMMENDATION	111
6.1 SUMMARY	111
6.2 RECOMMENDATIONS	115
REFERENCES	117
<i>Appendix A Groundwater chemistry</i>	<i>127</i>
<i>Appendix B Borehole core logging</i>	<i>129</i>
<i>Appendix C Fracture data from field measurement</i>	<i>134</i>

List of figures

<i>Fig. 2-1 Extension of the TMG in the southmost area of African continent</i>	<i>6</i>
<i>Fig. 2-2 Map stratigraphically showing the position of the TMG from basemen.....</i>	<i>8</i>
<i>Fig. 2-3 Map of Cape Fault Belt showing the stratigraphical and faulting distributions</i>	<i>11</i>
<i>Fig. 2-4 Historic earthquakes took place in the western branch of the Cape Fold Belt.....</i>	<i>12</i>
<i>Fig. 2-5 Post Karoo tectonic framework showing predominant structural feartures.....</i>	<i>14</i>
<i>Fig. 2-6 Brandvlei-Elkenhofdam megafault and its splay faults.....</i>	<i>14</i>
<i>Fig. 2-7 Picture showing Brandvlei – Eikenhofdam magefault zonet.....</i>	<i>15</i>
<i>Fig. 2-8 Map of isobath showing the vatiation of the TMG bottom.....</i>	<i>17</i>
<i>Fig. 2-9 Map of isopach showing the variation in thickness of the TMG Aquifer</i>	<i>17</i>
<i>Fig. 2-10 Fifteen hydrogeological units spreading over the TMG area</i>	<i>20</i>
<i>Fig. 2-11 Subdivision of hydrogeological unit 6 into four units</i>	<i>21</i>
<i>Fig. 2-12 A model of the TMG composite fractured rock aquifer system</i>	<i>22</i>
<i>Fig. 2-13 An example of horizontal terrane aquifer occurs in the Table Mountain</i>	<i>23</i>
<i>Fig. 2-14 Lithology and structural controlled aquifers.....</i>	<i>23</i>
<i>Fig. 2-15 Groundwater wellfields developed in the TMG.....</i>	<i>27</i>
<i>Fig. 3-1 Models of fault showing the evolution of fault architecture).....</i>	<i>31</i>
<i>Fig. 3-2 Factors impacting on the development of the fracture systems in the TMG</i>	<i>32</i>
<i>Fig. 3-1 Maps of the study area and Rietfontein deep hole..</i>	<i>36</i>
<i>Fig. 3-4 Spatial correlation and distribution of the fractures measured at Rietfontein.....</i>	<i>36</i>
<i>Fig. 3-5 Typical core sections from borehole G40145</i>	<i>37</i>
<i>Fig. 3-6 Types of fractures observed in the core from G40145</i>	<i>37</i>
<i>Fig. 3-7 Fracture density (fractures/cm) plot versus the depth of borehole G40145</i>	<i>38</i>
<i>Fig. 3-8 Types and variations of fracture coatings at borehole G40145 from 14 m below surface</i>	<i>41</i>
<i>Fig. 3-9 Map of the study area depicting extension of the TMG and selected domain areas</i>	<i>44</i>
<i>Fig. 3-10 Map showing Lineaments (red color) captured from Landsat ETM+ image.....</i>	<i>45</i>
<i>Fig. 3-11 Histogram for lineament lengths collectively shows a lognormal distribution.....</i>	<i>47</i>
<i>Fig. 3-12 The TMG outcrops for fracture measurement.....</i>	<i>48</i>
<i>Fig. 3-14 Frequency histogram of fractures vs fracture dip azimuth at per 10° interval.....</i>	<i>50</i>
<i>Fig. 3-15 Plot of cumulative frequency against fracture trace-length with cut-off at 100m, Gevonden.....</i>	<i>52</i>
<i>Fig. 3-16 Position of fracture central points generated by a uniform process.</i>	<i>53</i>
<i>Fig. 3-17 Relationship between fracture orientation and profile direction.</i>	<i>53</i>
<i>Fig. 3-18 Map showing the position of boreholes in Boschkloof wellfield</i>	<i>54</i>
<i>Fig. 3-19 Fractures generated on the 2D plan with the data derived from the field measurement.....</i>	<i>55</i>
<i>Fig. 3-20 Fractures generated on four comparable profiles.</i>	<i>59</i>
<i>Fig. 3-21 Drawdowns observed during the 72-hour pumping tests data at wells BK1 and BK4</i>	<i>59</i>

<i>Fig.3-22 Fracture generated based on the data derived from surface measurements</i>	60
<i>Fig.3-23 Fracture generated based on the data derived from surface measurements at Govendon</i>	60
<i>Fig.4-1 Schematic conceptual model of fractured and matrix rock media with different storativities</i> ..	66
<i>Fig. 4-2 Geophysical resistivity, gamma and density logs in the Rietfontein deep hole</i>	68
<i>Fig.4-3 Map schematically shows scale effect of porosity in the TMG</i>	71
<i>Fig.4-4 General four types of observed drawdowns and log time plot</i>	75
<i>Fig.4-5 Schematic map showing the expansion of depression cone in fracture flow systems</i>	76
<i>Fig.4-7 K Versus b_{er} by various roughness models using data measured from the TMG sites</i>	83
<i>Fig.4-8 Rock mass displacement and fracture closure under normal stress (after Goodman, 1974)</i>	85
<i>Fig.4-9 Hydraulic conductivity plot against depth of the Rietfontein, Boschklouf and Gevonden sites</i>	90
<i>Fig. 4-10 Hydraulic conductivity plot against depth of the TMG sandstone aquifer</i>	91

List of Tables

<i>Table 2-1 Stratigraphical succession of Table Mountain Group</i>	9
<i>Table 2-2 Groundwater abstraction from the TMG aquifers</i>	25
<i>Table 3-1 Chemical constituents of the groundwater from G40145 for representative months</i>	34
<i>Table 3-2 Statistic result of 216 fractures measured at Boschklouf</i>	55
<i>Table 4-1 Porosity estimated from the density logging result at Rietfontein deep hole</i>	67
<i>Table 4-2 Porosity derived from core samples and pumping tests</i>	69
<i>Table 4-3 Storativity of the TMG aquifer refers to various formations and areas</i>	71
<i>Table 4-4 Recommended storativity values for TMG aquifers (Jia, 2007)</i>	71
<i>Table 4-5 Calculated K values from surface fracture measurements</i>	82
<i>Table 4-6 Mechanical aperture correction coefficient C_{er}</i>	83
<i>Table 4-7 K values for bedding and structural fractures</i>	84
<i>Table 4-8 Fracture JRC and corresponding K values</i>	85
<i>Table 4-9 Data sets of fractures from surface measurements</i>	88
<i>Table 4-10 Computed different K values based on the data set of Table 4-9</i>	89
<i>Table 5- 1 Basic information of the boreholes at the Gevonden site</i>	96
<i>Table 5- 2 Physical properties of borehole and surface water</i>	96
<i>Table 5- 3 Statistic of the ^{222}Rn pulse number from different sources</i>	101
<i>Table 5- 4 Hydraulic properties from pumping tests at the Gevonden site</i>	107
<i>Table 5- 5 Computed equivalent K values for fracture blocks of interconnected fractures</i>	109

Chapter 1

Introduction

1.1 Background

The Table Mountain Group (TMG) is a huge aquifer system extends from the northwest of the Western Cape to the northeast of the Eastern Cape, consisting of a suite of sedimentary hard rocks produced in the Ordovician-Devonian period. The significance of the TMG groundwater for water supply in the arid or semi-arid areas of the nation has long been stressed due to the good water quality and a big potential of water abstraction from the fractured sandstones. For the purposes of water supply and resource preservation, the aquifer system has been extensively explored on locations from Utenhage artesian basin in the east to the Sandveld area in the west, since the 1980s. A big monitoring network of boreholes and springs has been established, from which water level and water chemistry data are periodically collected. However, current understanding of the TMG aquifer system is limited as regarding the hydrogeological settings, hydraulic properties of aquifers, and accordingly the groundwater storage and circulation.

Based on previous studies, tremendous borehole hydraulic test data are available for the analyses of aquifer properties on the traditional basis (Rosewarne, 2002). These data are valuable for the estimation of the intrinsic aquifer properties such as hydraulic conductivity (K), transmissibility (T), and storativity (S) and porosity (n). These estimated aquifer parameters are very critical in water resource evaluation, management, and groundwater development in the TMG area. An overestimate of T and S , for instance, may lead to water withdraw from the aquifer exceeding its normal capacity, and cause water level drop and aquifer degradation in a long-term water supply. Current studies on hydraulic properties of the TMG aquifer through field tests are mainly concentrated on the interpretation of testing data using the models based on such assumption that the aquifer are a geologic continuum. A lot of difficulty arise form the application of the models, since the fractured rocks are anisotropic and complex in geometric and physical features which might have been impacted by previous tectonic movement and current stress field. Therefore, a proper study on hydraulic properties of the TMG fractured rock aquifers, based on conceptual models, becomes very necessary.

Relevant researches associated with the TMG groundwater development have covered each field of hydrogeology ranging from aquifer delineation, through resource potential

evaluation, groundwater recharge and quality, to exploration techniques (Pieterse and Parsons, 2002). Explorations and exploitations in the TMG aquifers have produced plenty of valuable information and form the bases for in-depth researches. In terms of the hydraulic properties, previous studies have inescapably seemed to yield higher values of aquifer parameters through field testing or a short-term monitoring for aquifer capacity prediction than reality. This is due to some poor understandings of the subsurface features of the fractured rocks in which the key aspect is the determination of flow path and boundary condition when using existing models to interpret the aquifer responses during hydraulic tests. Previous studies have also showed that the groundwater in the TMG aquifers is prevalently dominated by secondary porosity, i.e. fractures or fracture networks. Significance of fractures control groundwater flow and storage in the aquifers has been long noted and studied by many researchers (Chevallier, 1999; Woodford and Chevallier, 2002), however, few researches have eventually investigated the characteristics and patterns of the fractures which exert a great impact on the aquifer properties.

A fractured rock aquifer is composed of a network of fractures that cut through a rock matrix. The characterization of fractured rock aquifers requires information on the nature of both the fractures and the rock matrixes. Fractures may be characterized in terms of the dimensions (aperture, length, width), locations (orientation, spacing, connectivity, etc.), and the nature of fracture walls (surface roughness, mineral fillings, coatings, etc.). The rock matrix is characterized by its pore sizes and spatial distributions, often expressed by effective porosity. Generally, the hydraulic conductivity of fractures is hundred times of that of matrixes, which has been expatiated in many academic documents. In the TMG sandstones, the fracture systems mainly control the permeability of rock masses and are major potential pathways for fluid flow. Because the distributions and attributes of fractures are not uniform either macroscopically or microscopically, the anisotropy of a fractured rock aquifer makes the determination of potential flow path difficult.

Ideally, fracture data should be gathered on fracture length, orientation, aperture, and density for developing a statistic or determinative model. Particularly the interconnection of fractures may play a key role on the determination of groundwater flow path. It is at times difficult to fully have these data for the characterization of fractures at a regional or a local scale. In this sense, some level of useful knowledge can be inferred based on the structural analyses of an area or a site. The tectonic and depositional history of a given area is generally available in some geologic literatures (McCathy and Rubidge, 2005; Newton et al, 2006),

which provide a concrete background for understanding the formation of fractures in the TMG sandstones.

Hydraulic conductivity, aquifer transmissivity and storativity, are frequently used as the key parameters to determine the aquifer's abstraction potential and sustainable yield. However, uncertainty and diversity of testing results often arise from various data sources at the same site or from multiple interpretation methods using the same testing data. Therefore, it is necessary to employ multidisciplinary approaches, such as geophysical and geochemical methods, in-situ hydraulic and laboratory tests, and digital process and numerical model (Karasaki et al. 2000; Kulatilake et al. 2003; Serzu et al. 2004), to estimate the hydraulic properties associated with groundwater flow and storage. Moreover, it is important to collate these data based on the understanding of the fracture network characteristics. Investigation and characterization of fractured rock as the basis of aquifer conceptualization are crucial, which present both geometric and hydraulic features of the fractures involved. The development of conceptual models on a basis of fractured medium analyses for the study of hydraulic properties of the TMG aquifers has rarely been studied in this poorly understood area. Because the TMG aquifers extend over a huge area, the scale-dependence of some of the hydraulic properties should be another important concern for water resource evaluation.

1.2 Research objectives

In South Africa, the TMG is one out of three major regional aquifers (dolomite, the Table Mountain Group and Karoo dolerite), which has a potential of bulk water supply to meet the requirements of irrigation and local municipalities in the Western and Eastern Cape provinces. Geographically, the TMG is the southmost hard-rock aquifer system in the African continent, surrounded by Indian and Atlantic oceans and generally yields groundwater of high quality characterized by low salinity (Smart and Tredoux, 2001). With the increased water demand from irrigation and urban areas, South Africa has launched a number of research and investigation projects to seek for a proper tool toward the integrated water resource management advocated by the Water Act of 1998. As part of the research of the TMG project on flow conceptualization and storage determination, this study on TMG hydraulic properties with relevant result is intended to provide a comprehensive understanding of the TMG fractured rock aquifers and a fundamental data set for the water resource management in the area. The major challenge of this study is to provide a proper estimation of the hydraulic

properties. Based on conceptual understanding of the TMG aquifer media, the following objectives are expected in this study to be:

1. A comprehensive understanding on the concepts of hydraulic properties and hydrogeological settings based on the analysis of existing geological and hydrogeological information.
2. Characterisation of fractures and fracture network through surface measurements, remote sensing imagery interpretation, and borehole loggings.
3. Establishment of conceptual models on the basis of the TMG aquifer type and groundwater testing data analyses.
4. Estimation of hydraulic properties involving the quantification of hydraulic tests (packer test and pumping test) conducted at different sites, numerical model based on hydraulic conductivity tensor to be applied to various types of fracture network for both 2D and 3D problems.
5. Porosity and storativity quantification using the analyses of core sample laboratory test, pumping and remote sensing data, and borehole geophysical logs.
6. Some site-specific studies established to have a better understanding of the TMG aquifers and associated groundwater behaviour.

1.3 Layout of this study

The abovementioned objectives can be reached with a combination of available site-specific data, related experience, and scientific knowledge of the TMG hydrogeology, geology/geological structure, and geomorphology. Characterization of hydraulic properties based on the analysis of these data requires not only an experienced interpretation of available data and a full understanding of the factors control groundwater processes, but also the application of GIS techniques and some other professional softwares. This study attempts to contribute a lot to the groundwater flow conceptualization and resource evaluation of TMG groundwater resources.

The structure of this dissertation has to be close to the objectives of this study. It begins with a brief background to this study and the objectives expected to be made in this study. For objective 1, current problems and basic concepts associated with the hydraulic properties of the fractured rocks will be introduced in Chapter 1. In Chapter 2, the background of TMG aquifers is addressed based on the description of geology and hydrogeology settings, aquifer delineation, the related researches in study area that will be reviewed.

Objective 2, 3, 4 and 5 will be covered in Chapter 3 and Chapter 4. Combined with the estimation of hydraulic conductivity and transmissivity, existing data from previous studies and current research will be collated and analysed to help establish conceptual models of the TMG aquifers. Based on the understanding of these models, different models or solutions are to be applied to the estimation of hydraulic properties. The applicability of these models or interpretation methods is also discussed, considering the media complexity for flow taking place in the fractured rocks.

Chapter 5 mainly covers objective 6 site-specific groundwater problems and spatial variation of the hydraulic properties in the TMG aquifers, intending to provide a close view and sound estimation of the parameters. Factors influence the spatial variations of main hydraulic properties are discussed taking into account the flow processed in the TMG aquifers.

In Chapter 6, a comprehensive summary will be made, a brief conclusion is drawn, and the suggestions for further studies are also recommended. The dissertation ends with the references.



Chapter 2

Hydrogeological background and literature review

2.1 Introduction

Currently, groundwater development in South Africa mainly occur in fractured rock aquifers in which three major aquifer systems comprising dolomite, the TMG sandstones, and Karoo dolerite are significant for regional groundwater supply. The TMG sandstones are exposed along the west and south coast of South Africa can also be regarded as the southmost regional aquifer system in African Continent, which yields high-quality groundwater. The outcrop of TMG extends from Vanhynsdorp in the northwest to Cape Peninsula in the south and then incurves eastward to Port Elisabeth, covering around 37000 km² out of the whole TMG deposit area of 248400 km² (Fig.2-1) confined in the Cape Fold Belt. Stratigraphically, with a deposit thickness ranging from 900 to 4000m, the TMG consists of a thick sequence of hard sedimentary rocks in a southeastward trough 500~425 Ma ago.

Based on the results of sustainable groundwater practices inside the TMG aquifers via borehole/spring abstractions, together with the cognitions on lithological characteristics, stratigraphic assemblage and structural fabrics of the TMG, it has been inferred that the TMG is a regional aquifer which extends to big depths (Issar, 1995; Weaver et al, 2002) and there

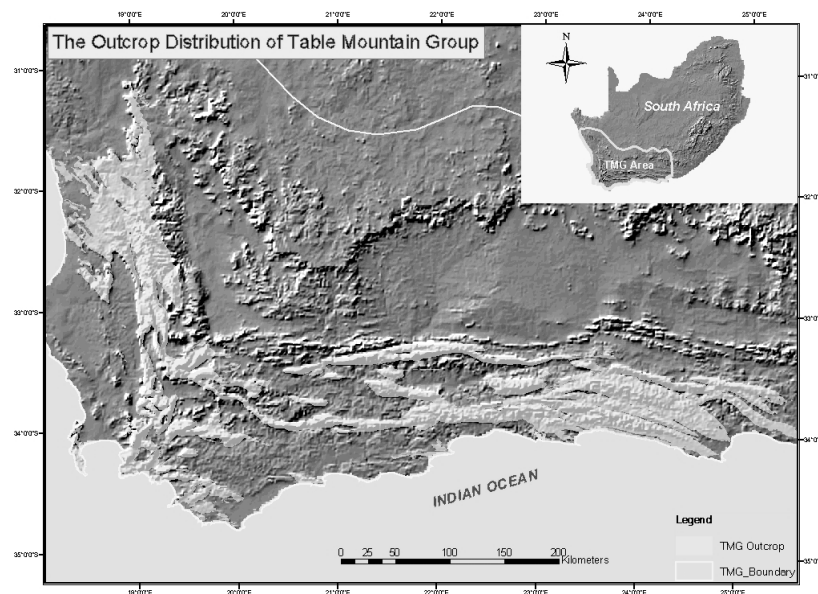


Fig. 2-1 Extension of the TMG in the southmost area of African continent with the outcrop mostly capping on the mountains from the west to the east

accordingly is a huge groundwater reservoir underneath the area. In addition, it is acknowledged that the aquifer systems are mainly dominated by fractured sandstones, siltstones, and sandwiched shales and mudstones. As underlain by Precambrian rocks and overlain by mid- to neopaleozoic basin deposits, and bounded by some regional faults such as Kango-Baviaanskloof and Worcester faults, the TMG aquifer system has been identified to have the potential for bulk water supply in the Western and Eastern Cape provinces. However, current understanding of the TMG aquifer system is limited as regarding the hydrogeological settings, geometric, physical and hydraulic properties of aquifers, and accordingly the groundwater storage and circulation.

As the important basis of hydrogeological settings, aquifer properties, groundwater storage, and circulation, it is necessary to have a gross view on the hydrogeological backgrounds with respect to geomorphology, stratigraphy, structural geology, and associated aquifer system and the status quo of groundwater development and current problems existed in the TMG study, mainly based on previous studies, and some of the current study.

2.2 Geological background

2.2.1 Geomorphology

The influences of geomorphologic features/patterns on groundwater behaviors in the TMG areas have been limitedly delineated. Regionally, the TMG covers mountains, wave-cut plains and intermountain drainage basins as the basic geomorphologic types in this area. The modern landform patterns of the TMG area largely resulted from post Karoo morphogenetic processes including the denudation of mountains and the formation of half grabens due to crust uplift in inland areas, peneplain and transgression along the coastal areas, which lead to the rolling landscapes with a relative relief of 200~1700m.

The mountain peak can reach 1900~2250m in Hex River Mountain, 1500~2000m along Langeberg and 1700~2000m on Swartberg Mountains. Compared with overlaying argillaceous rock formations and underlying basement rocks, the geomorphologic patterns of TMG are characterized by the highly stick-out mountains and steep slopes with quite thin or even no soil covers over its outcrops. Most of the mountains form the backbones of the TMG geomorphologies which are firmly controlled by the structures and lithologies. Among them, from west to east, Bokkeveldberg -Cedarberg – Skurweberg and Hex river mountains are dominant, and turning eastward to Langeberg- Outeniekwaberg Mountains. To the north there

are Witteberg-Swartberg- Baviaanskloof Mountains. In between these mountains there are intermountain basins and flood plains, most of which are covered by weather mantles from argillaceous rocks and fluvial deposits.

Eleven primary catchments fall into the TMG area, which are Berg, Olifant-Doring, Bree, Salt, Gounrits, Gamtoos and Sundays rivers from the west to the east and 551 quaternary catchments are involved. These catchments control not only the local base level of corrasion but also the water drainage systems. The rivers cutting through various formations of the TMG and structural units of the area produce the watercourses and slope systems, which lead to both the TMG rough and cragged surface and different relief mountain and hill systems. These definitely influence the groundwater systems in terms of recharge locations, interflow behaviors, and corresponding groundwater circulation above sea level.

2.2.2 Stratigraphy

South Africa is well known for its extraordinary long geological record spanning almost the entire geological history of the earth. One of the oldest lithostratigraphic units in the world in South Africa, i.e. the Palaeoarchaean greenstone belts, can be dated to ca. 3.5 Ga. The TMG was formed from the early Ordovician to the early Devonian during 500~425 Ma ago (Fig.2-2).

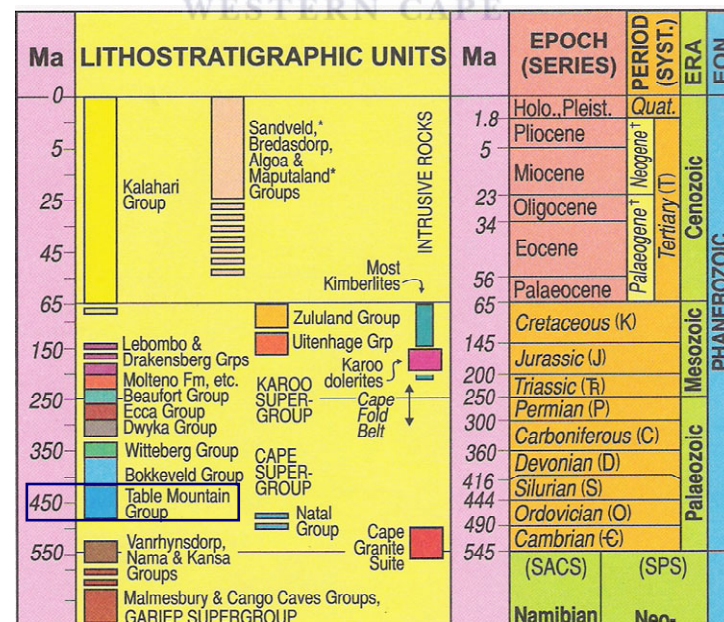


Fig.2-2 Map stratigraphically showing the position of the TMG from basement, in fact the oldest rock formations in South Africa can be dated back to 3.5 Ga (after Council of Geoscience, 2006)

Table 2-1 Stratigraphical succession of Table Mountain Group

Group	Subgroup	Formation	Geological symbol	Thickness (m)		Lithology
				subtotal		
Bokkeveld			D	4000		Siltstones, shales, sandstones
Table Mountain	Nardouw	Rietvlei/Baviaanskloof	Dr/ S-Db	1200	300	Feldspathic quartz arenite
		Skurberg	Ss		500	Quartz arenites
		Goudini	Sg		400	Arenite, minor siltstone, shale
		Cedarberg	O-Sc	70	50~150	Silty shales and shaly siltstone
	Peninsula	Parkhuis	Opa	2500~3100	100~150	Tillite, diamictite, quartz arenites
		Penninsula	Ope		1500~2000	Largely thick-bedded, coarse-grained quartzitic arenites
		Graafwater	Og		65~150	Thin-bedded sandstone, siltstone, shale and mudstone
		Piekenierskloof	Op		800	Quartzitic sandstone with coarse-grained to gritty zones and rudites
Basement		Underlying the TMG are the Malmesbury shales, the Gamtoos and the Kaaimans argillites, comprising a suite of moderately to lightly metamorphic sedimentary rocks; and cape granite suite.				

The stratigraphy and lithology of the TMG have been depicted in details by Du Toit (1954), Rust (1967; 1973), and De Beer (2002). Main stratigraphic units involved from the bottom to the top in the TMG aquifer system are Piekenierskloof, Graafwater, Peninsula, Parkhuis, Cedarburg formations, and Nardouw formations (Table 2-1). The basal Piekenierskloof formation, lying unconformably on basement rocks, consists of litharenites and rudites and is overlain by the semi-confining Graafwater shale/siltstone formation. These two units are only found in the western branch of the TMG. The most significant and thickest Peninsula formation is composed entirely of quartzitic arenites and is the most favoured aquifer for water quality and yields. This formation occurs across the whole extent of the TMG with a thickness ranging from 1000 ~ 2000 m. A thin shale/ shaly siltstone layer with an average thickness of 70 metres makes up the Cedarberg formation. As extensive as the underlying Peninsula, Cedarberg Formation acts as a confining layer or aquitard and effectively separates the lower and upper aquifers. The topmost of the TMG is the Nardouw subgroup, which is divided into three members of interlayered shale, sandstone, siltstone and quartzite because of its variable composition.

The TMG stratigraphic units had undergone a low grade of metamorphism due to folding and thrusting during the Cape Orogeny, resulting in the rocks of phyllites and quartzites rather than shales and sandstones (Hälbich and Cornell, 1983). Recrystallization and polygonisation of quartz grains are typical in quartz arenites; these cases are commonly intensified in the rocks near fault zones. On the other side, recrystallization of mineral grains implies the

reduction or disappearance of primary porosity and in this sense groundwater in the TMG rocks can be regarded as being dominated by secondary porosity of fractures and joints. In spite of these, the TMG rocks still remain many of the original sedimentary fabrics and are generally referred to be sedimentary rocks (Newton et al., 2006).

2.2.3 Geological structure

The TMG rocks have been reconstructed by several phases of crustal movements from the Permian to the Cretaceous, which created various types of discontinuities in the form of joints, faults and unconformities. Some of the discontinuities have been reactivated since the post Karoo tectogenesis which complicated the existing fracture systems or zones. These secondly structural voids in TMG sandstones and siltstones constitute most of the fracture spaces allowing groundwater storage and movement.

The TMG region was at the margin region of Gondwanaland. The subduction on the southwest margin of Gondwanaland in the Late Carboniferous - Early Permian led to the transformation of an old passive margin into a foreland basin (the Great Karoo Basin) with southerly sourced sediments. The tectonic convergence at plate margins in the Permo-Triassic led to four episodes of development of the Cape Fold Belt known as Cape orogeny during 278 Ma ~ 230 Ma (Hälbich, 1983). The formation of Cape Fold Belt, which extends from Australia through Antarctica and South Africa to South America (Fouché et al., 1992; McCathy and Rubidge, 2005), has posed a profound impact on the development of the TMG structural configuration and stratigraphical extension, and hence the hydrogeological setting.

The Cape Fold Belt is characterized by a series of northwest- to north-trending folds in the western branch, stretching from Stellenbosch to Vanhynsdorp, and by folds striking approximately east-west in the southern branch from Swellendam in the west to Great Fish River in the east. The two arms of folds meet in the structural syntaxis in the center with more complex folding and faulting (De Beer, 2002) (Fig.2-3). The Cape orogeny largely formed the structural framework of the TMG (Hälbich, 1983), which also produced a series of south-dipping imbricate thrusts affected both basement and cover rocks. Thrusts in the area, represented by Kango-baviaanskloof and Worcester faults, can be roughly divided into three categories: backthrust, forward thrust, and pop-up structures (Newton et al., 2006). Both of the regional faults mentioned here are usually regarded as regional boundaries of groundwater regimes, and the pop-up structures are critical in searching for groundwater in the TMG fractured rocks (Newton et al., 2006).

Breakup of Gondwanaland during the late Jurassic to the Cretaceous both created dextral shearing of the South African margin bounded by Agulhas-Falkland fracture zone and caused regional fragmentation and distortion of previous structural frames due to the compressive stresses were replaced by tensile stresses. Intraplate movements more likely took place along the existing thrust planes of relative weakness, which led to the development of half-grabens as Outshoorn and Worcester basins where the Mesozoic strata (e.g. Utanhage formation) were developed. Moreover, this tectogenesis has turned most of previous thrust faults into normal faults with a gross throw of over 6000m at Worcester fault, for instance, and an impressive throw at Kango-Baviaanskloof fault. Both in the eastern and western branches of the Cape Fold Belt, normal faults are widespread; especially the faults have been rotated clockwise due to the right-lateral movement along Agulhas-Falkland fracture zone in the eastern branch. In the structural syntax (Fig.2-3), the features of normal faults are much complicated as a set of north-east striking faults strongly transect or rebuild both west-east and north-west trending faults and folds. However, the existence of this set of faults implies that a predominantly dextral strike-slip movement in this area has ever taken place (1/250000 geological map, 3319 Worcester sheet).

The normal faults developed in the TMG have long been the targets for groundwater exploration and exploitation. This is the case for Quaternary active faults where the fault core

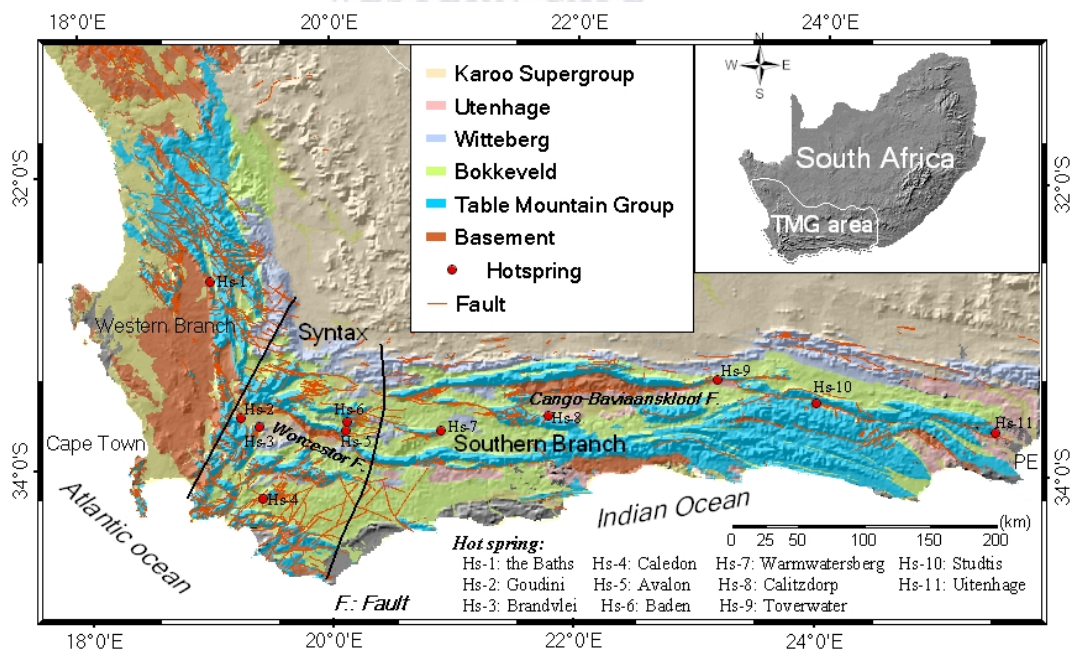


Fig. 2-3 Map of Cape Fault Belt showing the stratigraphical and faulting distributions of involved formations of the TMG, Pre-Cape rocks, and the younger Groups

materials are mostly uncemented, but misperception may arise when the fault zones are cemented and act as groundwater barriers. In fact, most of fault zones developed in the TMG sandstones and siltstones are evidenced to be lithified and act as aquicludes (Newton et al., 2006), such as Klein Bavaria fault north of Plettenberg Bay, Brandvlei – Eikenhofdam fault, and Kango fault etc.

2.2.4 Neotectonics

The impact of neotectonic activity from the Miocene to the Quaternary on groundwater in the TMG fractured rocks is yet unknown and has rarely been studied. With exception of earthquake, neotectonic deformation and its impact on the occurrence and motion of groundwater is imperceptible in most cases. However, this long-term deformation has undoubtedly imposed a great influence on the TMG rocks, especially such various-scale discontinuities as faults and joints. To have a better understanding of the TMG hydrogeology, it is necessary to take a look at post Karoo tectogenesis especially neotectonics. Currently, neotectonic study in South African onshore and offshore domains are derived from the interpretation on seismicity, fault rejuvenation, geomorphologic evidence, and estimation of stress field to meet the need of civil and industrial engineering work evaluations.

1. Seismicity

In general, earthquake can exerts an additional force on the rock masses within seismic influence zone. This momentary external force may change the properties of fractures such as aperture and connectivity, both of which are critical in controlling groundwater flow path in the fractured rocks. In particular rock masses nearby epicenter are more cracked after

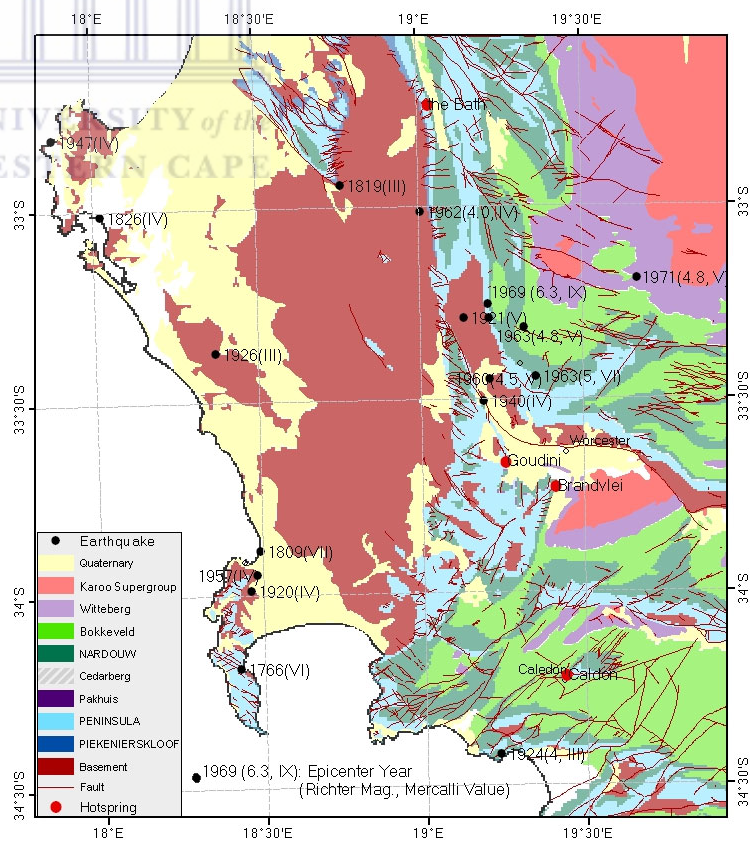


Fig. 2-4 Historic earthquakes took place in the western branch of the Cape Fold Belt from Ceres to the Cape Flat

an earthquake than before, from which the rocks can be prominent target for searching for groundwater (Andersen and Ainslie, 1994).

South Africa is in such an intraplate area that earthquakes take place under poorly constrained forces (stresses) and affect continental crust away from the seismic regions at the margin of tectonic plates (Andreoli et al., 1996). In the TMG area, seismic events characterized by low to moderate intensity are mostly concentrated in the western branch area of the Cape Fold Belt, from Ceres-Tulbagh to Cape Flat (Fig.2-4). In the last two century, there have been about 40 seismic events taking place in this region, in which the most frequently happened and the worst hit area is Ceres-Tulbagh where the earthquake on 29th Sep 1969 reached a magnitude of 6.3. This earthquake once dried off a nearby hot spring at Goudini, some 50 km away from the epicenter. Current hot spring water for one of the famous holiday resorts in Western Cape is abstracted from a 350 m deep borehole drilled after the earthquake.

2. Fault rejuvenation

Although the mechanism of inland seismicity has not yet been satisfactorily explained (Ransome and de Wit, 1992; Andreoli et al., 1995), using both “ridge push” and crust uplift models, evidence for the Late Tertiary to the Quaternary neotectonic activities is rapidly growing along with the data derived from both onshore surveys, and offshore geophysical and borehole investigations. Of this, the rejuvenation of faults at various scales has most been documented. Fouché et al. (1992) concluded that the tectonic movement in this area, corresponding to plate drifting, did not terminate after the Gondwanaland segmentation. Andreoli et al., (1996) suggested that post Karoo structural activity in southern African continental margin is mainly controlled by the structural configuration shown in Fig.2-5 where one the major component is Ceres-Prince-Edward fabric that covers the TMG area ranging from Groot River fracture zone (north limit) to Gansbairi-Quoin Point (south limit). According to his research, faulting structures that predominate neotectonics in this area mainly comprise the offshore Agulhas-Flankland fracture zone, Cape fracture zone which joins Cape-Tzaneen Fracture zone in the north of the TMG, and the onshore Worcester fault which was partially reactivated in the Neogene. The stress field (Bird et al., 2006, Umvoto, 2003) in Fig.2-5 implies that a NE 25° to NE 65° extension deformation dominates most of the TMG areas, but the direction and magnitude of principal stresses may change locally because the restriction of local structures especially the discontinuities in rock formations can divert stress distribution and concentraion.

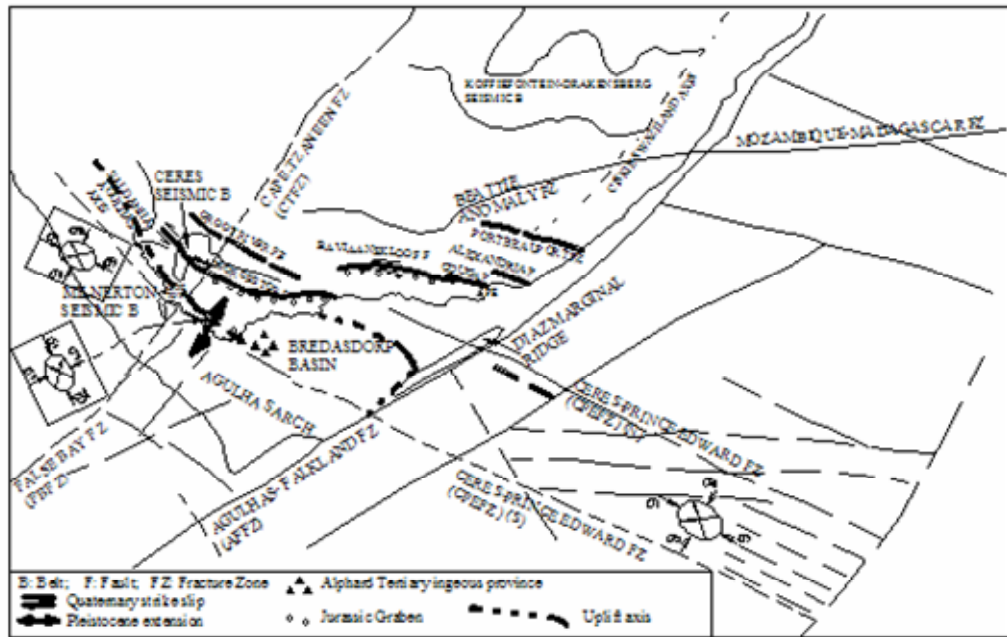


Fig. 2-5 Post Karoo tectonic framework showing predominant structural features such as Agulhas-Frankland Fracture zone and Cape-Tzaneen Fracture zone running through Ceres-Prince-Edward Fabric. These structural features control the post Karoo tectogenesis in the TMG area where some regional faults have been evidenced to be reactivated. (modified from Andreoli, 1996; Friese, 2007).

Compared with the neotectonic activities taking place at plate margins, the reactivation of faults in the TMG region is of low magnitude in terms of deformation. In the eastern branch of the Cape Fold Belt, the Kango-Baviaanskloof fault, for instance, was evidenced to have a left-lateral strike slip with a comparatively recent offset measurable in meters through investigation to slickensides and displaced river terraces at De Rust and Antoniesburge near Uniondale (Hill, 1988). In the western branch and structural syntaxis, the roughly W-E trending Worcester fault reveals a left-lateral slip movement (Andreoli et al., 1995). The rejuvenation of SE-trending Donkergat fracture zone between Quoin Pont and Gansbaai is well documented. The Miocene crust uplift along SE-trending Saldanha-Cape Agulhas axis was reported by Partridge and Maud (1987); this neotectonic activity caused extensive jointing, faulting, and folding in the calcified dunes in the wide west of Cape Agulhas.

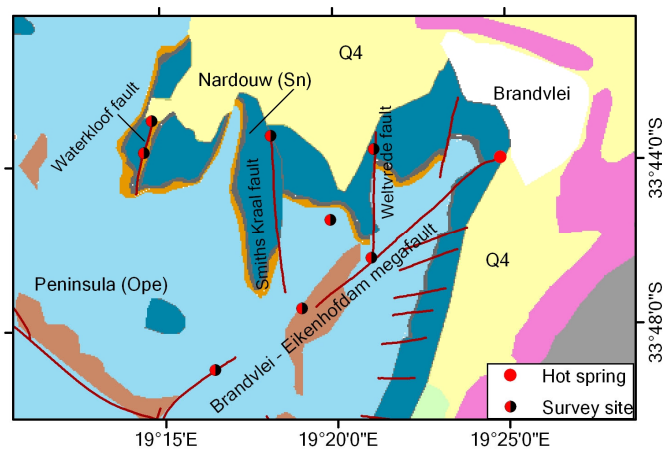


Fig. 2-6 Brandvlei-Elkenhofdam megafault and its splay faults developed in the TMG and basement rocks.

In the structural syntaxis, evidence for neotectonics is historically seismic events which are indications of crustal stress concentration at NW- and NE-trending faults. However, relatively recent fault movements can be tracked in some NS- and NE-trending faults, such as Brandvlei – Eikenhofdam megafault and its splays (Fig.2-6). At the fault zone of Brandvlei – Eikenhofdam fault near Brandvlei hot spring, the SW-trending scratches with uncemented iron oxides (Fig.2-7) extensively developed in the fault core cleavages have a plunge of $40^{\circ}\sim 50^{\circ}$. This probably indicates that this megafault has undergone a left-lateral strike-slip together with a SW-plunging movement in a comparatively recent time. From field surveys to the fault zones of the splays, such as the NS-trending Waterkloof, Smiths Kraal, and Weltvrede faults in the south of Rawsonville (Fig.2-6), the observed scratches with coating/filling materials of quartz and iron oxide, imply that these faults have experienced a strongly disturbed period but then low magnitude of displacement since post Karoo tectogenesis. In addition, clean scratches, identified at the depth of 110m and 65m in the borehole core samples from BH-1 and BH-2 nearby Waterkloof fault zone where the fault core material consists of recemented cataclasites and slightly metamorphosized sandstones, also evidence the recent movement or stress concentration.



Fig. 2-7 Picture showing Brandvlei – Eikenhofdam megafault zone (left) at Stettynskloof. Scratches developed in the cataclasite cleavages having a WS-NE trend with a plunge of 43° , indicating a recent left-lateral strike-slip movement of the fault. Filling materials are partially cemented iron oxides (right) and not silicified. Note: the vehicle is approximately facing northeast.

2.3 Regional hydrogeological setting

2.3.1 Delineation of the TMG Aquifer

The TMG aquifers largely consist of litharenites and rudites in Piekenierskloof formation, quartzitic arenites in Peninsula formation, sandstones and siltstones in Nardouw formations, and shaly members in Graafwater and Cerdaberg formations. Stratigraphy of the TMG in the Western Cape area was discussed by Rust (1967) who demonstrated its sedimentary sequence and regional extension in a southeastward trough and first time gave the TMG formations the academic nomenclature.

Generally, the TMG is strongly compartmented by basement rocks and faults/faulting zones created in the Palaeozoic and reconstructed during the Mesozoic tectonizations. As results, two major regional faults i.e. the Worcester fault and Kango-Baviaanskloof fault control the buildup frames of the TMG distribution to a very large extent. Reported throws of the two faults can reach 4000~6000 m that control the extension of the TMG to a big depth. Isobath of the TMG bottom (Fig.2-8), derived from eight main geological profiles and some 40 smaller geological cross sections across/over the TMG area, shows that the TMG extends to the depth of 4000~6000 m in the central area and northern areas. Lacune of the TMG commonly occur in the northwest and west coast areas where most of the TMG bottom exposes along the contacts with basement rocks, especially at the eastern border of the Cape Flat. Thickness of the TMG Aquifer largely ranges from 500 m to 4000m (Fig.2-9) that is consistent with the Cape Fold Belt extending southeastwards and then incurvating toward east. Both Fig.2-8 and Fig.2-9 indicate that the TMG may extend to a certain distance in the Indian Ocean to be the basement of the Mesozoic sedimentary rocks. The variation in depth and thickness of the TMG suggest that most the Aquifer in the study area is currently untouchable with respect to present exploration and exploitation techniques. Eleven thermal springs occur in the Cape Fold Belt (Fig.2-3) are exclusively the TMG deep circulation water with temperature ranging from 23° - 64°C (Meyer, 2002). Assume that the natural thermal gradient is 2°C per 100m and the average surface temperature 15°C, the circulation depth of these thermal springs is merely from 500 m to 2500 m. In terms of a natural groundwater circulation system, this probably implies that majority of the TMG stratigraphies extend below the limits of those thermal water circulation depths cannot be regarded as aquifers, although the existence of thermal water in the sea is unknown.

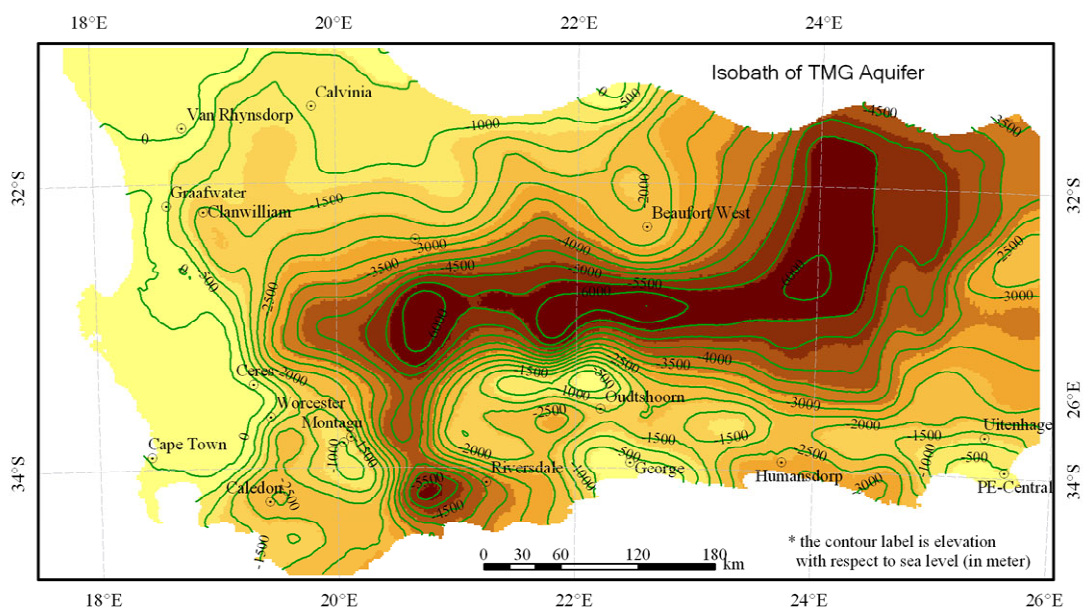


Fig. 2-8 Map of isobath showing the variation of the TMG bottom (buried depth) based on the study of cross sections through the whole TMG area

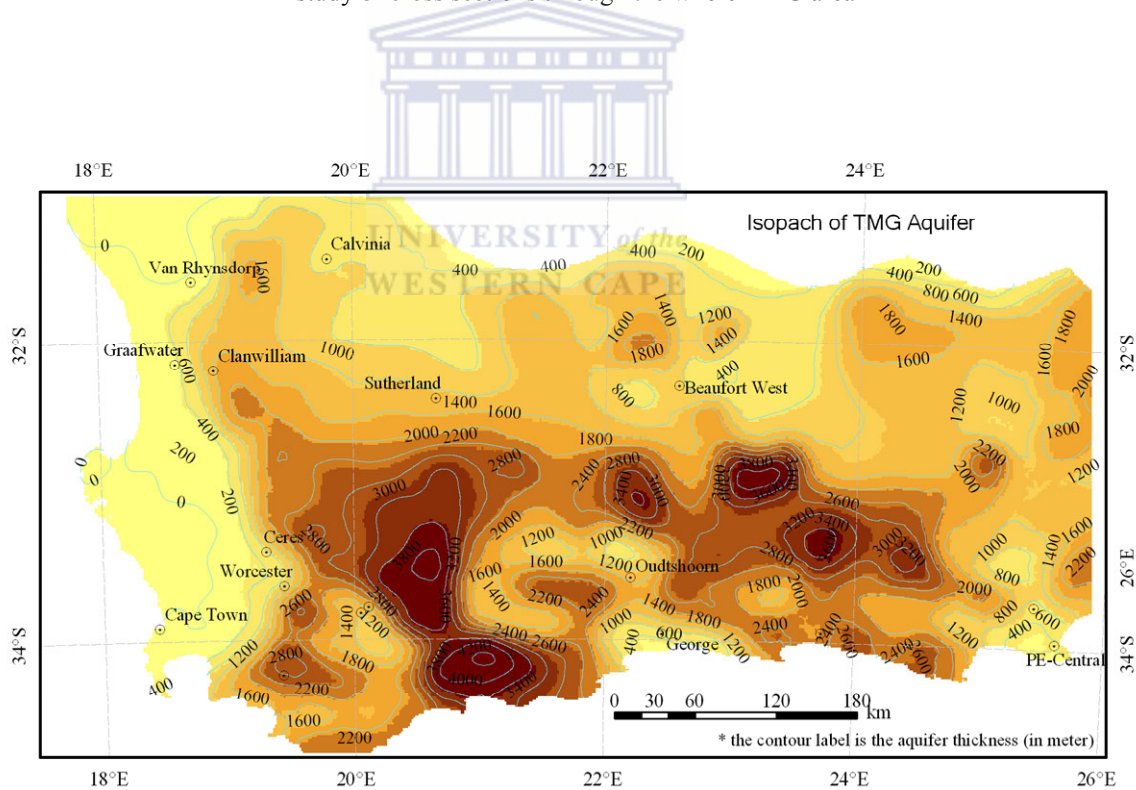


Fig. 2-9 Map of isopach showing the variation in thickness of the TMG Aquifer based on the study of cross sections through the whole TMG area

2.3.2 Division of hydrogeological unit

The TMG aquifer system in the Cape Fold Belt is, in general, conceptualized into three aquifer units as Peninsula Aquifer (Peninsula formation), Nardouw Aquifer (Nardouw formations), and interbedded Cedarberg Aquitard (Cedarberg formation) between the two main aquifers (Kotze, 2002). In particular, the Piekenierskloof Aquifer and its overlaying Graafwater Aquitard are only restricted to the western branch of the Cape Fold Belt. This kind of aquifer/aquitard demarcation is merely based on aquifer lithologies, although each of the units has unique hydrogeological characteristics regarding its physical and mechanical properties of rocks in response to previous tectonic deformations and later geomorphologic processes which may lead to variety of aquifer porosities, fracture configurations, spatial distribution such as depth extension, and proximity to recharge areas, etc.. A lithologic unit is not necessarily a hydrostratigraphic unit because the later is normally referred to as a formation, a part of formation or a group of formations in which there are similar hydrologic properties allowing for a grouping into aquifers and associated confined layers (Domenico and Schwartz, 1990). In fractured rocks, a hydrostratigraphic unit may consist of one or some lithological units with specific structural orientations and fracture networks where there is an independent groundwater circulation system for recharge, throughflow and discharge.

Regionally, the TMG aquifer system has been previously divided into five sections, probably based on regional water management, namely the Western Section (the CAGE area, Hartnaday and Hey, 2000), Central Section (Agter Witzenberg – Ceres – Hex - Koo Valley and Villiersdorp (Weaver et al., 1999), Klein Karoo Section (Kotze, 2002), eastern TMG Section (Plettenberg Bay to Port Elizabeth, Murray, 1996), and Coastal Belt (from Kleinmond to Mossel Bay, Fortuin, 2004).

In terms of the type of openings – primary or secondary, lithostratigraphy, physiography and climate, Vegter (2001) divided South Africa into 64 groundwater regions, in which 23 regions are within the TMG deposit area with 16 regions in its outcrop area. In his groundwater region demarcation and associated delineation, the TMG is not more hydrogeologically significant compared with the adjacent Bokkeveld Group and Witteberg Group.

The hydrogeological conditions of the TMG are more complex than the above delineations. The aquifer system within the Cape Fold Belt has complicated stratigraphic assemblages from Pre-Cambrian to Jurassic, which experienced the tectonic events and low-grade metamorphism from the Permian to the Cretaceous, resulting in various water-bearing fold/fault systems. As results, the TMG sandstones with low primary porosity are generally

regarded as fractured media in regional and local scales. With respect to groundwater circulation and storage, it was very common that the aquifer media, the behavior and nature of groundwater flow could be similar over a certain area but different from the others. For this reason, it is necessary to demarcate the aquifer system into distinguishing hydrogeological units. This is an important step in regional hydrogeological study and groundwater development and management in TMG area. This demarcation requires not only a detailed study on the aquifer media consist of basic stratigraphic units and structural fabrics, but also a careful identification of the boundaries of each proposed hydrogeological unit.

The hydrogeological boundary of the hydrogeological unit is firmly controlled by the features of lithology, geomorphology and fault, which could form the regional groundwater barrier, or recharge or discharge boundary. In the TMG area, the boundaries are summarized as the followings.

- 1) Contacts between the TMG and the Pre-Cape basement rocks such as Malmesbury, Kango, Gamtoos, and Kaaimans groups; and these contacts generally form the hydrogeological boundaries at the bottom of the TMG.
- 2) Contacts at TMG/Bokkeveld, TMG/Witerberg as the boundaries at the top of the TMG, where the TMG is mostly confined by the argillaceous rock formations.
- 3) Regional fault like Worcester fault and Kango-Baviaanskloof fault etc.
- 4) Basements and faults serve as boundaries at the same time.
- 5) Main rivers such as Breede River, Olifant-Doring River etc.
- 6) Primary catchemnts
- 7) Discharge boundary- coastlines along the Atalantic and Indian oceans.
- 8) The TMG north limit boundary where the TMG thins out.

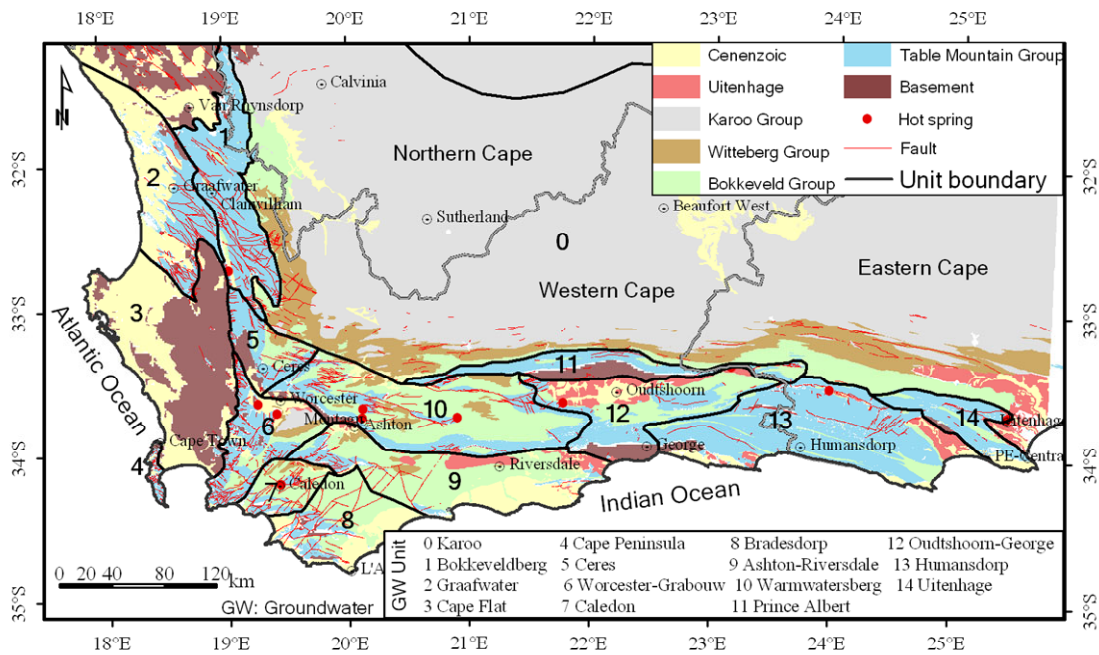


Fig. 2-10 Fifteen hydrogeological units spreading over the TMG area

According to the elements of a hydrodynamic system and the boundary conditions of groundwater storage and flow as mentioned above, the TMG aquifer system can be divided into 15 hydrogeological units (Fig.2-10). In addition, the Cedarberg shales act as aquitard at an aquifer scale, but should not be regarded as regional hydrogeological boundaries, as these shales are susceptible to mechanical displacement into regional discontinuities. The Graafwater formation are only restricted between the Piekenierskloof formation and the Peninsula formation and to the western branch of the TMG. As this area is highly fractured with the dense development of northwest and west-east trending faults, the Graafwater shale/mudstone formation can only be regarded as the local aquitard. Therefore the demarcation of hydrogeological units lithologically takes the TMG formations as a whole. Hydrogeological units classified at a scale of primary groundwater region may not coincide with regional groundwater flow; and these hydrogeological units are generally expected to provide a first-order focus for more detailed study in a regional scale. In this regard, there is no big difference in the demarcation from that of Xu et al (2007) who divide the TMG into 19 units.

Taking the geologic features and potential recharge areas and flow regimes into more detailed account, subdivision of each hydrogeological unit becomes necessary. The hydrogeological unit 6 (Worcester–Grabouw), for instance, can be subdivided into four subunits. Fig.2-11 shows that Worcester fault and basement rocks in the north, Kleinmond–Robertson fault zone in the east, the TMG/basement contact in the west, and the coastline in the south constitute the boundaries of the unit 6, whilst other three faults, including the

Brandvlei-Eikenhofdam fault in the middle, form the secondary boundaries of the four subunits. In the process of subdivision, the Goudini and the Brandvlei thermal springs are separated into different subunits, for each thermal spring represents an independent deep-water circulation system that should not be mixed at this scale. In terms of groundwater recharge, the hydrogeological subunit 6-4 (Fig.2-11) receives the highest annual precipitation and subunit 6-2 the lowest among the four subunits.

For more detailed demarcation of hydrogeological subunits, there has been and still tremendous work to be done, especially on the TMG geological structure and the identification of the characteristics of faults which have potential to become groundwater flow barriers or conduits. It is clear, from the subdivision of hydrogeological unit 6, that the fault and lithologic contact are both playing a key role in controlling secondary boundaries. The result of such subdivision shown in Fig. 2-11 is yet far from a close study to any specific aquifer, but the approach of subdivision can be analogized to the other hydrogeological units, provides a qualitative insight into scale-down regional groundwater regimes through the studies of hydrogeological conditions.

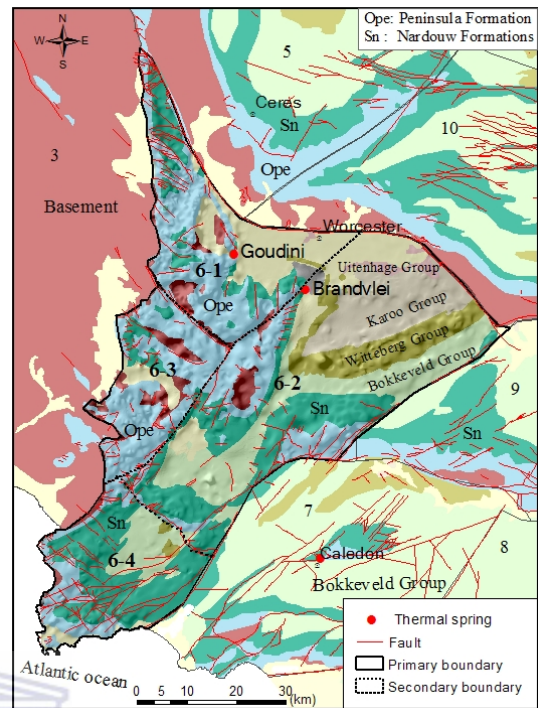


Fig. 2-11 Subdivision of hydrogeological unit 6 into four units based on structure, deep flow system, and recharge area.

2.4 Type of aquifers

The TMG aquifers can be regarded as the fortuitous combination of lithologic, tectonic and climatic features which cause the difficulties in the description and interpretation of their fabrics and dynamics. Currently, the majority of the TMG aquifer characterization is on the basis of aquifer formation analysis. With the study of geological cross-sections, the boundaries and possible flow path are often predetermined to describe a site-specific or problem-specific aquifer behavior, which are still an effective approach to characterize the thermal water flows since many subsurface features are yet unknown.

Based on the analysis of basic elements of aquifer system, Xu et al (2007) summarize the TMG aquifers into four categories:

- 1) Horizontal terrain aquifer system;
- 2) Fold strata aquifer system;
- 3) Fracture zone aquifer system; and
- 4) Composite aquifer system (Fig.2-12).

The horizontal terrain aquifers are limitedly occurred in the Cape peninsula and far northwest of the TMG area where the gentle-dipping TMG terrane controls both the extension of the aquifer and the topographical features that in turn influence the aquifer's recharge (Fig.2-13). Fold strata aquifer system includes the aquifers consist of syncline, anticline and monocline. This type of aquifer material is assumed to be homogeneous and is often use to explain the occurrence mechanism of some thermal springs in the TMG where the aquifer strata is bounded by relatively low permeable layers (Fig.2-14a). However, groundwater occurrence is not solely controlled by stratigraphy and its spatial distribution. On one hand, since there is almost no primary porosity in the TMG sandstone as will be discussed in next chapter, the majority of groundwater is dominated by various-scale fractures include faults, joints, and bedding planes. Because the characteristics of such structures show that the scale of fracture zone aquifers can vary from kilometer to meters, on the other hand, it is necessary to have more detailed study on the fracture systems for which there are yet no conceptual models to describe the fracture block sandstone aquifers as illustrated in Fig.2-14b.

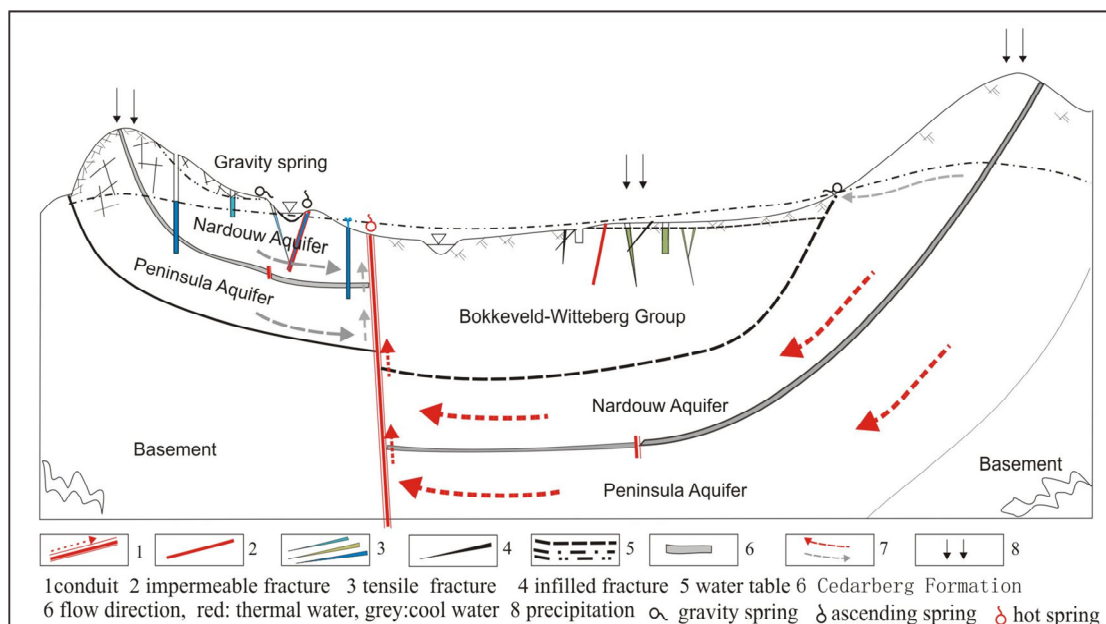


Fig. 2-12 A model of the TMG composite fractured rock aquifer system (after Wu, 2005)

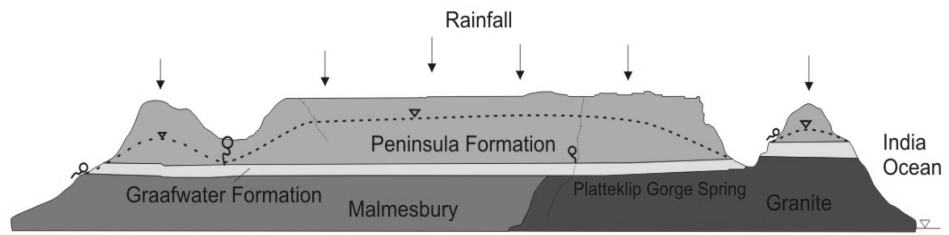


Fig. 2-13 An example of horizontal terrane aquifer occurs in the Table Mountain, Cape Town (after Xu et al, 2007).

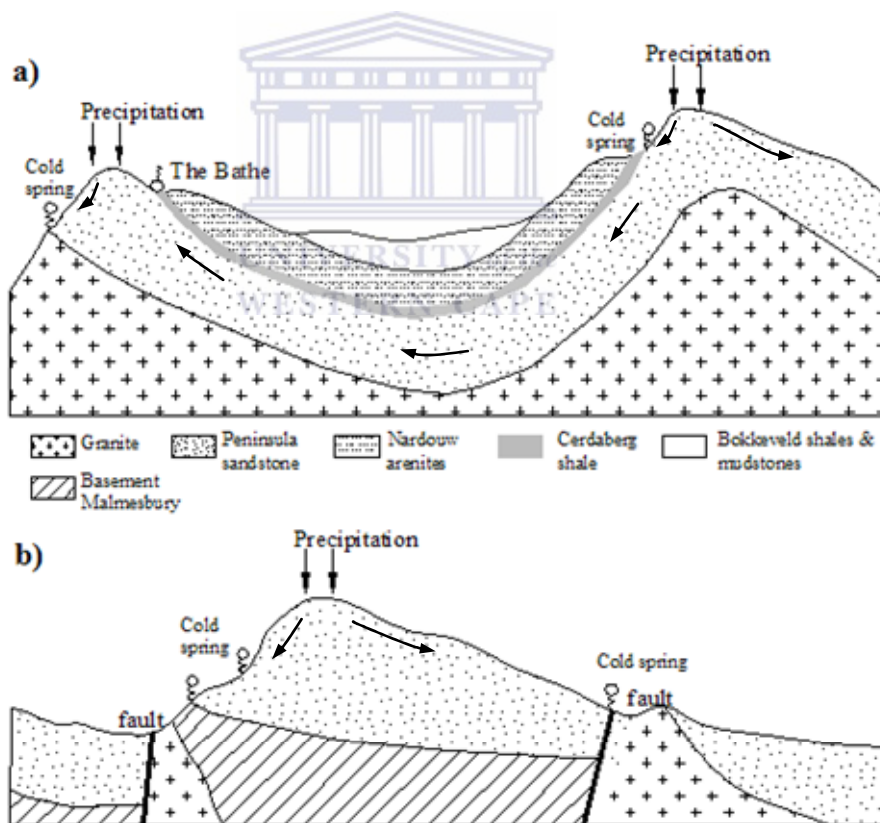


Fig. 2-14 Lithology and structural controlled aquifers, a) Syncline, the Bathe hot spring model, b) Fault and basement bounded outcrop model.

2.5 Current groundwater use

The TMG has become the focus of much investigation as a significant potential source of water supply for the southern regions of South Africa due to a large amount of high quality water stored. The TMG area is covered over large parts by the water management areas of the Department of Water Affairs and Forestry (DWAF), comprising the Olifants/Doring River in the west, Berg and Breede in the south and the Gouritz and the Fish/Gamtoos River in the east (DWAF, 2002). Statistical data show that present annual groundwater abstraction from the aquifers, approximating $5.56 \times 10^7 \text{ m}^3$ (Table 2-2), is only about 5.1% of overall water supply (about $9.0 \times 10^8 \text{ m}^3$) and 4.3% of entire groundwater discharge ($1.29 \times 10^9 \text{ m}^3$) estimated from the TMG aquifers (Jia, 2007). As surface water development has reached its peak in most areas, development of TMG groundwater is critical for future need and economic development. The figure of groundwater use presented here is probably under-estimated due to much private abstraction is out of the data list. However, considering current exploitation techniques and the cost for extracting groundwater from a maximum aquifer depth of 350 m below surface, the usable groundwater storage in the TMG rocks is estimated as $2.1 \times 10^9 \text{ m}^3$ (Jia, 2007), which implies that there is still a big gap for groundwater development in the TMG Aquifer.

There are more than 30 major users of groundwater, among them numerous towns are completely dependent on the TMG aquifer as their sole source of water supply, such as Steytlerville, Jeffreys Bay, St Francis Bay and Humansdorp in the east, Bredasdorp, Nepier, Struisbaai and Botrivier in the south and Lamberts Bay, Leopoldville and Graafwater in the west; and many other towns are partially dependent on the TMG groundwater during the dry season. From Table 2-2, it is clear that the present utilization of the TMG aquifers mostly exists in such areas where it has been developed; this hints at the great potential taking into the estimated water stored in the aquifers account. Table 2-2 also shows that 67.9% of groundwater abstracted from the fractured rock aquifers in the TMG is used for farmland irrigation, 20.0% of thermal water for holiday resorts, and only 12.1% is used for municipalities. Other minor users are the smaller scale farmers, homesteads and stock farms. Groundwater extraction covers a wide area but is localized and focused on points of consumption. Abstraction of $> 0.1 \text{ Mm}^3$ per annum for these and other towns shows the strategic and economic importance of the aquifer.

Table 2-2 Groundwater abstraction from the TMG aquifers
(After Meyer, 1998, 1999, 2001, 2002)

Area/Town	Water abstraction ($\times 10^6 \text{m}^3$)		Use	Year
	Amount	Percentage		
Albertinia	0.1	0.18%	Town	1999
Brandvlei-Sandrift	11.0	19.66%	Irrigation	2001
Bredasdorp	0.5	0.89%	Town	2001
Calitzdorp	0.1	0.18%	Town	2001
Ceres basin	8.0	14.30%	Irrigation	2001
Dysselsdorp	2.3	4.11%	Town	1999
Humansdorp	1.1	1.97%	Town	1998
Jeffreys Bay	1.8	3.22%	Town	1998
St Francis Bay	0.55	0.98%	Town	1998
Struisbaai	0.3	0.54%	Town	2001
11 hot springs	11.2	20.02%	Recreation	1999
Uitenhage	5.7	10.19%	Irrigation	1998
Vanwykdorp	2.3	4.11%	Irrigation	1999
Witzenberg valley	11.0	19.66%	Irrigation	2001
Subtotal	55.59	100%		

UNIVERSITY of the
WESTERN CAPE

2.6 Wellfield and study areas in the TMG

Prior to the late 1980's, early 1990's, large-scale abstractions in the TMG aquifers were restricted to Hex, Ceres, Breede, and Agter Witzenberg Valleys and small-scale municipal use by the towns along the coastal and inland outcrop areas. The more recently important developments of explorations and exploitations by means of TMG wellfields were Klein Karoo Rural Water Supply Scheme commenced in 1987, Boschklouf near Citrusdal in 1997/98, Hermanus in 2001/02, Koo Valley in 2002/03, and Cape Municipality being under way.

Previous studies on the groundwater resource in the TMG concentrate on the development of wellfields for water supply in the areas of Western and Eastern Cape provinces (Fig.2-15). The Klein Karoo Rural Water Supply Scheme, commissioned in 1987, was initiated for the water supply with a design yield of 4.7 million m^3/a from two wellfield areas, an Eastern Wellfield near Dysselsdorp and a Western Wellfield near Calitzdorp. Borehole monitoring has shown that the capacity of the scheme is only closer to 1.3 million m^3/a . The earlier

overestimation was a result of poor understanding of the hydrogeological setting and incorrect analysis of pumping test data from which the hydraulic properties of the aquifers were overestimated (Jolly, 2002). The scheme has also been followed by problems of iron bacteria formation in the boreholes developed in the Nardouw formations, which has led to clogging of screens and the need for continual rehabilitation of boreholes. As a result, the yield of Calitzdorp Wellfield has declined to a trickle.

The development of the wellfield at Boschklouf near Citrusdal in 1997~1998 triggered the full-scale groundwater research over the TMG area. Five boreholes with very high (one with $Q > 100$ l/s) flow yields, developed in the Peninsula formation near the intersection of two faults, were expected to provide a large quantity of water to meet the need of irrigation and municipality of Citrusdal. However, results from the evaluation of the pumping test data suggests that the long term sustainable yield of the wellfield is only 25 l/s and there exist a mutual interference among the boreholes and influence from a nearby river as the distance between the proposed production boreholes and the river is less than 80 m. These boreholes have only been used intermittently by the municipality in order to keep a relatively small drop of water levels.

A more recent development of the TMG wellfields is a water supply scheme in the Koo Valley, in the north of Robertson and West of Montague. This water scheme was initiated in response to a period of drought in the area and a subsequent shortage of irrigation water for the farmlands in Koo Valley. In order to have a sound estimate of sustainable yield in the wellfield, twenty-three exploration boreholes were drilled in 2002/2003. A sustainable yield of ~60 l/s estimated roughly through very few successful borehole pumping tests. However, subsequent groundwater abstraction and monitoring results show that this amount of water supply has also been overestimated, probably due to the overestimation of both hydraulic properties and recharge rate of the sandstone aquifer in the semiarid Klein Karoo area. These boreholes mostly only tap the Nardouw formations.

The biggest potential wellfield development in the TMG Aquifer is taking place in the mountains to the east of Cape Town. This project is intended to develop a pilot wellfield to a yearly water supply of ca. 3.5 million m^3 Cape Town Municipality. Yields of 100 l/s or 3.2 Mm^3/a have been proposed for some production boreholes with a total depth of over 1000 m. The investigation is being carried out for the City of Cape Town to see if the groundwater of the TMG aquifers can provide a significant supply to help alleviate future shortages in the Cape Municipality. The aim of this study is not only to develop a wellfield for bulk water supply, but also to see the potential ecological impact of large-scale groundwater abstraction

from high yielding boreholes/wellfields. It was originally proposed that only confined areas of the TMG Aquifer be exploited, i.e. where the Peninsula Formation is confined by the overlying Pakhuis and Cedarburg formations. However, this has apparently proved to be more difficult than originally thought and may not be feasible.

In 2003, Water Resource Commission (WRC) of South Africa launched a project – Flow Conceptualization and Storage Determination in the Table Mountain Group (TMG) Aquifer System - aimed at studying the properties and elements of the aquifer system, and groundwater resources in the area. By means of aquifer identification and conceptualization, the objective of the project is to determine groundwater storage and circulation, in which the estimation of aquifer hydraulic properties is a key aspect in this regard.

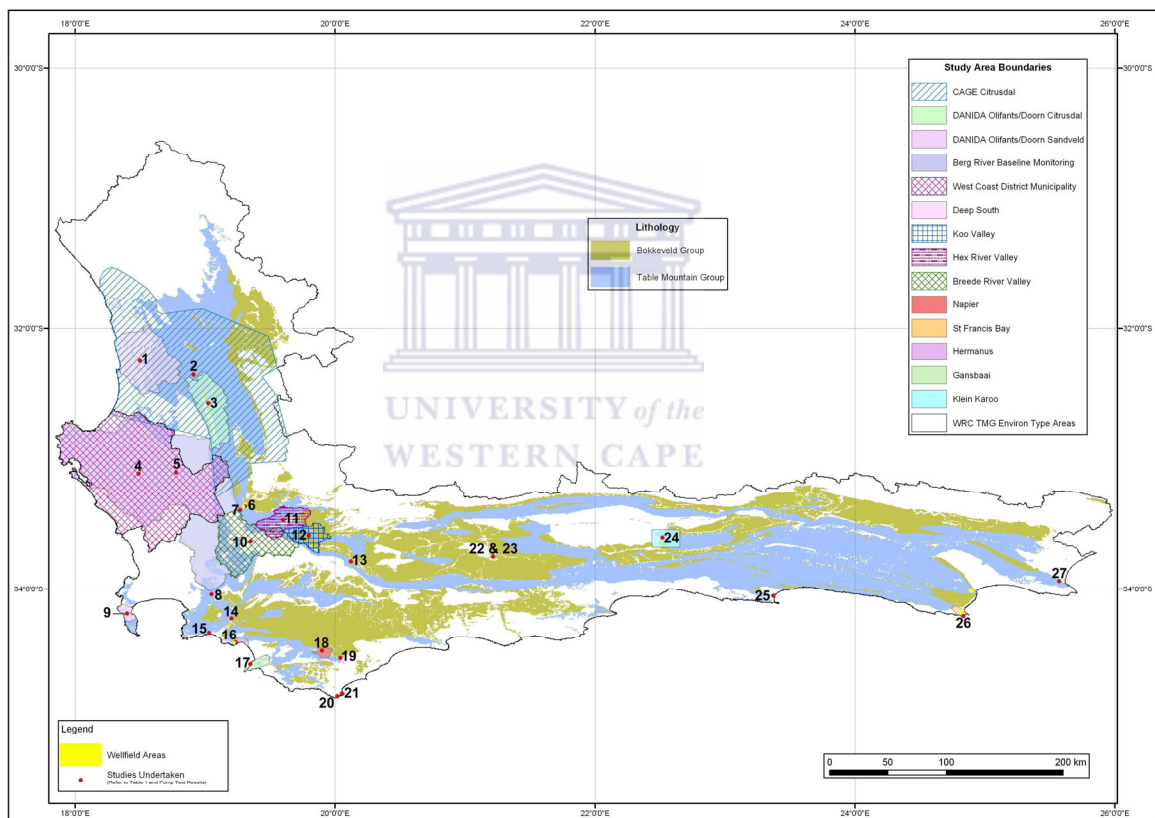


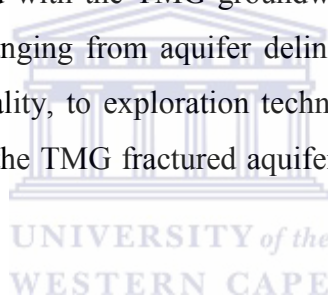
Fig. 2-15 Groundwater wellfields developed in the TMG

2.7 Summary

On a regional scale, the TMG Aquifer is both a heterogeneous and anisotropic entity, and a fractured rock aquifer system with unique features as regarding its stratigraphy, structure, and geomorphology. It is compartmentalized into various hydrogeological units, bounded by large faults, lithologies, and topographies. Various-scale TMG aquifers are the fortuitous

combination of lithologic, tectonic and climatic features. The establishment of hydrogeological units, associated subunits, and the analysis of aquifer types provide a regional view of the aquifer system and boundary conditions in the vast area, in which each unit has relatively independent properties of groundwater storage and circulation. The discussion of the TMG aquifer type raises the necessity of the aquifer media study, especially the study of fractured media which shows prominence in controlling groundwater of the TMG aquifers.

The TMG Aquifer has been exploited to a large degree throughout its extent from the west in the Sandveld and Citrusdal area, through the south and east in the Hex River and Koo valley, to the Klein Karoo and Uitenhage. With exception of thermal artesian flow, large part of the aquifer storage is still technically unavailable. The development of wellfields is economically important to alleviate the problem of water shortage in these regions, but must be carefully managed for sustainable utilization of the natural resources in a long term. Relevant researches associated with the TMG groundwater development have fully covered the fields of hydrogeology, ranging from aquifer delineation, resource potential evaluation, groundwater recharge and quality, to exploration techniques (Pieterse and Parsons, 2002). Groundwater development in the TMG fractured aquifers have yielded lot of information for the further research.



Chapter 3

Aquifer media

3.1 Introduction

On a regional scale, the TMG Aquifer is a heterogeneous and anisotropic entity, but in most cases it can be regarded as homogeneous and anisotropic on a local scale. Thin section studies have proven that even in pure quartzitic sandstones from unfolded beds of the TMG, intergranular pore spaces are completely filled by secondary quartz overgrowths, making these host rocks nearly impermeable (Hälbich and Cornell, 1983; De Beer, 2002). It is only where they are fractured by folding, and/or faulting that the rocks develop a secondary porosity and become fractured aquifer media. This point is also supported by the thin section analysis of sandstone samples from both Peninsula formation and Nardouw formations in this study.

Fractures are referred to as joints and faults, as well as varied discontinuities over different scales and lithologies due to crustal tectonic driving forces (Pollard and Aydin, 1988). They could act as groundwater conduits or as barriers to groundwater flow relative to shallow and deep flow. The analysis of the TMG aquifer types in Chapter 2 provides a regional view of the aquifer fabrics and possible groundwater flow paths in which the aquifer media are generally homogeneous and isotropic. However, different from porous media such as the Quaternary deposits on the coast and river valleys, the indurated TMG rocks are extremely anisotropic.

Current methods used for analyzing groundwater flow and storage in fractured rocks are based on the assumption that groundwater flows through a geological continuum (Wang et al, 2002). These methods are generally applicable to porous media, but have limited applicability when groundwater is governed by highly anisotropic fractures or fracture network. Field observations show that there is almost no a uniform groundwater level from site to site. This suggests that water levels and associated maps are not anymore capable of characterizing a meso- to large-scale flow. Even in a single wellfield at the scale of hundred meters, the groundwater in boreholes does not completely communicate one another, such as the Malkoppaan site of Lambert's bay and the Gevonden site of Rawsonville where some of nearby monitoring boreholes do not respond to the water level drop at the pumping holes. In fact, groundwater occurring in fractured rocks like the TMG sandstones is mainly flowing

through the fractures, controlled by the fracture geometry and associated hydraulic properties. In the absence of fracture information, it is extremely difficult to have a better understanding on the aquifer response to hydraulic tests and perform an analysis on the related aquifer properties. It is hence of hydrogeological significance to study the properties of the fractured media.

Currently, among the hydrogeological problems faced in the TMG fractured rock aquifers, none is as challenging as the establishment of conceptual model through the characterization of aquifer media. The study of such problem is limited in the TMG because of its regional and local complexity, though many efforts have been contributed to the investigation of the characteristics and patterns of the fractures that exert a great impact on aquifer properties (Chevallier, 1999; Woodfords and Chevallier, 2002, Hartnady and Hey, 2002a).

Based on previous studies and current research, in this chapter, the characterization of the TMG fractured media on regional and local scales is to be done using remote sensing interpretation, core sample study, and analysis of fracture field measurement data, intending to develop an initial conceptual model that is expected to be helpful for a better understanding of the TMG fractured rocks and can be applied to and in turn be refined by the quantification of aquifer properties. In addition, the study of aquifer media should include the delineation of aquifer types for which one can refer to the Section 2.4 in Chapter 2.

3.2 Fault

It is well acknowledged that fault to a large extent plays a key role in the occurrence of groundwater in the TMG sandstones. So far, almost all the major wellfields for water supply schemes in the TMG area are developed in the vicinity of fault zones, such as Vermaaks River (Kotze, 2002), Boschkloof (Hartnady & Hay, 2002b), St Francis Bay (Rosewarne, 1993a), Ceres (Rosewarne, 1993b), and so on. Where the faults intersect the regionally oriented structure they may become a preferred locality for the production boreholes. This suggested that the secondary splays of regional faults are currently major zones for groundwater targeting.

However, through field investigation to the Vermaaks River fault, Hälbich and Greef (1995) found that there were hard breccias and cataclases widely developed in both of the 9km long fault and its secondary splays. In Eastern Cape the Coega Fault cutting southeastward through the Uitenhage artesian basin results in separating the basin into two different groundwater

systems (Maclear, 2001). In fact, most of fault zones developed in the TMG sandstones and siltstones are evidenced to be lithified and act as aquicludes (Newton et al., 2006), such as Klein Bavaria fault in the north of Plettenberg Bay, Brandvlei – Eikenhofdam fault, and Kango fault etc.

Of particular interest of borehole siting for groundwater development is the architecture of faults which could have a big effect on the mode of groundwater occurrence. Generally, to distinguish from the country rocks, the elements of a fault include fault core and fracture zones at both walls (Ciane et al., 1996). Current state of a fault is the result of geological processes; especially neotectonic activities might have an additional impact on the fault fabrics. However detailed information of neotectonics is yet not available except some evidences show that the area has undergone a relatively low magnitude of fault reactivation, for instance, evidenced by earthquake events in the western and southern branches of the Cape Fold Belt. Fig.3-1 presents the conceptual models of the fault possibly occur in the TMG area regardless of the mode of faults, in which there are four types of fault architecture. Obviously, the majority of the TMG faults fall in category **d)** where the fault cores are largely recemented and often serve as groundwater barriers (Fig.3-1e), whilst the fracture zones act as the conduits. This sheds light on localized groundwater targeting, but more detailed work needs to be done for a better understanding of the megafaults, such as the Worcestor and Cango Faults which are apparently related to the occurrence of thermal springs in the Cape Fold Belt.

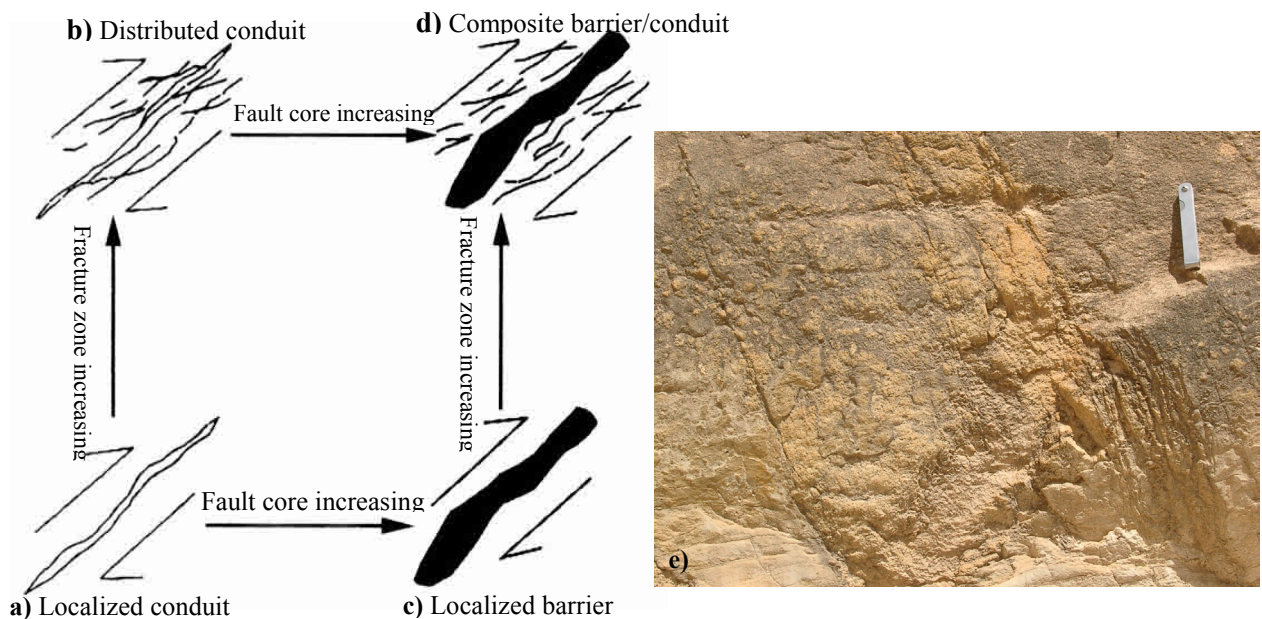


Fig. 3-2 Models of fault showing the evolution of fault architecture (After Ciane et al., 1996).
 e) Breccias constituting fault core material in very common in the TMG area.

3.3 Classification of fractures

The classification of fractures is conventionally based on the mode of rock deformation or displacement that represents a broad mechanical classification (Pollard and Aydin, 1988; National Research Council, 1996):

- i) Dilatant fractures;
- ii) Compaction fractures; and
- iii) Shear fractures/faults.

To designate the TMG fractures into the above classes, one must have not only the data of a single fracture as abovementioned but the analyses of fracture networks such as termination, hierarchy, and connectivity as well. In this study, it was extremely difficult to collect these data to identify the modes of such structures on the surface or in the hole, although the aerial and satellite imagery have been used to interpret the fractures and fracture networks, since most of the area are covered by weathered materials. However, geological structures of the TMG in the Cape Fold Belt have been developed and modified by multistages of tectonics. The development of these fractures is summarized in Fig.3-2, which may help to explain the complexity of the fracture system in the study area. On one hand, the structures have been developed by multistage tectonic events and modified by later morphogenetical processes resulting in both various types of folds/faults and specific fracture systems in the TMG areas.

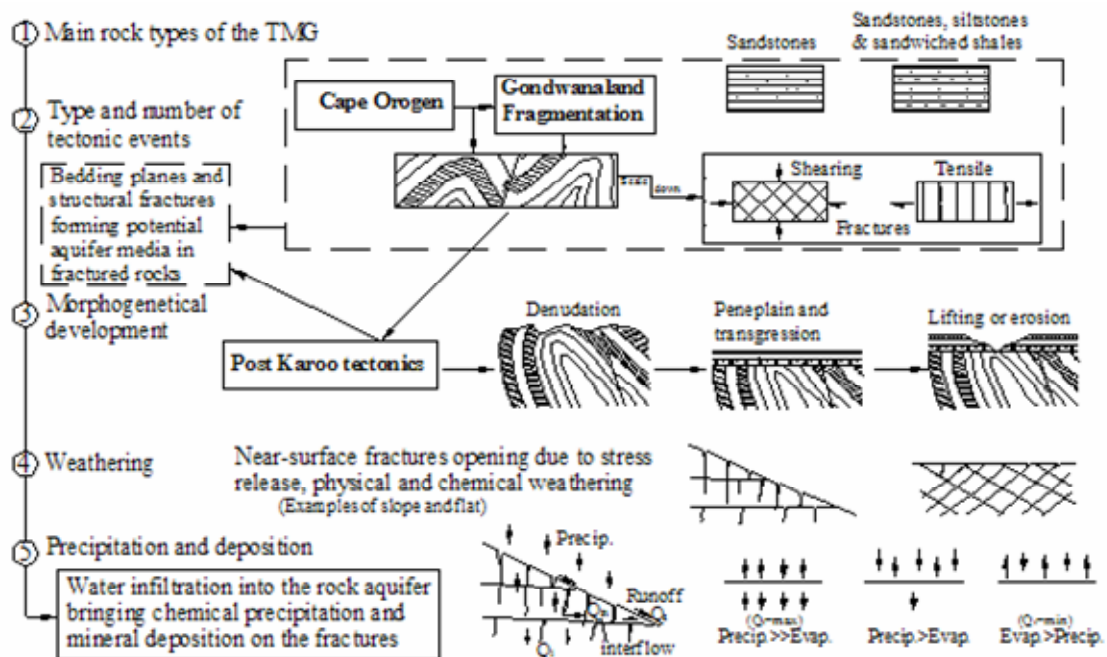


Fig. 3-3 Factors impacting on the development of the fracture systems in the TMG sandstone formations (modified from Ewer, 1985)

On the other hand, the infiltration of meteoric water and precipitation of secondary minerals on the fracture walls tend to complicate the properties of the fractures. As the current state of the fracture network has resulted from long-term geologic processes, the most concerned property is the percentage of open fractures where groundwater could be stored and the interconnectivity of the open fractures where flow could take place.

Thus the classification of fractures as the **open** or the **closed** may have more hydrogeological meaning to the study of a fractured rock aquifer if it is realized that open fractures are a precondition for groundwater flow in the aquifers.

3.4 Core sample study – a case at Rietfontein deep borehole

There are many approaches to study open fractures and their interconnectivity such as borehole image scanning, borehole radar, injection and tracer tests, and so forth. Often core logging is unable to directly sort out the features of open fractures due to the deformation of many core samples by stress release and disturbance during drilling. But the topography and the mineral fillings/coatings of the core fractures may help to distinguish some susceptible zones of open fractures. Moreover, it is expected that fracture scanning from the core samples can yield useful information for the characterization of fracture network that has a direct effect on groundwater flow. For this reason, a case study was done at the Rietfontein wellfield in the Sandveld area, where a deep borehole was drilled to a depth of 800 m. In this study, the characteristics of the fracturing in the rock aquifer around a deep borehole in the TMG are examined and analyzed, using surface fracture measurements and core sample data. Information on fractures and fracture coatings was collected and analyzed by scanning borehole cores. The main objective is to provide a qualitative insight into the fracture characteristics and associated hydrogeological conditions by assessing fracture spatial correlation and precipitation of secondary minerals on the fracture walls. The main results of this case study have been published and please refer to Lin et al (2007).

3.4.1 Introduction to site hydrogeology

The site is located at the farm Rietfontein, 10 km west of Graafwater, Western Cape (Fig. 3-3). Borehole G40145 was drilled between 1998 and 2001 to a depth of 800 m and screened to a depth of 168 m. It is the deepest of about 25,000 holes in the TMG area. The borehole passes through the Piekenierskloof Formation, the basal formation of the TMG, from 0 to 754 m depth and Precambrian metamorphic basement rocks for the remaining depth. During the drilling process, core samples were carefully collected for further analysis; traditional

downhole geophysical tests such as vertical electrical resistivity (VER), gamma (NN log), and rock density logs were completed to 380m below the surface, in an attempt to identify the lithologies and fracture zones and to establish a conceptual framework for the hydrogeology in the vicinity of the borehole (Titus et al. 2002).

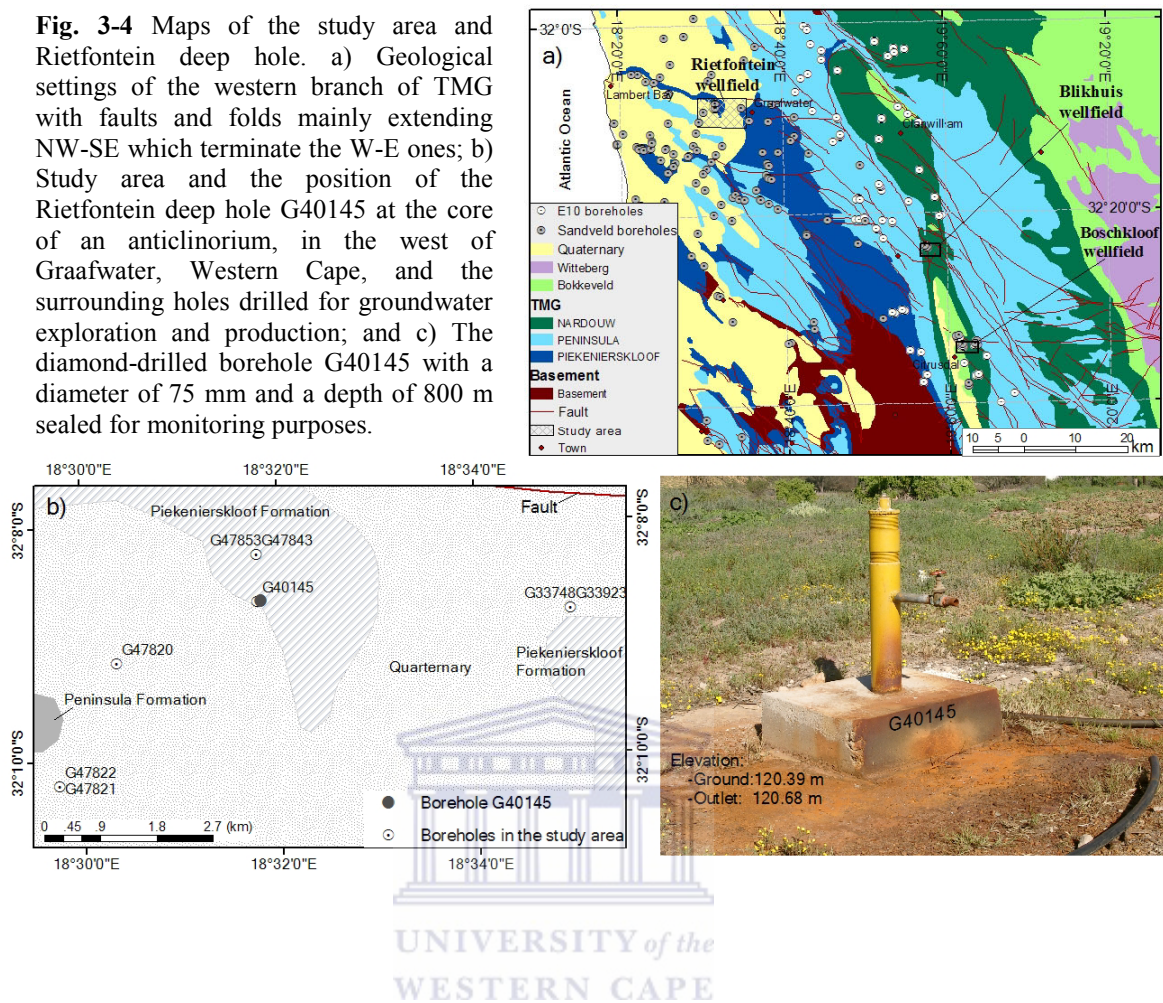
The Piekenierskloof Formation in the study area represents alluvial-fan and braided-river complexes deposited on uneven bedrock topography created during the folding and lifting of Neoproterozoic Pan-African mountain belts along the west coast prior to 500×10^6 years ago. The lithology is characterized by mottled sublitharenites and quartzarenites, with a 100m thick conglomerate at the base, followed by sandstones and siltstones; altogether the thickness of the Piekenierskloof Formation is 800 m. It is also characterized by minor sandwiched iron-rich shales which affect the groundwater quality in terms of color and smell. The basement rocks are slightly sulphur-bearing metamorphic rocks.

During the drilling of borehole G40145 (Fig. 3-3b and c), an initial artesian flow of 0.3 l/s was identified from three intervals (about 170 m, 210 m and 380 m below surface). Water samples have been collected monthly for both in-situ and laboratory analyses since April 1999. The average water temperature is 20.8°C. Electrical conductivity (EC) has varied between 1350 and 2560 $\mu\text{S}/\text{cm}$, pH between 5.7 and 6.8, and the artesian flow yield has dropped drastically from 0.33 l/s to 0.01 l/s in only two years probably because of large water abstractions from surrounding boreholes. The groundwater is sodium-chloride dominant with an average of 82% Na-Cl content (283.80 mg/l as Na, 534.34 mg/l as Cl) and with an absence of carbonate (Table 3-1). The major chemical constituents have changed over time with iron and sulphate having the most significant changes. Similar to most of TMG groundwaters (Smart and Tredoux 2002), this borehole water is ferruginous with a dissolved iron content within 0.1~1.2 mg/l. The presence of iron gives an undesirable reddish color to the borehole surroundings due to the precipitation of $\text{Fe}(\text{OH})_3$ from the hole overflows (Fig. 3-3c).

Table 3-1 Principal chemical constituents of the groundwater from G40145 for representative months

Sampling date	Chemical content (mg/l)							
	Na ⁺	Ca ²⁺	Mg ²⁺	Si ⁴⁺	K ⁺	Cl ⁻	SO ₄ ²⁻	NO ₃ ⁻
2000-8-25	298.98	29.59	34.75	5.03	10.84	556.82	37.59	0.04
2001-9-7	284.41	49.40	22.00	5.06	10.26	559.99	14.32	0.04
2003-11-17	268.00	25.30	29.43	3.84	7.93	486.21	6.00	0.11
	F ⁻	PO ₄ ³⁻	Fe ²⁺	Mn ²⁺	Zn ²⁺	Cu ²⁺	Cd ²⁺	As ³⁺
2000-8-25	0.28	0.03	1.18	2.00	0.004	0.002	0.002	0.05
2001-9-7	0.25		0.88	1.96				
2003-11-17	0.26	0.02	0.06	2.53	0.014	0.044	0.009	0.13

Fig. 3-4 Maps of the study area and Rietfontein deep hole. a) Geological settings of the western branch of TMG with faults and folds mainly extending NW-SE which terminate the W-E ones; b) Study area and the position of the Rietfontein deep hole G40145 at the core of an anticlinorium, in the west of Graafwater, Western Cape, and the surrounding holes drilled for groundwater exploration and production; and c) The diamond-drilled borehole G40145 with a diameter of 75 mm and a depth of 800 m sealed for monitoring purposes.



3.4.2 Fracture geometry

3.4.2.1 Fractures from surface measurement

Borehole G40145 is situated at the core of an anticline extending to the northwest (see Fig. 3-3b). In order to study the effect of fractures on borehole hydrogeological conditions, it was necessary to determine the surface characteristics of the fractures in the vicinity of the deep hole. The measurement of fractures was carried out within an area of about $90 \times 60 \text{ m}^2$ using a line scanning method which is roughly perpendicular to structural lines. The measured elements mainly included orientation, distance, aperture and roughness; and some of the fracture lengths were also traced. The fracture lengths traced range from 0.8 m to 20 m whilst the apertures have a wide range of 0.1 to 2 mm due to the effects of weathering. With respect to fracture orientations, Fig. 3-4 shows the spatial variation of the orientation and density of 289 measured fractures composed of bedding planes and steep structural fractures. According to the field measurements, the bedding planes trend to the NE from 50° to 90° with gently-

dipping angles of 2° to 10°, while three sets of steep fractures were identified having average trends of N67E (67° east of north), S25W and S23E with the average dips of 78°, 71° and 77°, respectively.

3.4.2.2 Fracture from core logging

In general, downhole geophysical data are useful for interpreting the variation of lithologies. But they can be inaccurate or even inapplicable for identifying fractures and associated properties at depth. Hence, it was necessary to re-scan and re-log the core samples to sort out the fractures developed in the lithologies of the Piekenierskloof Formation, especially when borehole image techniques were not applied during the drilling.

Fig. 3-5 illustrates 4 typical core sections, at the given depth intervals, to represent what the rocks of the

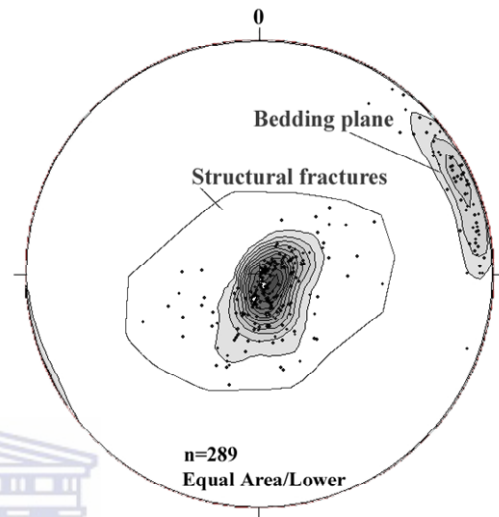


Fig. 3-5 Spatial correlation and distribution of the fractures measured at Rietfontein, in which the solid circles represent normals to the fractures, the density ranging from 0 to 27.85 with a contour interval of 2.7, and the area of the small circle for density grid cell is 1% of the diagram area.

Piekenierskloof Formation look like, the basic types of fractures, and the mineral fillings and coatings on the fracture surfaces. The fractures observed in the core are sub-horizontal bedding and steep structural fractures which is similar to the fractures present on the surface. Regardless of the dip direction, the dip angles of both bedding fractures (1°~12°) and steep structural fractures (60°~85°) from the top to the bottom of the hole are compatible with those observed on the surface.

Geometrically, the core fractures are not evenly straight but rough or undulating and have been potentially deformed during drilling. For this reason, drill-induced fractures should be excluded in the process of core logging. With respect to fracture shape and assemblage, 5 types of common patterns were delineated from the core sections (Fig. 3-6):

- a) Bedding and steep fractures crossing each other is commonly developed in the brittle hard sandstones.
- b) Bedding (planes) fractures are dominant in most shale and other thin layers.
- c) Vertical and sub-vertical fractures intersecting bedding fractures.

- d) A complex of bedding and steep fractures intersecting with a few terminations.
- e) Intersection and termination of sub-vertical fractures.

The assemblage patterns in Fig.3-6a, c and d roughly represent the well-connected fractures developed in sandstones, while Fig.3-6b and e indicate the poorly connected fractures in shales and some sandstones/siltstones. From the topography and coating of the core fractures, generally, steep fractures are more likely to be open than other types. Bedding fractures developed in shales and other thin layers are mostly closed except for those at sandstone/shale contact zones.

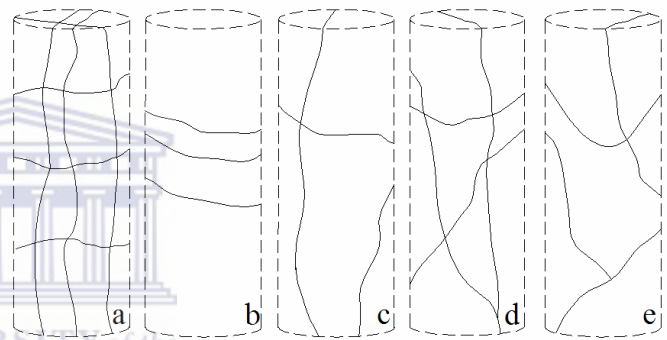
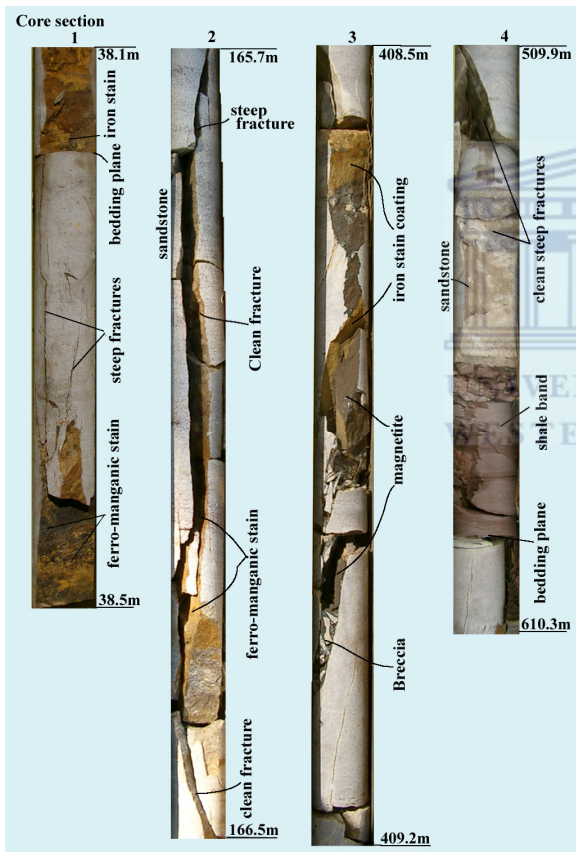


Fig. 3-5 Typical core sections from borehole G40145 at various depths ranges from the top to the bottom of the hole, showing not only lithology, but also fracture coatings. Most of the coatings on the fracture surfaces are iron and manganese stains (section 1, 2 3), while the magnetite occurs as vein material. Note that the steep fracture in section 3 is partially coated and partially clean, and a clean fracture surface is shown in section 4.

Fig. 3-6 Types of fractures observed in the core from G40145 with respect to fracture shape and assemblage (please refer to the text for an explanation of a to e).

3.4.2.3 Fracture density at depth

Besides the above analyses, fractures are also characterized by density or intensity, which are often compared with lithologic logs, and the result of geophysical investigation and hydraulic conductivity estimation. The density of fracturing in fractures/cm was computed for all the fractures - bedding and structural fractures - observed between core depth tags without regard

to the fracture orientation, fracture mode, and rock type. A frequency plot of 7242 fractures, observed with a logging interval of 2~6 m, following the intervals of core tags from the top cut-off at 14m depth to the bottom at 785m depth, is shown in Fig.3-7. The core of TMG rocks ends at a depth of 754 m below surface. This plot, with an average density value of 0.114, shows that the density of fractures gently decreases with depth. In comparison with traditional frequency distributions, it has very weak spatial correlations, for the linear correlation coefficients between the fracture density and depth are 0.28, 0.33 and 0.16 with respect to linear, exponential and power distributions, respectively.

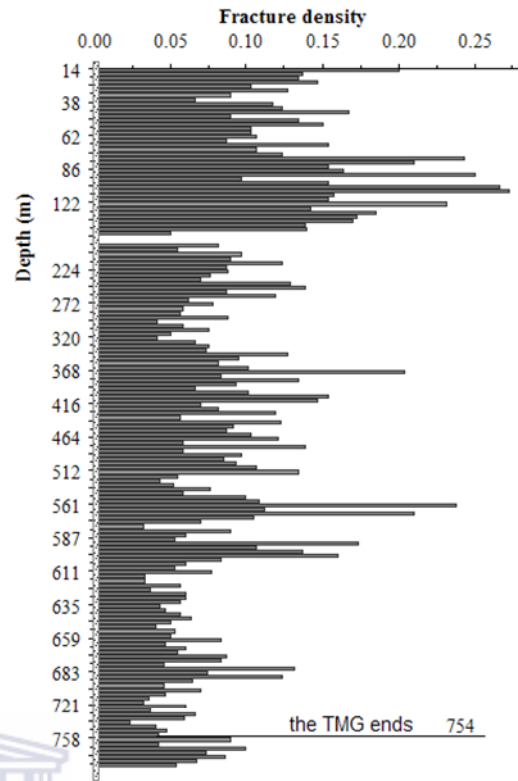


Fig. 3-7 Fracture density (fractures/cm) plot versus the depth of borehole G40145, computed at borehole depth intervals of 2~6 m except for the depths of 170~187 m due to core missing (Lin et al, 2007)

Snow (1968) points out that fracture spacing increases with depth, while aperture decreases.

Although the density generally decreases with depth and 33% of fractures are concentrated in the top 160-m portion of this borehole, fractures are not substantially depleted with depth in the sandstone predominant portion. The general shape of the density plot is an undulating pattern where relatively highly fractured zones are located in the depth ranges of 70~125 m, 344~410 m, 560~598 m, and 668~697 m. However, these highly fractured zones or the logging intervals of higher densities are not consistent with the positions of conductive zones which are open to the groundwater flow into the borehole.

3.4.3 Hydraulically active fracture

As shown in Fig.3-2, the processes of mineral filling and coating in a fracture network due to physical or chemical precipitation, and deposition due to groundwater circulation tend to change the nature of fracture walls. However these processes take place underground are extremely complicated and difficult to be detected directly. In general, coating materials may occur where the fractures are relatively open to flow, whereas fluid diffusion preferably happens at a state of comparatively stagnant water from which the chemical and physical precipitates tend to clog the potential flow path, leaving few fracture to be competent. The

cognition of such processes is resulted from the examination of core samples collect from the TMG rocks, especially those from fault zones. Thus it is necessary to have an investigation into the hydraulically active fractures via the study of coating materials. The relationship between fracture filling/coating and hydraulically active fracture or flow path is barely studied in the TMG sandstones. A notable work was done by Paces et al.(1996) who focused on the analysis of fracture coating data in a tunnel in the unsaturated zone of Yucca Mountain, USA. A hydraulically active fracture as used here refers to a fracture open to flow both in the past and present. Thus it represents the maximum number of fractures currently open to groundwater flow.

The groundwater from borehole G40145 is weakly acidic, ferruginous, manganiferous and is also characterized by the absence of carbonates. The anions are mainly Cl^- , SO_4^{2-} and NO_3^- (Table 3-1). The cations such as Fe^{2+} , Mn^{2+} , Ca^{2+} , Mg^{2+} and Zn^{2+} are prone to precipitation as hydroxides through hydration during migration in this weakly acidic and oxidized environment and form the majority of the fracture fillings/coatings. This environment also provides desirable conditions for iron bacteria to establish themselves and create a reddish-brown ferric hydroxide ($\text{Fe}_2\text{O}_3 \cdot n\text{H}_2\text{O}$) precipitate.

Petrographic evidence suggests that most of the iron that now resides in oxidized authigenic phases was derived from solutes mobilized through dissolution of older iron-bearing authigenic minerals, particularly from the iron-rich shales. The presence of the secondary minerals in the form of fracture coatings consequently provides an indicator of hydraulically active fractures.

For the fractures in between the core depth tags of borehole G40145, both total fracture length and the length with coatings were counted, while the length of a whole or a portion of a single fracture was counted as well to collect the fracture coating data. Most of the coatings are fixed on fracture surfaces. Unfortunately, the fracture coatings are too thin to sample, but they can be divided into 4 categories based on their physical features such as color, smell, and fabric as the followings:

- a) Reddish-brown and loose iron and manganese stains which are mainly limonite and less frequently hematite, with minor manganese stain;
- b) Dark reddish and hard magnetite;
- c) Gray sporadic thin clay minerals marked by pyrophyllite deposits;
- d) Pyrite crystals.

Type-a) coatings occur on the surfaces of fractures with little or no diffusion into the matrix rocks, implying that the groundwater in the rock aquifer was not stagnant. It is also

obvious that the coating materials such as limonite and hematite have been transported and precipitated due to past or current groundwater flow; and that these coating materials are in turn indicative of hydraulically active fractures, and to a large extent groundwater flow has been mostly confined to the space where these fractures dominate. However, the other three types of coatings are not definitely related to flow. In particular, the sporadically deposited pyrophyllite and magnetite were probably formed under great pressure and temperature (Velde, 1984) where the fractures can be regarded as clean or closed to hydraulic activity. Pyrite crystals only occur at the very bottom of the hole, and may be attributed to the original fluid intruding from the sulphur-bearing basement rocks.

In order to characterize the spatial variation of the fracture coatings, a line-scan technique is used first to compute the intensity of the coatings. Similar to the statistics of fracture density, the intensity of fracture coatings is expressed as the ratio of fracture length with coatings to the total fracture length in between core depth tags. Then plotting the intensity data against borehole depth, the downward distribution of hydraulically active fractures is presented. On average, 23.3% of the fractures are occupied by different types of coatings in the depth range of 14 to 800 m (Fig. 3-8). In the relatively shallow zone above a depth of 125 m, the number of hydraulically active fractures increases with depth with a maximum coating intensity of 0.9 at 122 m. Below 125 m, the number decreases and by 570 m hydraulically active fractures are absent. In particular, about 99% of hydraulically active fractures occupied by ferromanganese coatings are less than 400 m deep, while the most active ones are located between 85 and 135m depth. At depths of less than 145 m, fracture coatings are mostly composed of ferromanganese substances both in gently-dipping bedding planes and steep structural fractures, but the coatings in steep fractures become predominant below that depth (Fig.3-8a).

Using the spatial variation and types of coatings to determine the degree to which fractures are hydraulically active, four zones are recognized as follows:

- i) 0~150 m – High;
- ii) 150~400 m – Medium;
- iii)400~570 m – Low;
- iv)570~800 m (or deeper) – hydraulically inactive fractures.

In this case, the relations of borehole depth with fracture types and coating types provide a statistical basis for determining the degree of hydraulically active fractures and its hydrogeological implication. As a result, it is concluded that:

- i) Groundwater flow is controlled by both gentle-dip bedding planes and steep fractures in the near-surface zone above 150 m, but is dominated by steep fractures in the deeper part of the aquifer below 150 m depth.
- ii) The majority of groundwater flow occurs above 400 m depth and tends towards zero below that depth.
- iii) No groundwater flow could take place below 570 m depth in the study area and adjacent areas of the TMG fractured rock aquifers with an analogous assemblage of structure and lithology.

Based on the above analyses, the depth model of groundwater circulation is not necessarily applicable to all areas of the TMG rock aquifers in respect of proposed borehole planning. It may be extrapolated to analogous areas with a similar assemblage of structure and lithology. In terms of groundwater protection zoning and numerical flow modeling of the TMG area, the model may help to explain the properties of the fractured rock aquifers in general and to establish the conceptual model considering the lower limit of aquifer depth in particular.

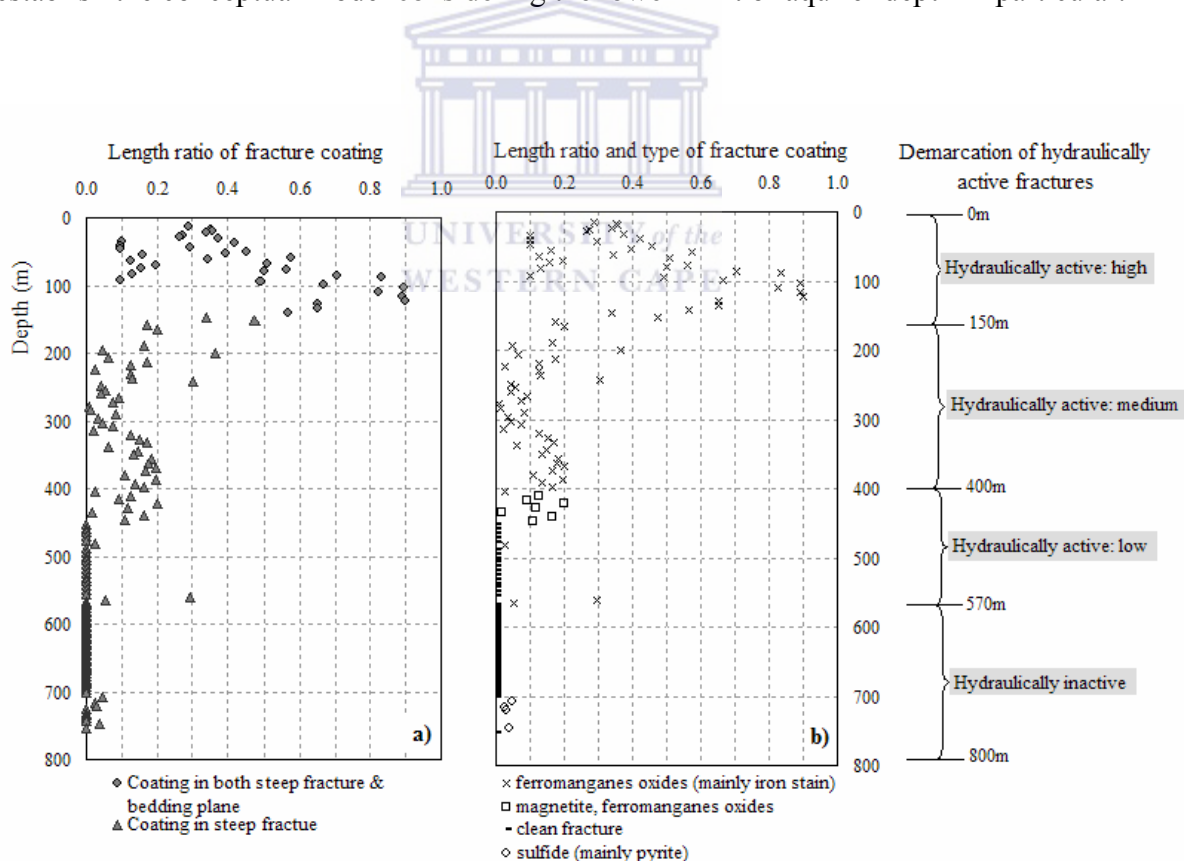


Fig. 3-8 Types and variations of fracture coatings at borehole G40145 from 14 m below surface, showing the distribution of hydraulically active fractures which have become absent from a depth of about 600 m. a) Fracture coatings distinguished in both bedding and steep fractures; b) The distribution of different types of fracture coatings with depth (Lin, et al, 2007)

3.4.4 Implication of the hydraulically active fractures

The analyses of fracture coatings have clearly indicated the distribution of hydraulically active fractures, although such fractures cannot be regarded as any flow paths. It can be assumed that the hydraulically active fractures represent the maximum number of currently open fractures and that most groundwater flow takes place in those interconnected open fractures. From a statistical perspective, these assumptions give a limiting state for the relation of hydraulically active fracture with currently open fractures and groundwater flow.

From the demarcation of hydraulically active fractures, it appears that groundwater flow in the study area is controlled by the fractures without regard to their orientation in the near-surface zone above 150 m, but is dominated by steep fractures in the deeper parts (below 150 m). The main reason for this is that the subhorizontal bedding fractures are more vulnerable to lithostatic pressures than the steep fractures and tend to close with increasing depth. It also appears that the majority of groundwater occurs above 400 m depth and is rarely found below 400 m depth. Furthermore, the top of the hydraulically inactive fracture zone clearly indicates that groundwater flow could not take place below a depth of about 570 m.

The main water strikes in the deep hole G40145 range from depths of 170 m to 380 m below surface, which is similar to other areas of the TMG fractured rock aquifers. In the adjacent wellfields of Boschkloof and Blikhuis (Fig. 3-3a), for example, the strongest flow yield encountered in borehole BK1 and BK4 in the Boschkloof wellfield was 100~120 l/s and 95~109 l/s at a depth of 154 m and 294 m, respectively (Hartnandy and Hay 2002b). Comparatively, the groundwater situation in a deep borehole (over 600 m in depth) at Blikhuis field is more typical, where the main water strikes are in the depth range of 345~370 m with an accumulative artesian flow of 3.35 l/s. Although another two conductive zones were found at 434~444 m and 475~485 m depths, the additional flow rate was merely 0.05 l/s and 0.3 l/s, respectively. There was no water encountered below 490 m in the Blikhuis deep hole (Hartnandy and Hay 2001c).

3.5 Application of remote sensing data

With the increasing availability of high-resolution imagery of the earth, there have been more hydrogeologists to make use of remote sensing techniques to study, on a large scale, hydrogeological conditions (Schowengerdt *et al*, 1979; Mabee *et al*, 1994; Kresic, 1995; Drury *et al*, 2001), site investigation (Sander *et al*, 1996; 1997), groundwater monitoring (Rodell and Famiglietti, 2002), and groundwater protection and resource evaluation (Koch

and Mather, 1997; Bressan and Anjos, 2003). As groundwater is not readily perceptible from remote sensing data, surface indicators have to be used to infer the subsurface condition which controls groundwater occurrence. Lineaments captured from imagery often provide a crucial clue on the interpretation and analysis of fractured rocks and associated groundwater flow regimes. The main assumption that underlies all lineament analyses is that the linear features (O'Leary *et al*, 1976; Waters *et al*, 1990), when properly identified, represent the surface manifestations of transmissive fracture framework of low permeability rocks (Degnan *et al*, 2002). Lineaments are usually characterized by azimuth and length distributions, length density (L_d , total length of lineaments per unit area), frequency (L_f , total numbers of lineaments per unit area), and intersection point density (L_c , total numbers of lineament intersection points per unit area). Preparation of lineament map is hence important for groundwater study in fractured rocks, especially when they are incorporated with other pertinent maps via GIS integration.

3.5.1 Lineament mapping

The selected areas are situated at the southern and western branches of the Cape Fold Belt, comprising a series of folds and faults extending NW-SE, NE-SW and approximately W-E. Due to the lithologies and geomorphologies, many of the TMG outcrops are well exposed as bare rocks but extremely difficult to access. This has potential to use remote sensing data to study the hydrogeological conditions on the basis of lineament analysis in the fractured rocks. As lineament analysis requires the location and distribution of lineaments that represent the fracture-correlated features, the choice of a study area should have very good rock exposures on images. Thus areas with too many or too big barren lineament windows have to be excluded. This may reduce the selectivity of available study areas, but increases the quality and consistency of lineament data interpreted. For this study, seven domain areas labeled as A1~A7 with the size ranging from 6.25~225 km² (Fig.3-9) in the southwestern TMG outcrops are screened out from many candidate ones for lineament and density map analyses.

Meaningful interpretation of lineaments that are associated with the structural framework is largely dependent on the quality of imagery, acquaintance of area background, and the approach of acquiring lineament data. In this study lineament mapping was done using Landsat ETM⁺ imagery (UTM zones: S-34-30) that covers west half of the TMG area. The existing lithostratigraphic, geomorphologic, and structural information are also used for reference during the mapping. The imagery comprises seven multi-spectral bands and one panchromatic band. It has already been linearly enhanced and projected before being loaded

up to the GIS software. In comparison with conventional aerial photography (1/50,000), the imagery has better spatial resolution which allows to trace lineaments with 65-m minimum length (approximately twice of its spatial resolution). To enhance the confidence of lineament interpretation, multiple interpreters were employed during the lineament tracing. The data from various interpreters were carefully compared and then combined to one shape file. In the mean time, each of the lineaments was identified to avoid the non-fracture-correlated lineaments as much as possible. The major problem encountered during the lineament tracing with the images was sun azimuth effect (Woodford and Chevallier, 2002) which created a bias toward northeastern striking lineaments, therefore much patience was required to identify such linear features. After the mapping of a domain area was done, each lineament length and orientation was computed for the distribution and density analyses. The mapping and statistic results of the lineaments in the seven domain areas are presented in Fig.3-9.

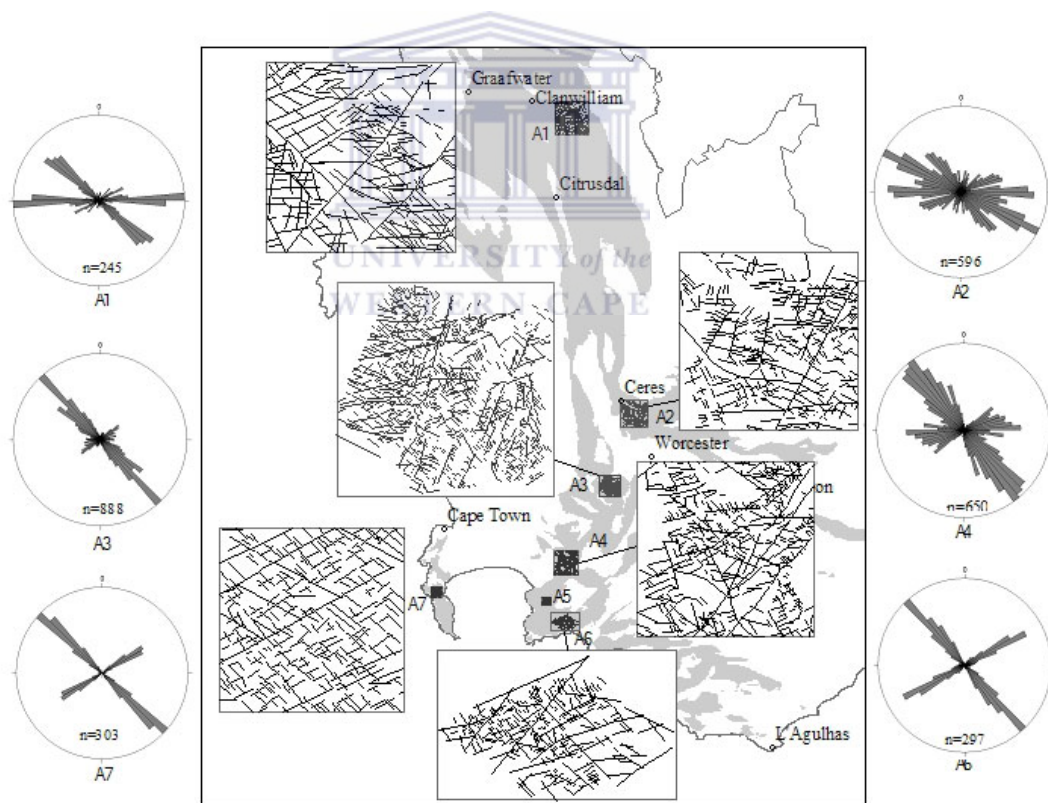


Fig.3-9 Map of the study area depicting extension of the TMG and selected domain areas for lineament analyses; seven selected for lineament study labeled from A1~A7 and their corresponding lineaments captured from satellite image and rose diagrams. The size of the areas for lineament analyses are: A1, 225 km²; A2, 144 km²; A3, 45 km²; A4, 144.5 km²; A5, 6.25 km², A6, 16 km²; and A7, 25 km².

3.5.2 Lineament analysis

Distribution patterns of lineament lengths and orientations are very useful for the study of fractured rock aquifers (Kulatilake and Panda, 2000), especially in the case where the measurement of fracture lengths and orientations on the surface is unable to yield sufficient data. A quantitative analysis was carried out to determine the distributions of lineament orientations and lengths in each domain area. Lineaments characterized by azimuth and length are computed with an exhaustive method using our Visual Basic for Application (VBA) scripts developed in ArcMap. The results of directional analysis show that there principally are three striking directions: NE-SW, NW-SE, and approximately E-W in the seven domain areas (Fig.3-9). According to the distribution of the orientations, these areas can be grouped into four categories probably representing different fracture patterns and tectonic stress conditions from the north to the south of the study area: 1) A1 in the northwest; 2) A2 in the core of structural syntax zone; 3) A3 and A4 in the middle south; and 4) A5, A6 and A7 in the southmost where the lineaments are merely striking to NE-SW and NW-SE. Moreover, the strikes of lineament closely have to a normal distribution with different orientation compartments as one of which is shown in Fig.3-10.

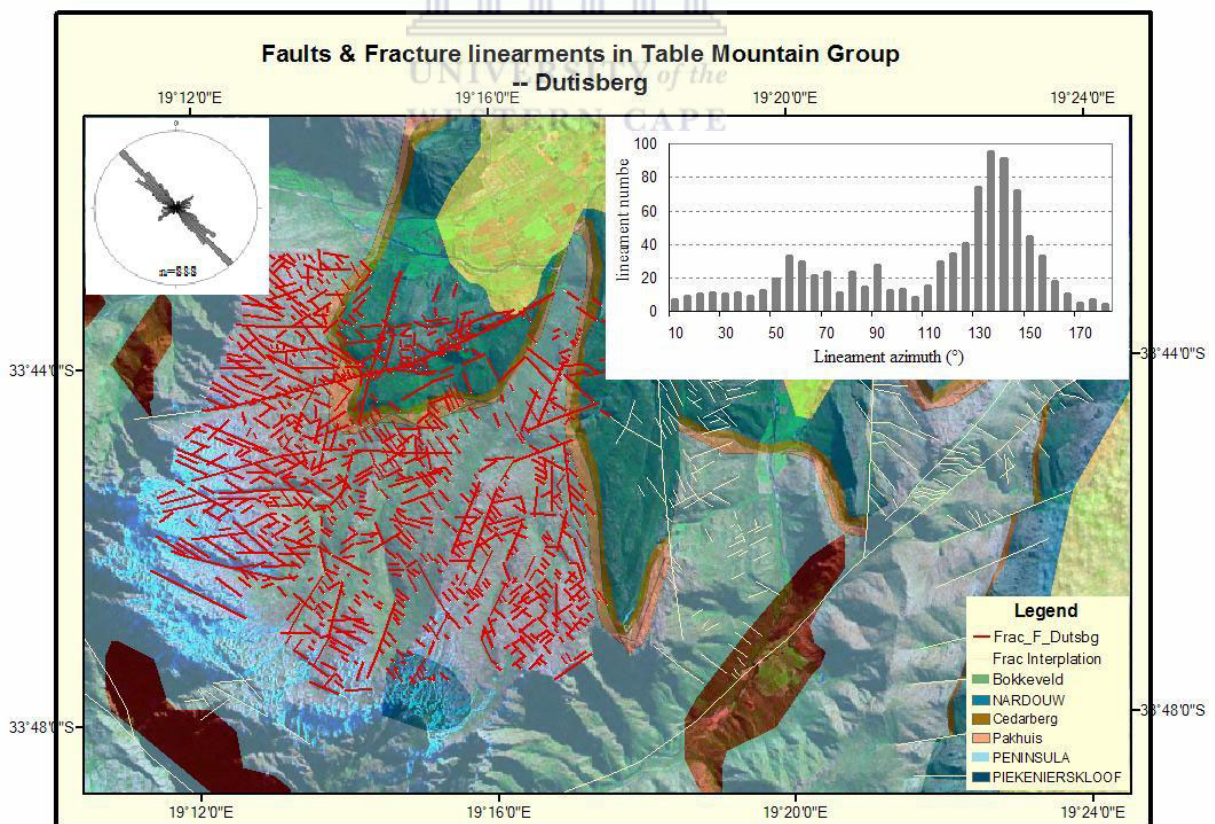


Fig. 3-10 Map showing Lineaments (red color) captured from Landsat ETM+ image and their orientation pattern, incorporating with the geological information at domain area A3.

It is well known that fracture length has a significant impact on the connectivity in a fracture network. Currently, the studies of fracture connectivity pattern are largely derived from generated models via stochastic analysis of measured fractured data. Kulatilake et al (2003) suggest that lognormal, gamma, and exponential distributions are the best models to characterize fracture semi-trace lengths based on probability analysis with data from field measurements in gneiss rock masses. An exponential distribution of fracture trace-length is applied by Park et al (2002) to study the hydraulic properties in granite. On a microscopic scale, the elementary fracture, with few long fractures tend to have a lognormal distribution resulting from X-ray scanning of core samples (Pyrak-Nolte et al, 1997). In fact, not only the lithologies over which the fractures develop, but also the methods of fracture scanning and length computation, have a big influence on the length distribution patterns.

In this study, the length of lineaments is computed by points on each tracing line to avoid the possible bias for non-beelines, using VBA script developed in ArcMap. Recorded lineament length ranges from 60 m to 17450 m with mean values ranging from 351 m to 1984 m in the seven domain areas. No significant differences in the distribution of lineament length can be found from the number-length histograms (Fig.3-11). They all appear to have a lognormal distribution with various mean value and standard deviation. This distribution pattern is thought to be prevailing in the TMG sandstone terrain, regardless of the size of a domain area. According to the universal presence of similarity of fracture systems at different scales, this distribution pattern can probably be introduced to the smaller-scale fracture systems, especially where difficulty is often encountered on the weathered grounds to have sufficient trace-length data to represent the statistic population.

On a microscopic scale, the aperture value of a fracture is perhaps proportional to that of fracture length (Zimmermann et al., 2003). The same context is supported as well by the work of Gavrilenko and Gueguen (1998) who assume a linear relationship between fracture aperture and length. The previous work indicates that information of fracture aperture can accordingly be obtained from that of fracture length. Based on lineament data analysis and field verification, Liu and Bodvarsson (2001) are able to establish the relationship between fracture aperture and fracture length which follows a power law with the exponent of 0.3~0.5:

$$B=c \cdot L^d \quad (3-1)$$

Where B – fracture aperture, L – lineament trace-length, the constant c and d , which could be varied due to the statistic results. This relationship between fracture length and aperture tends to become meaningful in the study of large-scale hydraulic properties.

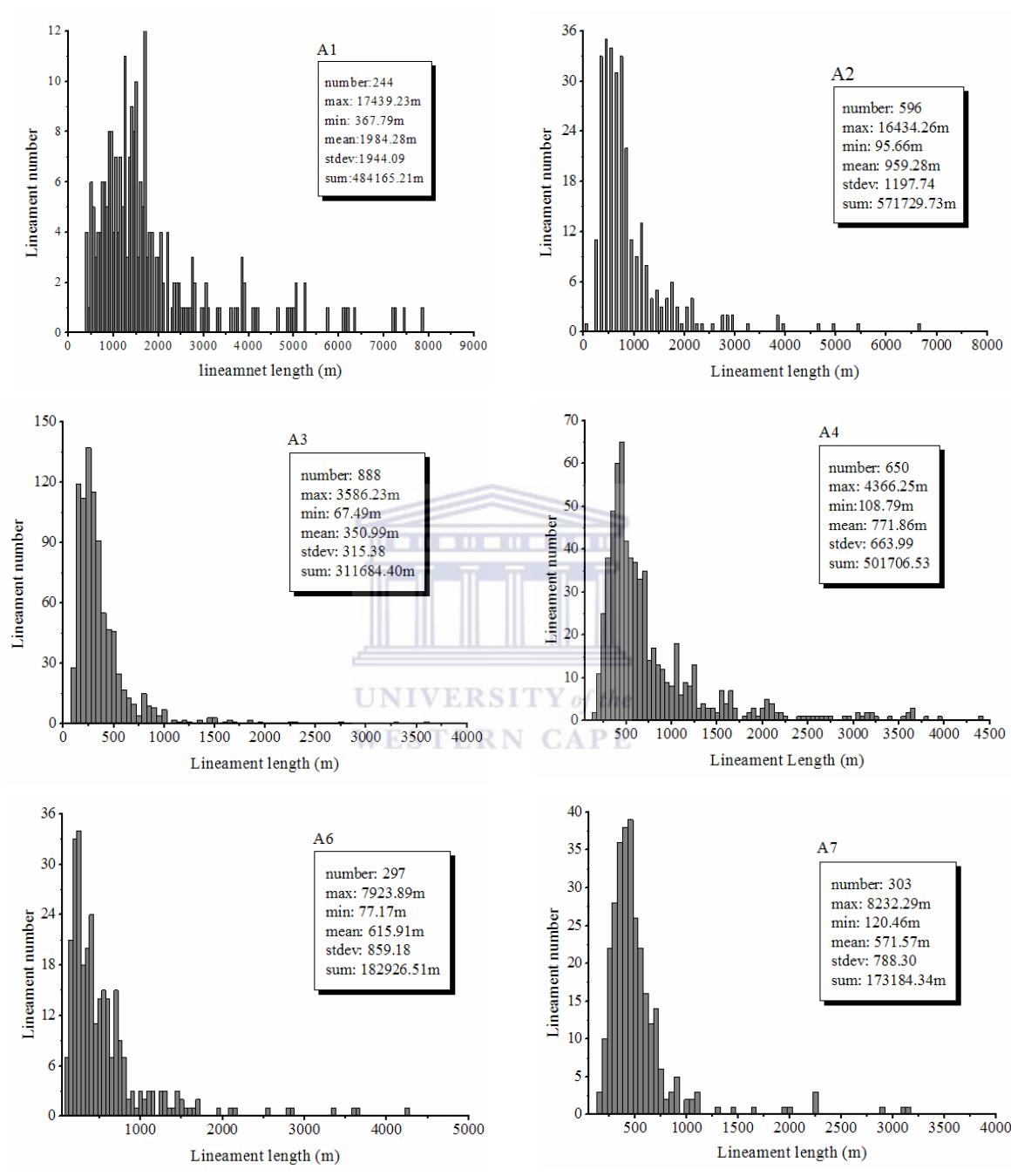


Fig.3-11 Histogram for lineament lengths collectively shows a lognormal distribution together with the statistic parameters derived from the lineament data of domain area A1~A7, in which A5 with the same distribution is not included.

3.6 Fracture characterization with data from field measurements

The fracture measurements carried out on medium to large scales by means of remote sensing imagery interpretation and statistics are intended to draw out the framework of fracture network with length more than 60 m. If properly interpreted, fractures with size larger than site scale (above the cut-off of 60 m) can be presented in a 2D space. This is obviously an effective approach to present the backbone of fracture systems in a specific region where the rocks are well exposed. However some drawbacks inevitably arise from the quality of outcrops and the misinterpretation of fractures when the lineaments are not actually controlled by fractures. The interpretation results need to be confirmed in the field. Furthermore, fracture data from site surveys and field measurements can be statistically analyzed for both the characterization of the TMG fractured rocks and production of hydraulic conductivity information by properly organizing the data measured at sites.

3.6.1 Fracture field measurement and data statistics

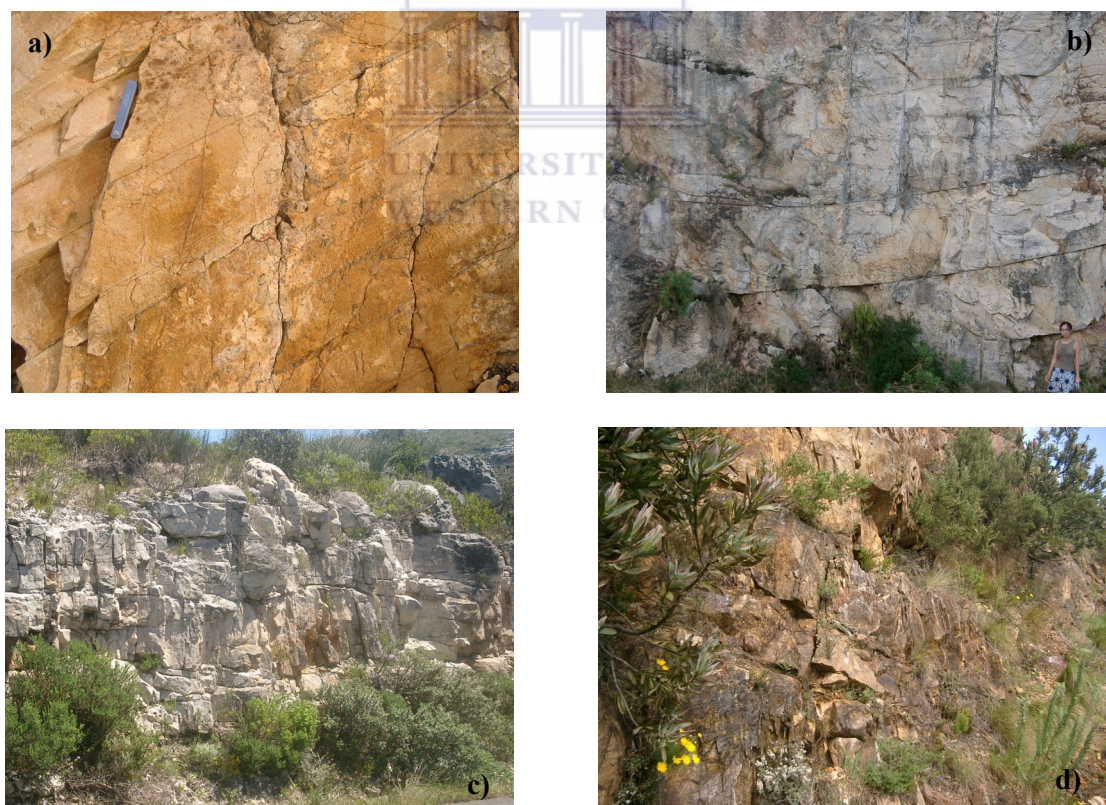


Fig.3-12 The TMG outcrops for fracture measurement. a) A close view of the TMG sandstone near a fault zone at the north of Grabouw; b) the Peninsula sandstone outcrop at Teewaterskloof west; c) Peninsula sandstone at Simon's Town; and d) the Nardouw sandstone outcrop at Aseljagberg.

Field measurements of fractures for the purpose of collecting fracture data over the TMG outcrops to compensate for the interpretations of satellite imagery have been carried out. Selected sites for the detailed field surveys and investigations on much smaller scales are located in different structural domains of Cape Fold belt. Ideally, fracture data should be

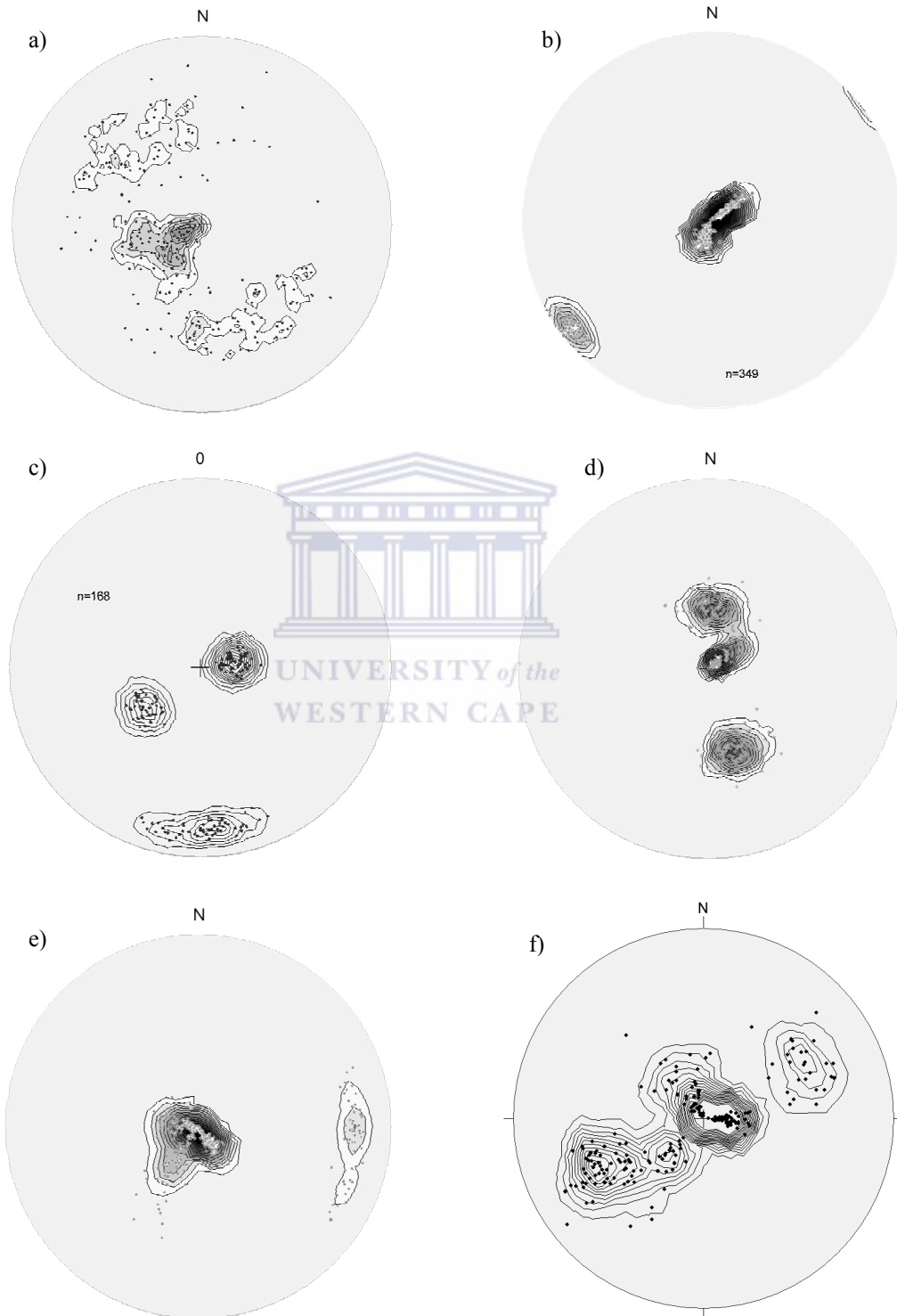


Fig3-13 Spatial frequency distribution of fractures measured at sites in the Western Cape: a) Teewaterskloof east; a) Teewaterskloof west; c) Montague tunnel; d) Eselagberg; e) Gevoden; and f) Boschklouf, in which the solid circles represent normals to the fractures. For density computation, equal area method is used with grid cell area as 1% of the diagram area, using lower hemisphere projection.

gathered on fracture elements, i.e. length, orientation, aperture, and density for developing a statistical or deterministic model. Most of the fracture element data could be properly collected in the TMG sites, except the fracture length due to the difficulty of tracing along the fractures as most of them are buried by soils and vegetations. In order to have sufficient representative measurement samples, the size of measurement sites is often required to be more than 60 m in either length or width with good sandstone outcrops (Fig.3-12).

Statistics on fracture geometries (dip azimuth and dip angle, spacing, aperture, and length) at selected sites are used to analyze the distribution of these parameters and form a solid basis for the study of aquifer properties such as hydraulic conductivity (Lin and Xu, 2006). With respect to the distribution of each fracture element, it is well established that fracture length often obeys a lognormal distribution, which has been proved by the data captured from satellite imagery, and orientations and aperture roughly follow normal distributions. Fracture density that is dependent on the fracture spacing is assumed as uniform distribution in case of only one type of rock material such as Peninsula or Nardouw sandstone, but it could be diverse over different rock formations. The fracture data measured at selected TMG sites show that there are mainly 3 to 4 sets of fractures (Fig.3-13), including bedding fractures. Fig.3-13 suggests that approximately normal distribution of fracture orientation as regarding to individual set of fractures (Fig.3-14), which is quite similar to that of lineament statistical result.

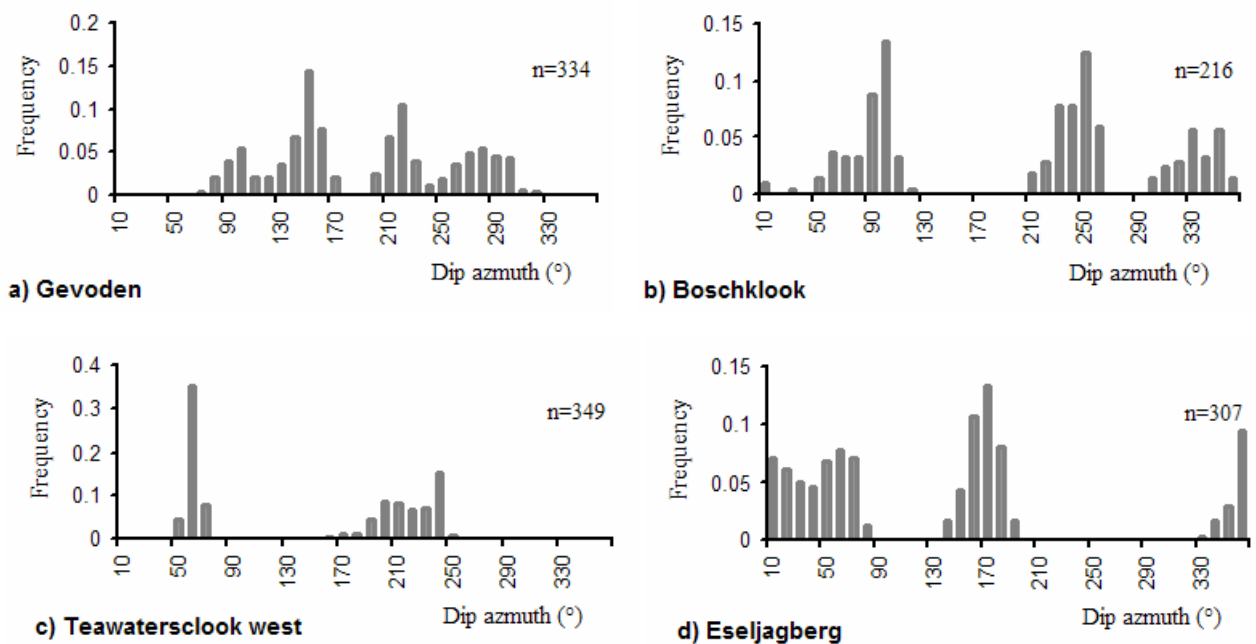


Fig. 3-14 Frequency histogram of fractures vs fracture dip azimuth at per 10° interval, showing the dipping directions at each selected site are compared due to different sets of fractures, in which n is the number of fracture measured.

3.6.2 Stochastic realization and connectivity of natural fractures

In the context of fracture hydrogeology, the interconnection of fractures has been recognized as one of the key feature in controlling the flow system in fractured rocks (Margolin et al., 1998). Many efforts have contributed to the study of fracture connectivity through randomly reproducing fracture reality (Bradbury and Muldoon, 1994) largely based on the distribution of each fracture element (orientation, length, density). When these statistical data are incorporated with other parameters such as aperture and particularly connectivity of fractures, the hydraulic properties of fracture network can then be estimated (Mourzenko et al, 1999; Dreuzy et al, 2000). In this regard, percolation theory can be an effective tool to delineate the connectivity of a fracture network. Random fracture reality applied to quantitatively determine the percolation threshold mostly assumes that fractures are well connected so as to allow flow to move from one side to the other. Moreover, the determination of percolation threshold uniquely requires information of fracture number or density, which suggests at times thousands of fractures might be involved in a flow system. In study of fracture system at the uranium mine in France, Long and Billaux (1987, cited by Witherspoon, 2000) found that only 0.1% fractures out of 65740 generated ones contribute to flow at the site scale. In situ borehole tests (Karasaki et al, 2000; Halihan et al, 2005) have also shown that fractures developed in a rock mass are not always fully connected. Fracture interconnection may depend on both geometric and physical properties such as orientation, aperture, length, termination, and fracture filling.

Based on the assumption that groundwater in the TMG sandstones is governed by fracture networks, and in light of the field evidence, fractures have been generated, in this study, with the data derived from field measurements. The intention of the realization is to present, on a site scale, the geometric interconnection of fractures with the length ranging from meters to tens of meters, and subsequently to yield a type of conceptual model that may be applied to the estimation of hydraulic properties as will be discussed in the later chapter.

3.6.2.1 An approach to fracture realization

The process of fracture realization is conducted using a random process with the distributions of fracture elements which can be summarized from the field or site measurements data. Fundamental elements include fracture orientation (strike, dip azimuth and dip angle), fracture length and the distance (spacing) of each set of fractures, in which the number of fractures measured has to be enough to represent the population of fractures at the measuring site.

As discussed above, fracture orientation follows a normal distribution that can be observed from Fig.3-14. Lognormal distribution is adopted for fracture length from the data of remote sensing by considering the similarity of fractures at various scales (Fig.3-15). Since it is extremely difficult to have enough trace-length data measured on the TMG exposure, fracture length population is only represented by less than 40% of the measured fractures with the length scale in meters to tens of meters.

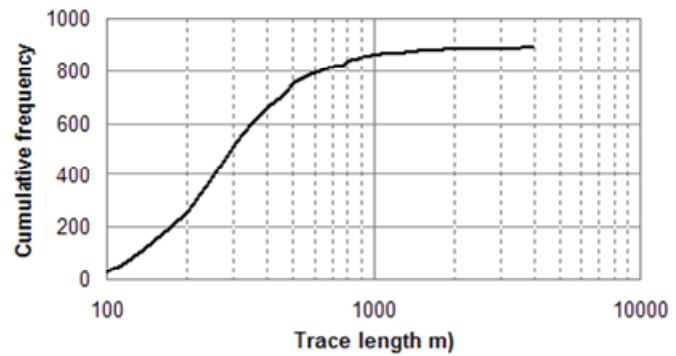


Fig.3-15 Plot of cumulative frequency against fracture trace-length with cut-off at 100m, at site Gevonden (see Fig. 3-11-A3), approximately showing a lognormal distribution.

Random realization of fractures is based on the statistical data of each fracture set. With respect to the number of each fracture set, many key studies on discrete fracture network (DFN) use multiple fracture numbers, which seems to meet a density value for the study of connectivity. Without doubt, such way for fracture number at a study domain tends to amplify the uncertainty of the statistic results on fracture elements on the measurement scale. Other than using an uncertain number, in this study, the number of each set of fractures is determined by their spacing in a domain, and accordingly the position of fractures is assumed to be a uniform distribution.

Based on statistical feature of fracture data, it is able to use the function of “random number process” embedded in Excel to geometrically generate the fractures on surface and on profile respectively. Then the fracture data generated in Excel is loaded up to ArcGIS where the graphical process is conducted using a VBA subroutine developed in ArcGIS; geometric connectivity analysis is also done in ArcGIS automatically.

The realization of fractures on 2D plan (on surface) only needs to have the input of stochastically generated data of fracture strike, length and density (for the number of fracture sets). In order to remove the boundary effect in which position of each fracture offsets out side of the study domain, central coordinate (x,y) should be used to position each fracture during the generating process (Fig. 3-16).

It is acknowledged that groundwater flow in the fracture system is not a 2D problem, but a 3D one. This requires presenting the fracture media on 2D profiles in which the generated fracture data of length, dip angle and density are necessary. However, different from the

realization of fractures on a 2D plan, the real dip angle of each fracture needs to be projected on the profiles with different strikes (direction) before the data can be generated. Fig. 3-17 illustrates the projection from a real dip angle (β) to apparent one (α) which can be performed using the following relationship:

$$\tan \alpha = \sin \phi \cdot \tan \beta \quad (3-2)$$

Where ϕ ($\phi = 0^\circ \sim 90^\circ$) is the included angle of profile strike and fracture strike. In the meantime, fracture length is changed as well, by assuming the fracture takes a rectangle shape with an aspect ratio of 1.5:1 (the same hereinafter); whereas the rotation of profile does not have a big impact on the change in fracture length on profile.

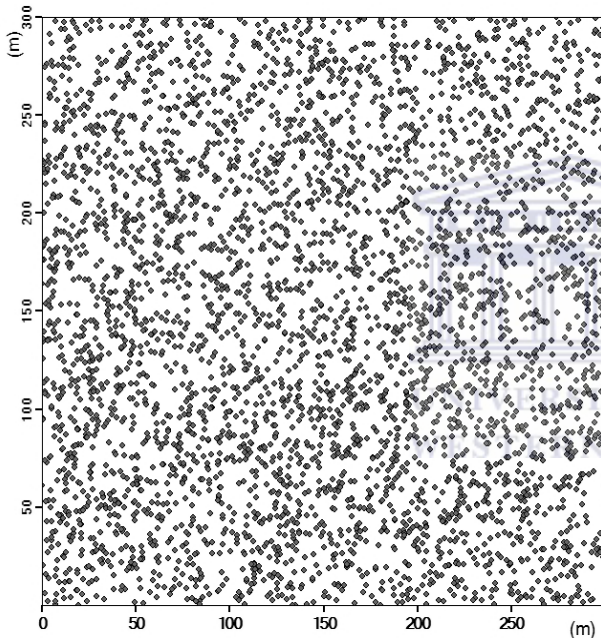


Fig.3-16 Position of fracture central points generated by a uniform process in the study domain of 300m×300 m at site Boschkloof.

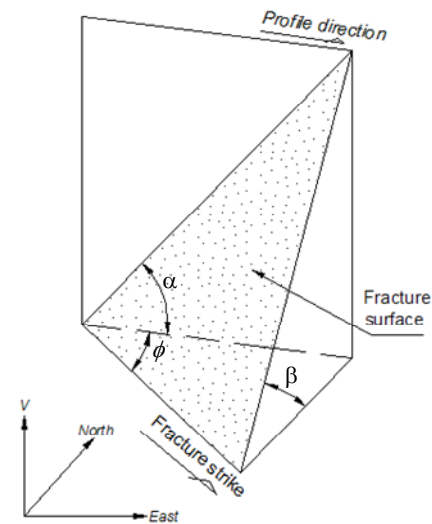


Fig. 3-17 Relationship between fracture orientation and profile direction, in which ϕ is the included angle of fracture strike and profile direction, β the fracture dip angle, and α is the apparent dip angle of fracture projected on the profile.

3.6.2.2 Application to field data

Fractures data in this part of study is derived from the field measurement of the site Boschkloof in Citrusdal area (Fig.3-3a), Weastern Cape, where there are five borehole with the depth ranging from 174 m to 350 m drilled in the sandstone of the Peninsula formation in 1997~1998 (Fig. 3-18). These boreholes are located in the vicinity of a N-W trending fault

that extends in kilometers that has been identified as a flow barrier, while the N-E trending fault is actually a lineament feature with unknown properties (Hartnady and Her, 2002b). During the borehole drilling, the blow yield of the boreholes was reported to be very high compared with another wellfields developed in the TMG, especially in borehole BK1 and BK4 the yield value reached 95 l/s and 120 l/s respectively. It is the success of this wellfield that motivated a full study of the TMG Groundwater.

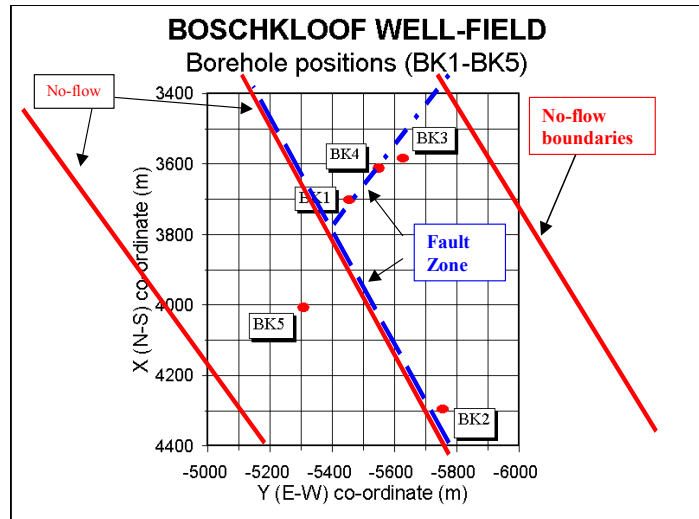


Fig.3-18 Map showing the position of boreholes in Boschkloof wellfield. Field measurement of fractures was taken on the Peninsula sandstone exposure between the borehole BK1 and BK3 (Courtesy of Gerrit Van Tonder, also see Hartnady and Hey, 2002). Note that the N-E striking fault is a lineament feature.

Characterization of this site and associated groundwater flow is based on the interpretation of stratigraphies, structure, and pumping test data and another field observation during the drilling (Hartnady and Hey, 2002). Herein, it is not necessary to completely present these results, but study the fractures from the other angle.

Table 3-2, Fig.3-13f, and Fig.3-14b collectively show the basic fracture data results from that of the field measurement on the exposure of Peninsula sandstone where total 216 fractures, about 5.2% of the fractures to be generated (Table 3-2), are examined. Five sets of fracture are identified and parts of the length measured. In table 3-2, set 1 represents bedding fractures together with the fractures of set 4, have relatively gentle dip angles and control the length element with a less density comparing with the other three sets. Steeply dipping fractures of set 2, 3 and 5 appear to predominate over the density distribution in the sandstone because of their relatively low spacing. It should be pointed out that the fracture trace-length collected at the site ranges from 1.9 m to 35 m and consequently this study can be defined as regards the problem on a site scale.

Fracture realization is based on the statistic and parameter distribution of each fracture element as have been previously discussed. Fractures are generated in a study domain of $300 \times 300 \text{ m}^2$, on both 2D plan and 2D profiles with various profile directions. It is expected to present the fracture networks on this site scale because both the borehole lengths are less than

350 m and the lower limit the main water strike is located at the depth of 294 m in borehole BK4.

Geometric nature of the fractures perhaps is different at depth as discussed by Shapiro et al (2007), due to the difference in lithology and stress state of fractures. For the realization of fractures on 2D profiles, partially based on the core sample study at the adjacent Rietfontein site, it is necessary to propose such assumption that the fracture orientation and density do not change much at depth in the locally homogeneous Peninsula sandstone.

Table 3-2 Statistic result of 216 fractures measured at Boschkloof

Set	Sample number	Dip angle/Dip direction (°)		Length (m)			Spacing (m)	Number generated
		Mean	Standard deviation	Mean	Standard deviation	Number measured		
1	57	40/244	10.28/40.09	16.31	1.66	16	0.41	730
2	50	77/330	10.44/17.48	7.29	1.40	22	0.27	1110
3	55	79/94	4.53/5.77	5.06	1.49	19	0.34	860
4	27	40/62	8.68/12.63	13.94	1.31	8	0.68	440
5	27	63/211	11.87/8.52	4.50	1.61	20	0.30	1000

3.6.2.3 Connectivity pattern of fractures

Similar to many other stochastic studies, the fractures generated on both the 2D plan and vertical profiles more represent the assemblage of fractures than the real position of each fracture in the site because of their random coordinates. Therefore, each generated domain reflects the mode of fracture occurrence and the connectivity pattern that is embedded in the features of natural fractures.

To continue the field data application of the Boschkloof site, Fig.3-19 shows these fractures on the plan where four profiles with the strikes from NE40° to

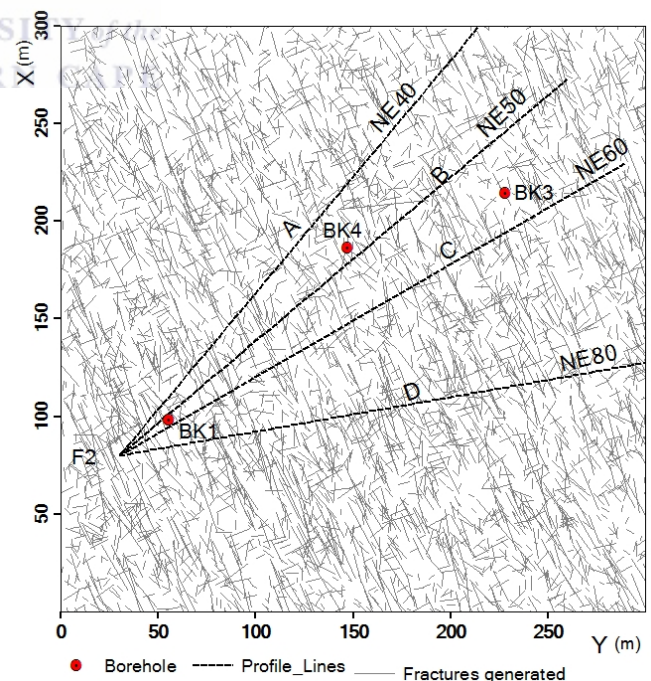


Fig.3-19 Fractures generated on the 2D plan with the data derived from the field measurement at Boschkloof wellfield with five boreholes. The study domain area is 300×300m², in which the dashed lines are profile lines for profile fracture realization labeled by A to D.

NE80° are positioned for the fracture realization on vertical profiles. The intention of fractures realization on multiple profiles is to comparatively analyze such connectivity pattern that may help to explain some unique flow phenomena in the TMG fractured rocks, and thus help to establish a site-scale conceptual model for studying aquifer properties and borehole hydrogeological condition in a statistical sense, such as how to average out a suite of relevant hydraulic properties to apply to groundwater modeling, or how to effectively use a contour map of borehole water levels to present groundwater flow trends on a local or even a regional scale.

Fig.3-20 shows the generated results including both the whole fractures (Fig.3-20A1~D1) and the relatively large fracture clusters (Fig.3-20B2~D2), together with three boreholes projected on four neighbor profiles with the intervals of strike azimuth from 10° to 20° in which the profiles A, B, and C are close to the line determined by connecting borehole BK1 through BH4 to BK3, while the profile D is relatively apart from the line (Fig.3-19). It is clear that the interconnected fractures on each profile collectively exhibit a mode of separated fracture blocks which commonly show an anisotropic feature of the fracture networks. It is also clear that the profile direction has an impact on the connectivity pattern in terms of the size and plunge of the connected blocks. Except the profile D, fracture blocks on the profiles A, B and C similarly present another feature that the largest connected block extends accordingly most range of the domains but none of them breaks through the boundary on both sides (bottom to top or left to right side) (Fig.3-20A2, B2, and C2). This suggests that the connectivity patterns are collectively dependent on the factors of orientation, length, and density of fractures and implies that in a study domain only part of the fractures are able to be involved in a flow system. For example, on profile B the number of interconnected fractures from block 1 to block 5 is 954, 127, 224, 99, and 167, respectively, accounting for 23%, 3.1%, 5.4%, 2.4%, and 4.1% of the total 4140 fractures.

Such connectivity pattern does help to explain the existence of multiple water strikes or conductive zones where groundwater is coming from different fracture (blocks) systems probably without hydraulic connection. However, validity of the connectivity pattern needs to be compared with the results from field observation. From borehole observations, the phenomena of multiple water strikes or several conductive intervals in a borehole or no hydraulic communications taking place between the holes in a wellfield are common in the TMG sandstone aquifers. In the Boschklouf site, for instance, at least two conductive intervals were identified in boreholes BK3 and BK4 (but only one in BK1), whereas the borehole BK2 appeared to be isolated from the other three. Moreover, it was observed that the groundwater

in boreholes BK1 (major water strike 98.7m elevation) and BK4 (major strike 30.3m elevation) were connected at the depth of the major water strikes (Hartnady and Hey, 2002b). Distance between BK1 and BK4 is 127.4m, from which it is obvious that the northeastern plunge of the conductive zone is 28°. This value falls in the fractures of set 4 with the dip angles ranging from 20° to 52° and the length of these fractures are just second to bedding fractures (Table. 3-2). Field observation (Hartnady and Hey, 2002b) also showed that groundwater in borehole BK3 was not necessarily connected to the other two although they were sited almost on a profile line. This evidence indicates that three boreholes were probably not sited on a single fault zone (Fig 3-18); contrarily, the fault may have been blocked to function as a fracture zone.

When looking into the drawdown observations during the constant discharge (CD) pumping tests conducted at borehole BK1 and BK4, with the same level of discharge rate which can match the same magnitude of blow yields observed from the boreholes during the percussion drilling, it is found that the types of drawdown curve are different from each other (Fig. 3-21). Compared with borehole BK4, drawdown observed in BK1 during the CD test is very close to that of Theis flow, whereas drawdown in BK4 exhibits a stepwise mode. From both of the drawdown curves, it appears that the groundwater is coming from two different aquifers, but there is hydraulic connection between the both boreholes as abovementioned.

The stepwise mode of drawdown is very common in the TMG sandstones and many other fractured rock aquifers in South Africa (van Tonder et al, 2001) and is often explained as being set off by multiple boundary effects. This is true if only one flow system is intercepted by a borehole. When a borehole like BK4 intercepts at least two fracture flow systems, question of whether the stepwise drawdown is attributed to simultaneously dynamic response of these two flow systems to the external pumping stresses may arise. On one profile, it is noted that the multiple realizations of fractures by the same statistic data do not change the mode of connected fracture blocks, which means the stability of the connected blocks is quite high. On a single site, the connectivity patterns are directionally different, as above-discussed, which always suggests the potential of preferential flow path in the study domain and implies the existence and necessity of studying groundwater problem in a three dimension. From site to site, the pattern of fracture connectivity varies mainly in terms of connected block size as additionally shown by results from the Rietfontein and Govendon site in Fig.3-22 and Fig.3-23.

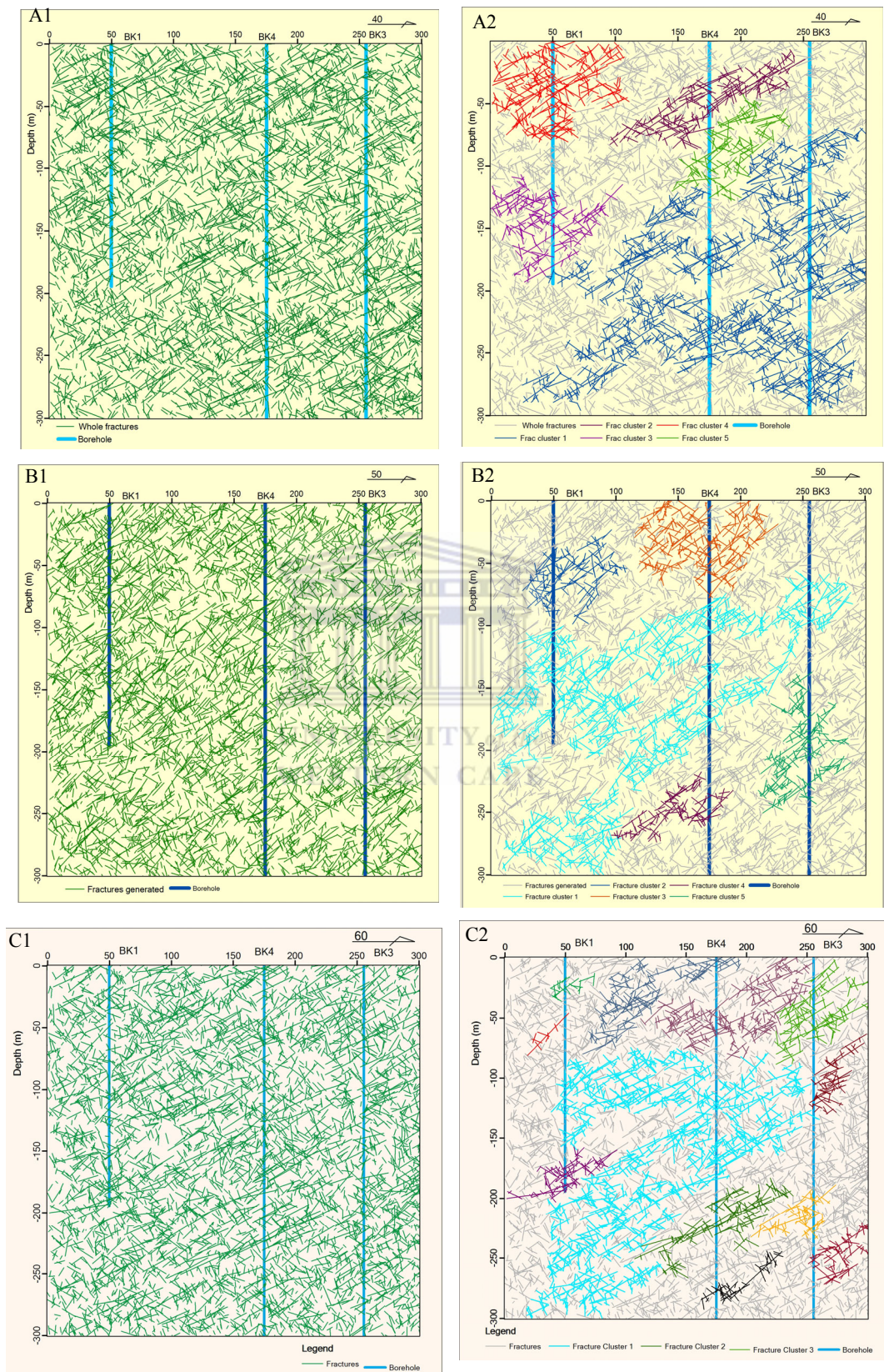


Fig. 3-20 (to be continued in the next page)

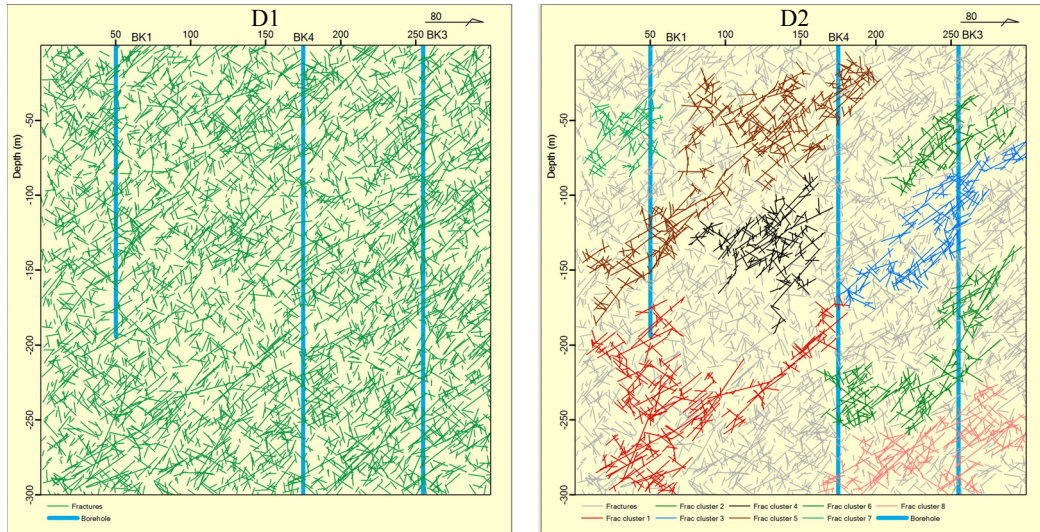
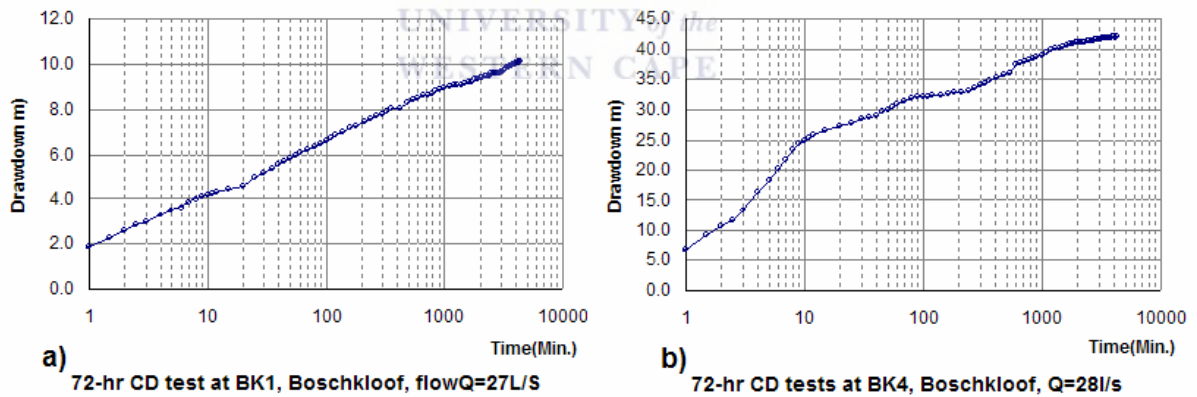


Fig.3-20 Fractures generated on four comparable profiles based on the data derived from surface measurements (Table 3-2) at a size of 300×300m. 1) The left, the whole fractures on each profile. 2) The right, relatively large interconnected fracture blocks geometrically show the connectivity patterns at this site scale with the involvement of boreholes.



a) 72-hr CD test at BK1, Boschkloof, flow $Q=27L/S$

b) 72-hr CD tests at BK4, Boschkloof, $Q=28l/s$

Fig.3-21 Drawdowns observed during the 72-hour pumping tests data at wells BK1 and BK4

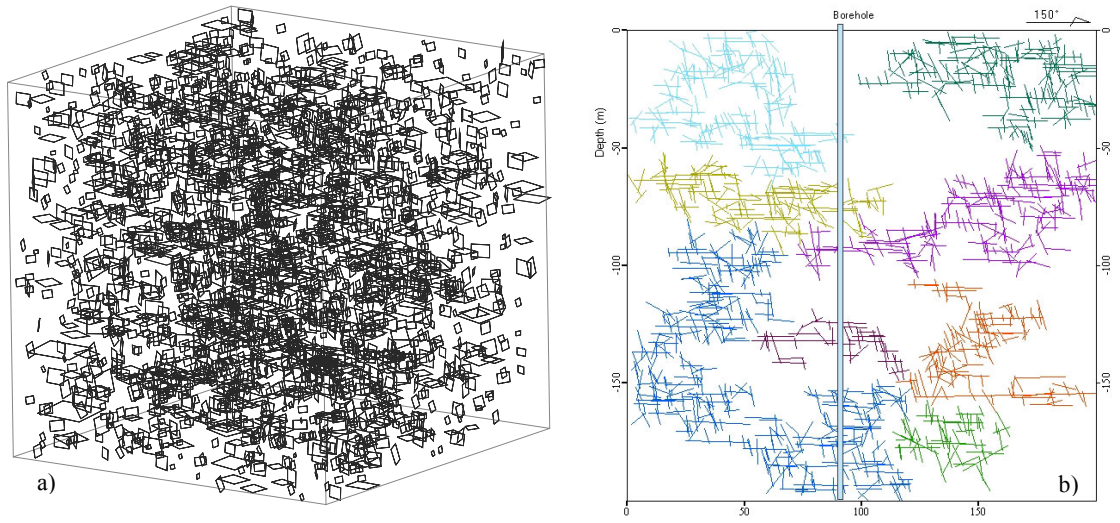


Fig.3-22 Fracture generated based on the data derived from surface measurements at the Rietfontein at a size of 200×200×200 m. a) A northwestward view of 3-D visualization of rectangle fractures with a fracture length/width ratio of 1.5, in which the small black blocks indicate the well-connected fractures. b) The interconnected fracture blocks geometrically show a connectivity pattern at a borehole scale. With the involvement of a borehole, it may present the conceptualization of groundwater flow could come from different fracture systems without hydraulic communications in a single hole. Note that the fractures are projected and generated on profiles with a strike of 150°–330°.

UNIVERSITY of the
WESTERN CAPE

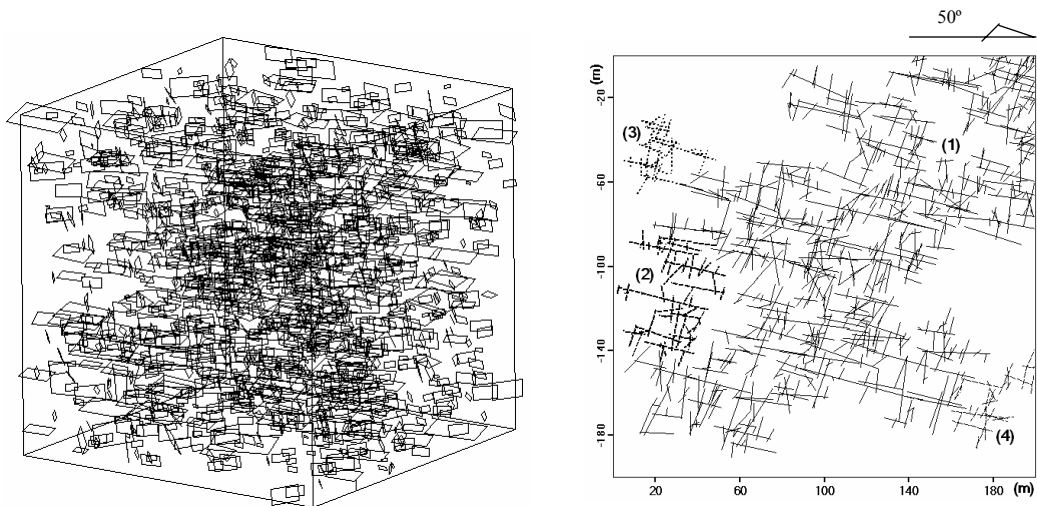


Fig.3-23 Fracture generated based on the data derived from surface measurements at the Govendon site at a size of 200×200×200 m.

3.7 Summary

Based on previous studies and current researches, the characterization of the TMG fractured media on regional and local scales is performed, through the interpretations of existing geological data and remote sensing imagery, the study of core samples, and the analysis of fracture field measurement data, from which an initial conceptual model of fracture network is developed. This model can help to have a better understanding of the TMG fractured rocks media and can be applied to the quantification of aquifer properties.

According to the experience of groundwater development in the TMG area, fault structures have attracted much attention in the development of wellfields for water supply. Most of the fault zones developed in the TMG sandstones and siltstones are evidenced to have been recemented and act as aquicludes. Based on the study of fault architecture, a conceptual model of fault is proposed, which stresses that fracture zones at both walls of a fault core may become a particular interest of borehole siting; this suggests that the groundwater occurrence and flow path are dominated by fractures or fracture network.

In the context of hydrogeological setting, it is better to classify fractures in the TMG sandstones into two categories of the open and closed than conventional classification based on the mode of rock deformation. To investigate such types of fractures, a case study on core sample fractures in an 800-m deep borehole at the Rietfontein site is then introduced. Data from fracture field measurement, and fracture core sample and coating scanning are comparatively analyzed, which yield the results in the distribution of orientation, and the variations both fracture density at depth and fracture coating intensity at depth. These results are informative for the characterization of the TMG fracture media; in particular the analysis of fracture coating, which has never been done in the TMG, discloses a mode of hydraulically active fractures at depth.

For the study of a regional problem, remote sensing can be an effective tool, especially when incorporating with GIS technique. For the characterization of fractures on a regional scale, lineaments captured from imagery often provide a crucial clue on the interpretation and analysis of fractured rocks. Using Landsat ETM⁺ imagery, a quantitative analysis is carried out by VBA subroutine developed in the software ArcMap to determine the distributions of lineament orientations and lengths in seven domain areas, from which a universal lognormal distribution of lineament length is established. This distribution pattern can be introduced to the smaller-scale fracture systems, especially where difficulty is encountered on the weathered grounds to have sufficient trace-length data to represent the statistic population.

For the site-specific groundwater problems, because the existing data for characterizing fractured rocks of the TMG are very limited, field measurements on fracture elements are carried out over the sandstone outcrops at selected sites. Based on statistic features and distribution pattern of the fracture elements, fractures on both 2D plan and profiles, and in 3D domains are generated using random processes, from which the connectivity is qualitatively examined. These results generally show that the interconnected fractures collectively exhibit a mode of separated and anisotropic fracture blocks (networks). Such connectivity pattern is thought to be general in the TMG sandstones, especially where the TMG rocks are exposed but not confined by overlaying geological formations. Because the basic data have been measured at different structural domain and lithologies, the generated results and subsequent fracture connectivity is accordingly representative. In order to verify the validity of the generated model, a brief case study was carried out in the Boschklouf site, from which some of the field observations of groundwater phenomena can be explained by the models.



Chapter 4

Hydraulic properties

4.1 Introduction

Groundwater problems in fractured rock aquifer are traditionally evaluated and monitored using considerably designed wellfields from which water level, quality and flow quantity are measured, and field testing such as pumping/packer tests are conducted. On one hand, interpretation of the data obtained from laboratory and field tests is used to quantitatively yield the intrinsic aquifer properties (hydraulic properties, including storativity/specific yield and hydraulic conductivity/transmissivity), which is based on the assumption that groundwater flows through a geological continuum. When the representative elementary volume (*REV*) of an aquifer does exist, the interpreted results become applicable to the evaluation of groundwater flow and storage in fracture rocks. However, in porous media the *REV* can be very small; in a fractured rock aquifer the *REV* may be very large or even does not exist in many cases (Kulatilake and Panda, 2000; Wang et al., 2002). Therefore, on the other hand, groundwater flow through a fracture has been analyzed with such consideration that the flow conduit is exclusively governed by the fracture under a certain hydraulic pressure. Based on the same consideration, many researchers have tried to experimentally find out the existing relationship between the hydraulic properties concerning flow through a single fracture (Lomize, 1951, Louis, 1974). When groundwater flow is assumed to be laminar through a couple of parallel plates, the flow can be featured with Cubic Law (Snow, 1965, cited by Snow, 1969). Talobre (1957, cited by Jaeger, 1972) proposed an alternative expression of Cubic Law to present water flow through a set of fractures by taking into account the fracture number density. When using the Cubic Law to assess the flow in a fractured rock with multiple sets of fractures, a method of flow superposition is employed for these fracture sets (Tian, 1988; Lin and Xu, 2006). The validity of the Cubic Law has been examined and discussed by many authors (Witherspoon et al, 1980; Brown, 1987; Thompson and Brown, 1991) through theoretical analyses and laboratory tests. There are arguments on the application of these methods to estimate flow and relevant hydraulic properties in natural fractures, nevertheless methods based on the Cubic Law are still an effective tool to quantify the groundwater flow and hydraulic properties. The key aspect of the quantification depends on a proper characterization of fractures or a fracture network.

As has been previously discussed, the TMG fractured rock aquifers are anisotropic with unique features as regarding its lithology and various-scale fractures. Currently, major problems faced are the lack of information on the properties of the fractured rock aquifers at various scales for the characterization of shallow and deep groundwater circulation. The overestimation of wellfield/aquifer productivity is a common phenomenon. Incorrect estimation of aquifer conductivity and transmissivity can result in wrong evaluation on abstraction rate as can be seen in the Vermaak River wellfield in the Klein Karoo, where yields of 4.7 Mm³/a were estimated but actual figures achieved were only 1.3 Mm³/a. Moreover, the overestimation of storativity, and the incorrect calculation of recharge and transmissivity may lead to the aquifers' overdraft, and subsequent lowering of water levels and decrease in water quality. This is due to poor understanding of the subsurface features of the TMG rocks in which the key aspect is the determination of flow path and boundary condition when using existing models to interpret the aquifer responses to hydraulic tests or pumping scenarios. Previous studies have also showed that groundwater in the TMG aquifers is prevalently dominated by secondary porosity, i.e. fractures or fracture networks as discussed in Chapter 2.

Based on previous studies and current research, this chapter focuses on the determination of the hydraulic properties of the TMG aquifers, including porosity/storativity and hydraulic conductivity/transmissivity. The study of porosity is expected to link to the study of storativity through multiple approaches, for which the relation between these two terms will be discussed. Currently, transmissivity estimations of the TMG aquifers are largely derived from the analysis of hydraulic test data, especially pumping tests, therefore the mathematical solutions from the data interpretation and the applicability of the interpreted results are discussed through the analysis of the commonly encountered drawdown curve types. Since hydraulic conductivity (K) of the TMG aquifers is mainly controlled by fractures or fracture networks, a new tensor approach is proposed. Using the basic fracture data measured on the surface, different types of K values will be calculated. The results are also expected to compare with those from field tests and in turn the tensor model can be calibrated to meet the changes in fracture features and fracture setting conditions, from which a depth model of K is proposed and comparatively studied with the data from hydraulic tests.

4.2 Porosity and storativity

4.2.1 Relationship between porosity and storativity

Porosity and storativity are both important hydraulic parameters for the estimation of groundwater storage. The former (n , in percentage) is defined as the ratio of pore volume to the total volume of rock sample. The latter (S , dimensionless) is defined as elastic efflux or influx volume of water by per unit change in piezometric head in per unit area of a confined aquifer with a thickness of D . The relationship between the both can be expressed by the specific storage (S_s) which is developed by Jacob (1940):

$$S_s = \rho g(\alpha + n\beta), \quad (S = DS_s) \quad (4-1),$$

where ρ is the fluid density, g the acceleration of gravity, β the compressibility of the fluid (for water at 25C is $4.48 \times 10^{-10} \text{ m}^2/\text{N}$), and α is the compressibility of rock mass denoted by the reciprocal of its bulk modulus (K_v , N/m^2).

The S_s expression is one of the earliest studies to address the hydromechanical coupling problem. It was initially derived from compression process of porous media (soil) stressed by abstracting water from a confined aquifer. During the abstraction of confined water, decrease in water level leads to increase in the effective stress acts on the soil particles, resulting in the compression of the soil; in the meantime decrease in piezometric head leads to the expansion of the confined water, resulting in elastic efflux. Extrapolating to an isotropic rock mass, the bulk modulus K_v is often estimated by Young's modulus through the relation:

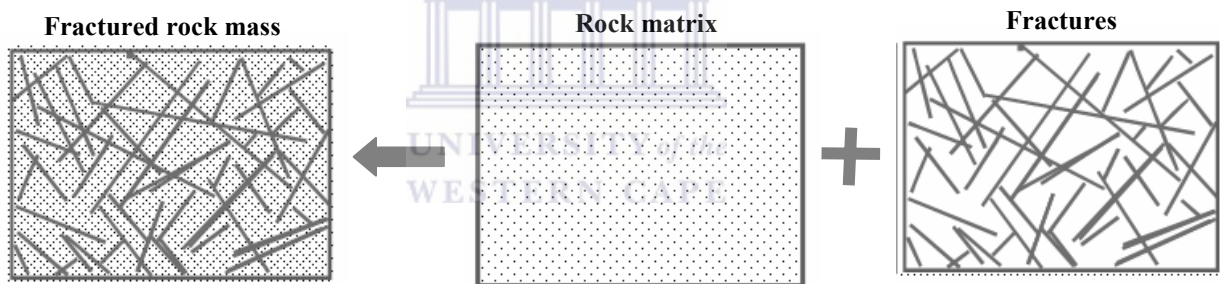
$$E = 3K_v(1 - 2u) \quad (u \text{ is the Poisson's ratio}) \quad (4-2),$$

However, for an anisotropic rock mass where fractures develop, bulk modulus of the fractures must be introduced and the specific storage of the fractures takes the similar form to that of the matrix rocks.

$$S_f = \rho g(\alpha_f + n_f\beta) \quad (4-3),$$

in which α_f is the compressibility of fracture determined by the reciprocal of bulk modulus of the fractures (K_f , N/m^2) which is generally less than K_v by couple orders of magnitude, n_f is the fracture porosity which can be estimated by total aperture of fractures. Thus, using the S_s to represent the specific storage of a matrix, the specific storage of a fractured aquifer is sum of both S_s and S_f as illustrated in Fig.4-1. In this regard, the fractured rock seems to be a dual porosity medium.

Assuming that the total aperture of fractures is generally in millimeters to centimeters, and the aquifer thickness range from meters to tens of meters, it is obvious that storativity of matrix rocks can be much higher than that of fractures on a borehole scale. It was report by Woodford (2002b), based on the study of Van Tonder and Xu (1999), that storativity of highly permeable fractures are usually very low in the order of 10^{-4} to 10^{-7} , whilst that of the matrix is much higher (i.e. 0.005 to 0.05). This indicates that fractures in a rock aquifer can dominate the flow system, but groundwater storage is mainly controlled by the rock matrix. The ratio of both values suggests that storativity term contributed by fractures can perhaps be discarded in the estimation of aquifer storage. However, it should be noted that there is always a lower limit size of fractures or lower cut-off in the study of fractured media. With respect to the TMG sandstones, the storativity of rock matrix can perhaps be regarded as the contributions of fractures at various scales, because there is almost no primary porosity through the thin section studies as mentioned in Chapter 2, and because there are micro-fractures found by Dr. Paul Carrey during the onscreen examination and interpretation of the thin sections with rock samples from the TMG sandstones. If this point is true, there must be



a scale-dependent problem of porosity as regarding the apertures of fractures at different scales.

Fig.4-1 Schematic conceptual model of fractured and matrix rock media with different storativities

4.2.2 Porosity

As discussed above, porosity of the TMG rocks includes two components, i.e. matrix porosity and fracture porosity; both of them have impact on the storativity of the aquifers; they can be expressed as follow (Cook, 2001).

$$n = n_f + n_m(1 - n_f) \quad (4-4),$$

where n , n_f , and n_m stands for total porosity, fracture porosity, and rock matrix porosity, respectively.

It is extremely difficult to determine both of matrix porosity and fracture porosity at the same time, because there is yet no borderline to distinguish one from the other, which is dependent on the scale of problem studied. In general, porosity of a rock mass is obtained from laboratory test of rock sample, well pumping test, and borehole geophysical logging (e.g. density, sonic, and neutron logs); fracture aperture is used to represent the fracture porosity of a rock in particular.

Fig.4-2 shows some of geophysical logging results from the Rietfontein deep borehole (see Fig.3-3), including resistivity (Ohm/m), Gamma (cps), and density (g/cm^3) logging data, from which lithologies of the Piekenieskloof formation in the borehole can be roughly identified. In order to avoid the uncertainty of geophysical loggings, further more, the logging results are compared to those of box-up core photos and core logging information. According to Titus et al (2002), in the three common types of rocks, bulk density of sandstone is 2.65 g/cm^3 on average, similarly siltstone is 2.45 g/cm^3 , and shale (band) 2.35 g/cm^3 . From the result of density logging, the porosity of the rock formation can be estimated using the following well established equation:

$$\rho = n\rho_f + (1 - n)\rho_s \quad (4-5)$$

in which n is the porosity, ρ is the bulk density, ρ_f the pore fluid density, and ρ_s matrix density. Assuming that the matrix density of sandstone is 2.75 g/cm^3 , siltstone is 2.62 g/cm^3 , and shale 2.57 g/cm^3 , calculation of the porosity for different rocks then is performed.

Table 4-1 Porosity estimated from the density logging result at Rietfontein deep hole

Lithology	Density (g/cm^3)		Porosity (%)	
	Range	Average	Range	Average
Clean sandstone	2.53~2.72	2.65	1.7~12.6	5.7
Fractured sandstone	2.1~2.52	2.30	13.1~37.1	16.4
Siltstone	2.35~2.55	2.45	4.3~16.7	17.1
shale	2.25~2.50	2.35	4.5~20.4	14.0

As can be found in Fig.4-2, there is no spatial correlation of the density logging data, so the porosity result derived from the density data is rather shown in a range of porosity than presented at depth. Porosity of the rocks from the density logging shows a wide range in which many of the calculated values fall in the range of porous media. Although the results

shown in Table 4-1 reveal an increasing trend in the porosity value from clean sandstone through siltstone and shale to highly fractured sandstone, these porosity data have some limited applicability only if the lower limit of the porosity of each rock type represents a relatively intact rock. This is because the bore wall has been long exposed during the extended drilling process, and consequently there is always a tunnel effect as stress concentration or release, resulting in the deformation of rocks near the bore wall to increase fracture porosity.

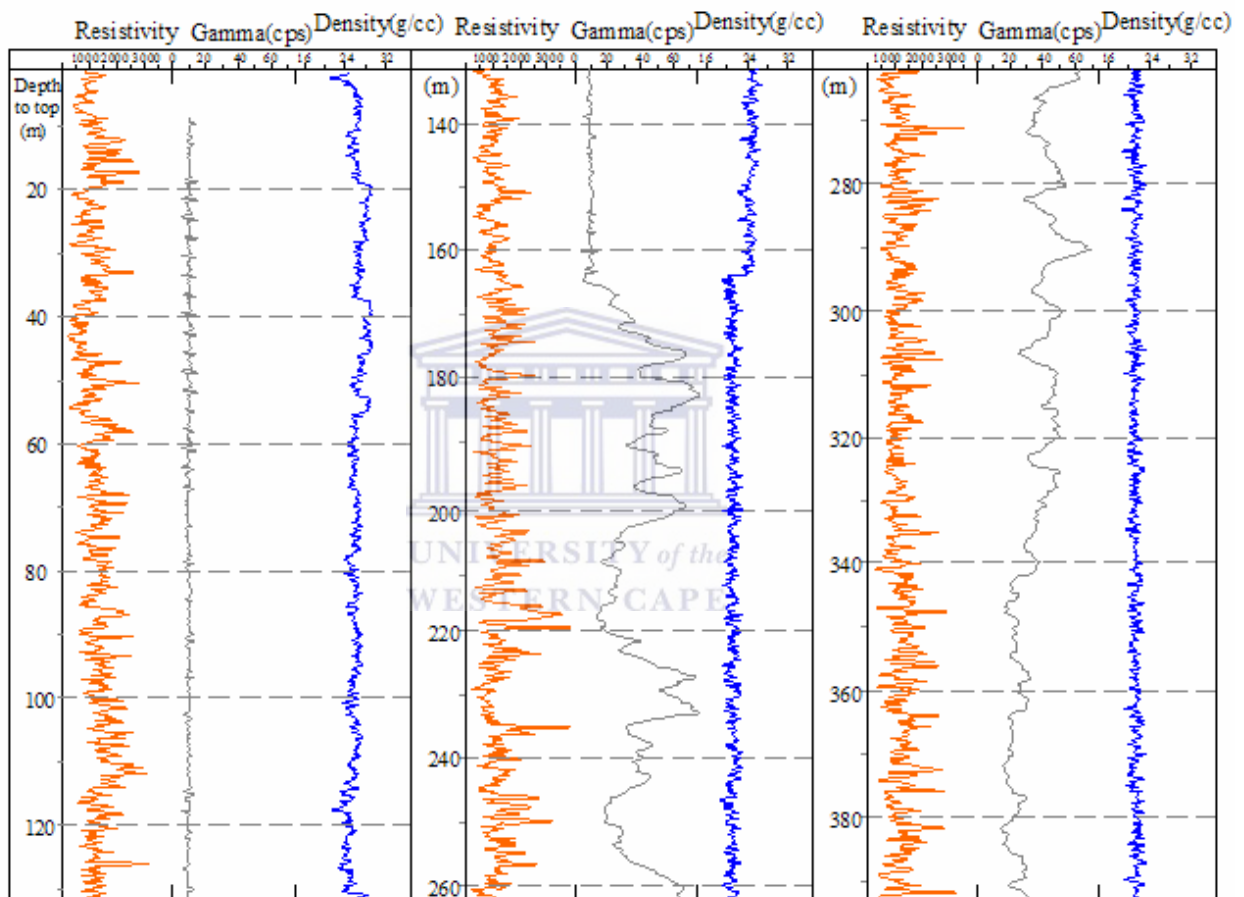


Fig. 4-2 Geophysical resistivity, gamma and density logs in the Rietfontein deep hole.

Table 4-2 shows a wide range of porosity resulted from various measurements, including laboratory test of core samples, in situ fracture aperture measurement, pumping test, and the application of satellite imagery. Generally, porosity of core samples and in situ aperture measurements represent a scale of meters. Porosity derived from pumping test is actually derived from storativity of a rock mass on a scale of tens of meters, which is highly dependent on a sound estimate of bulk modulus of the rock mass studied. Since remote sensing data can only be used for capturing the fractures with length of more than 100m, porosity from the

interpretation of lineaments is representing a study area in the scale of kilometers. The scale effect of porosity of the TMG rock is schematically presented in Fig.4-3, which can be recommended to the further work in this aspect for the estimation of aquifer storativity through porosity approach.

Fig.4-3 also reveals that porosity varies much even being measured at the same scale. For example, porosity analyses of few of the TMG core samples have been carried out (Table 4-2), using volumetric method. The result shows that the porosity of the TMG sandstones ranges from 1.0~3.6% with an average of 2.5%. These values greatly depend on both laboratory methods and selections of core samples. Moreover, the effect of stress release of the core samples after they are taken away from the original condition could have another impact on the estimation of porosity, from which difficulty of in-situ measurement and determining the variation of porosity at depth could arise. On the other hand, only the visible fracture measured could lead to the porosity value underestimated because the discarded micro-fractures in the rock mass still have a contribution to the n value.

Table 4-2 Porosity derived from core samples and pumping tests

Type of measure	Sample Depth [m]	Porosity [%]		Reference
		Range	Average	
Core samples	3322 -3420 [7 samples]	1.9 – 2.3	1.5	Core samples of Soekor boreholes. After, Roswell and De Swardt, 1967. non-TMG rocks
	122 – 154 [11 samples]	0.6 – 1.7	1.4	
	1 – 152 [49 samples]	0.9 – 5.4	3.1	
	10 – 107 [7 samples]	1.2 – 3.0	2.2	
	42.5 – 135.5 (5 samples)	1.2 – 3.6	2.5	
	Unknown (1 sample)	1	1	
Pumping tests	Koo Valley	0.01 – 0.35	0.06	Pumping tests, Jacob
	Kammanassie	0.11 – 0.22	0.15	Kotze (2002)
	Boschkloof	0.1 – 0.01	0.05	Umvoto (2000)
	Gevoden	0.21 – 1.2	0.57	Pumping tests, Jacob
Field measurement	Kirstenbosh,	0.04	0.26	Sandstone block measurement
	Rawsonvill,	0.52		Rock surface measurement
	Montague	0.22		Rock surface measurement
Remote sensing	Rawsonville		1.24×10^{-6}	Area shown in Fig.3-10

4.2.3 Storativity

Storativity can be obtained from the interpretation of well pumping tests, and tests of both rock mechanical property and porosity of rock mass. There is no available data for the latter which requires tremendous work including the identification and sampling of rock mass, and laboratory or field testing. Currently the storativity and other hydraulic properties of the TMG aquifers are generally derived from the interpretation of well pumping tests. In almost all of the existing wellfields, from the west Citrusdal municipality through Klein Karoo semiarid area to Uitenhage artesian basin developed in the TMG, such hydraulic tests have been conducted by different researchers and a lot of information have been yielded, from which the results of storativity are summarized in Table 4-3. These results show that storativity of the TMG fractured aquifers falls in a wide range of 10^{-2} to 10^{-5} , derived from the interpretation of data through various methods mostly based on Theis's theory for confined aquifer. In absence of detailed time-drawdown information, additional discussion on the applicability of the storativity values cannot be made. However, uncertainty of the results from the testing data is quite common in the fractured rock aquifers because of both the diversity of observed drawdowns and difference in the interpretive methods. In this sense, the storativity seems much preferable to be used in a value range rather than fixed value for regional studies.

For the estimation of storage and characterization of flow, the S value of less than 10^{-3} have been applied to groundwater resource evaluation for the TMG aquifers at a national scale by Vegter, 1995. Based on the study of Jia (2007), the storativity range of Peninsula Aquifer and Nardouw Aquifer respectively, is recommended as listed in Table 4-4 for the estimation of regional groundwater storage, in which the range of high value of 10^{-3} to low value of 10^{-5} is used as the value range of the storage coefficient of confined Peninsula Aquifer, and the range of 5×10^{-3} to 1×10^{-4} is assigned to the specific yield of unconfined Peninsula Aquifer. In terms of application, the scale-dependency of storativity should be considered, of which the variation can be regarded as that of porosity from a small scale to large scale as shown in Fig 4-3. Moreover, total discharge rate of 355 l/s of the 11 hot springs (Meyer, 2002) representing a kind of regional storage of the TMG aquifers probably indicates a limited storativity at the regional scale.

Table 4-3 Storativity of the TMG aquifer refers to various formations and areas

Wellfield	Formation	Reference	Storativity	Transmissivity (m ² /d)	Analysis method
Citrusdal	Peninsula	Umvoto-SRK (2000)	1×10 ⁻³ to 7×10 ⁻⁴	<10 to 200	FC* Recovery
Struisbaai	Peninsula/Nardouw	Weaver (1999)	8.6×10 ⁻³	15 to 200	Cooper-Jacob
Uitenhage	Peninsula/Nardouw	Maclear (2001)	2×10 ⁻⁴ to 5×10 ⁻²	<10 to 400	Unknown
Kleinmond-Bot River	Nardouw	Parsons (2001)	1 to 5×10 ⁻⁴	70 to 320	Jacob and FC
Klein Karoo	Peninsula/Nardouw	Kotze (2000)	1×10 ⁻⁴ to 1×10 ⁻²	10 to 200	FC
St Francis-on-sea	Nardouw	Rosewarne (1990)	1.8×10 ⁻³ to 3.3×10 ⁻³	55	Gringarten & Witherspoon
Rawsonville	Peninsula	UWC Groundwater Group (2006 to 07)	6.9×10 ⁻⁴ to 2.8×10 ⁻⁵	9 to 30	Cooper-Jacob, fault barricaded

* Flow characteristics method

Table 4-4 Recommended storativity values for TMG aquifers (Jia, 2007)

Aquifer Type	Range	Storativity	
		Specific yield (Unconfined)	Storage coefficient (Confined)
Nardouw	Low	7.0×10 ⁻⁵	7×10 ⁻⁶
	Medium	3.5×10 ⁻⁴	7×10 ⁻⁵
	High	3.5×10 ⁻³	7×10 ⁻⁴
Peninsula	Low	1×10 ⁻⁴	1×10 ⁻⁵
	Medium	5×10 ⁻⁴	1×10 ⁻⁴
	High	5×10 ⁻³	1×10 ⁻³

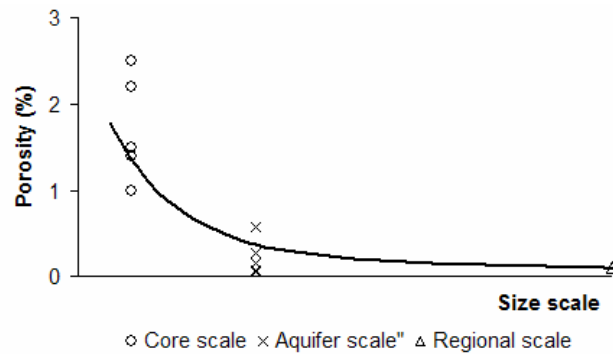


Fig.4-3 Map schematically shows scale effect of porosity in the TMG

4.3 Transmissivity of the TMG

4.3.1 Solution to hydraulic test

In a flow system, permeability (k) of the aquifer is one of the key hydraulic parameters to characterize the aquifer's ability to transmit groundwater from a high hydraulic head point to a low one. Considering the nature of fluid, hydraulic conductivity (K) is often used to represent aquifer's permeability. When taking into account the aquifer thickness (D), transmissivity (T) term is then used. This parameter of permeability becomes meaningful in terms of groundwater management for a specific aquifer. The relationship of these three is presented as follows:

$$K = k \cdot \frac{\rho g}{\nu}, \quad T = KD, \quad (4-6),$$

in which, ν is dynamic viscosity of fluid ($\text{N}\cdot\text{s}/\text{m}^2$).

In general, well pumping test provides an effective approach to estimating the average transmissivity of an aquifer; this approach is largely based on the traditional theory such as Dupuit, Hantush and Theis solutions, and etc, for a broad variety of aquifers and different boundary conditions at the external pumping stresses (Renard, 2005). Presently the most active interpretation techniques based on the Theis solution include straight line analysis and type curve matching of observed drawdown. The frequently used straight line analysis is based on a kind of asymptotic method and often yields both the early time and late time values from the determination of hydraulic properties, especially for fractured aquifers. It can be found from many textbook that the Theis solution is derived from the following well established equation for the radial transient flow in a confined aquifer.

$$\begin{cases} \frac{\partial^2 s}{\partial r^2} + \frac{1}{r} \frac{\partial s}{\partial r} = \frac{S}{T} \frac{\partial s}{\partial t}, & t > 0, S = S_s \cdot M \quad 0 < r < \infty \\ s(r, 0) = 0 \\ s(\infty, t) = 0, \quad \left. \frac{\partial s_w}{\partial r} \right|_{r \rightarrow \infty} = 0, & t > 0 \\ \lim_{r \rightarrow \infty} r \frac{\partial s}{\partial r} = -\frac{Q}{2\pi T} \end{cases} \quad (4-7)$$

in which s is the drawdown during the pumping test with a constant flow rate Q , r the distance to pumping well, t the time from the start of pumping test, T the transmissivity, S is the storativity and M thickness of the confined aquifer. By a series of inverse Hankel and other transformations, the Theis solution of the above equation with the specific conditions is:

$$\begin{cases} s = \frac{Q}{4\pi T} W(u) \\ u = \frac{r^2 S}{4Tt} \end{cases}, \quad W(u) = \int_u^\infty \frac{e^{-u}}{u} du \quad (4-8),$$

where $W(u)$ is defined as the Theis well function. It should be note that the validity of the governing Eq. (4-7) and the subsequent Theis solution are initially base on the following assumptions:

- 1) Confined aquifer with uniform thickness, horizontal dipping and isotropic properties.
- 2) Water of a constant discharge rate is pumped out a completely penetrating well with an infinitesimal radius.
- 3) Natural gradient is zero before the groundwater withdraw.
- 4) Darcy's law is governing flows.
- 5) Elastic release of the aquifer is instantly over, namely no aquifer storage effect takes place.

In Eq (4-8), the well function $W(u)$ can be opened up with serial number technique and truncated into approximate expression as the following:

$$W(u) = -0.577216 - \ln u + u + \frac{1}{4}u^2 - \frac{1}{18}u^3 + \dots + (-1)^{n+1} \frac{1}{n!}u^n$$

$$\xrightarrow{\text{if } u < 0.01} W(u) \approx -0.577216 - \ln u = \ln\left(\frac{2.25Tt}{r^2 S}\right) \quad (4-9),$$

To replace the well function of Eq.(4-8), the drawdown then is:

$$s = \frac{Q}{4\pi T} \left(\ln \frac{2.25T}{r^2 S} + \ln t \right) = \frac{2.3Q}{4\pi T} \left(\log \frac{2.25T}{r^2 S} + \log t \right) \quad (4-10).$$

This simplified $W(u)$ is generally termed Cooper-Jacob well function that normally causes less than 5% of error to the drawdown with $u < 0.1$. Therefore, this drawdown can be alternatively presented as:

$$\begin{cases} s = a_p + b_T \log t \\ a_p = b_T \log \frac{2.25T}{r^2 S}, \quad b_T = 0.183 \frac{Q}{T} \end{cases} \quad (4-11)$$

During a constant discharge pumping test, the piecewise data of drawdown (s_i) and time moment (t_i) used to be recorded in the form of unequally spaced data. Although more recently developed equipment such as Diver is able to capture the equally spaced data, it needs to be calibrated through thermometric and barometric compensations; and those data are currently scarce in many sites of the TMG. Assume that the relationship between drawdown s and log time t is linear as described in Eq. (4-11), using straight-line technique, the determination of parameter a_p and b_T in Eq. (4-11) may be easily carried out by means of least-square method

from which the T and S are estimated. In a single well test, given radius of the well is r_w , parameter a_p and b_T is presented as follow.

$$b_T = \frac{n \sum_{i=1}^n (s_i \cdot \log t_i) - \sum_{i=1}^n s_i \sum_{i=1}^n \log t_i}{n \sum_{i=1}^n (\log t_i)^2 - (\sum_{i=1}^n \log t_i)^2}, \quad a_p = \frac{\sum_{i=1}^n s_i - b_T \sum_{i=1}^n \log t_i}{n} \quad (i = 1, 2, \dots, n) \quad (4-12)$$

This kind of straight-line technique is frequently used to estimate both aquifers' transmissivity and storativity with data from pumping tests. However, problem arises when observed data set does not approach to a straight line.

4.3.2 Result from hydraulic test

In the TMG fractured aquifers, T values estimated by the methods mostly based on Theis Formula generally fall in a wide range from 9 to 400 m²/d with a big difference of two orders of magnitude (Table 4-3). From these results, it is extremely difficult to establish a regional understanding of the aquifer properties. The variation of the T values is largely due to the complexity of the aquifers with diverse hydrogeological settings, reflecting the anisotropic nature of the hydraulic property from both site to site and even borehole to borehole at a single site. At times interpretation models for hydraulic tests also yield a big uncertainty of the hydraulic property without carefully distinguishing the aquifer response to hydraulic test, particularly in a fractured aquifer. Except the Gevonden site where the pumping tests were conducted by the author, data from the other sites with unknown testing conditions posed many difficulties for further analysis on the estimation of aquifer hydraulic properties.

However, from the observed drawdowns during the pumping tests in the TMG aquifers, there are generally four categories of drawdown curves conceptualized in Fig.4-4 which represent different modes of the aquifer response to pumping tests:

- a) Approximate straight-line type with the linear relation of drawdown with log time roughly show a radial flow pattern, for which the straight-line interpretation technique can be applied.
- b) The stepwise drawdowns are commonly observed during constant-discharge pumping tests in the TMG fractured aquifers, from which estimation of aquifer hydraulic properties generally yields multiply results; and applicability of the T and S values seem to be very limited.

- c) Approximate S-type of drawdown curves is the other one kind of familiar drawdowns observed in the TMG aquifers, from which the early-time and late-time T and S values are generally calculated to represent the intrinsic aquifer properties.
- d) This type of drawdown curve is seldom observed in the TMG aquifers, but represents a kind of aquifer response to external stress, from which the T and S values can be tremendously small.

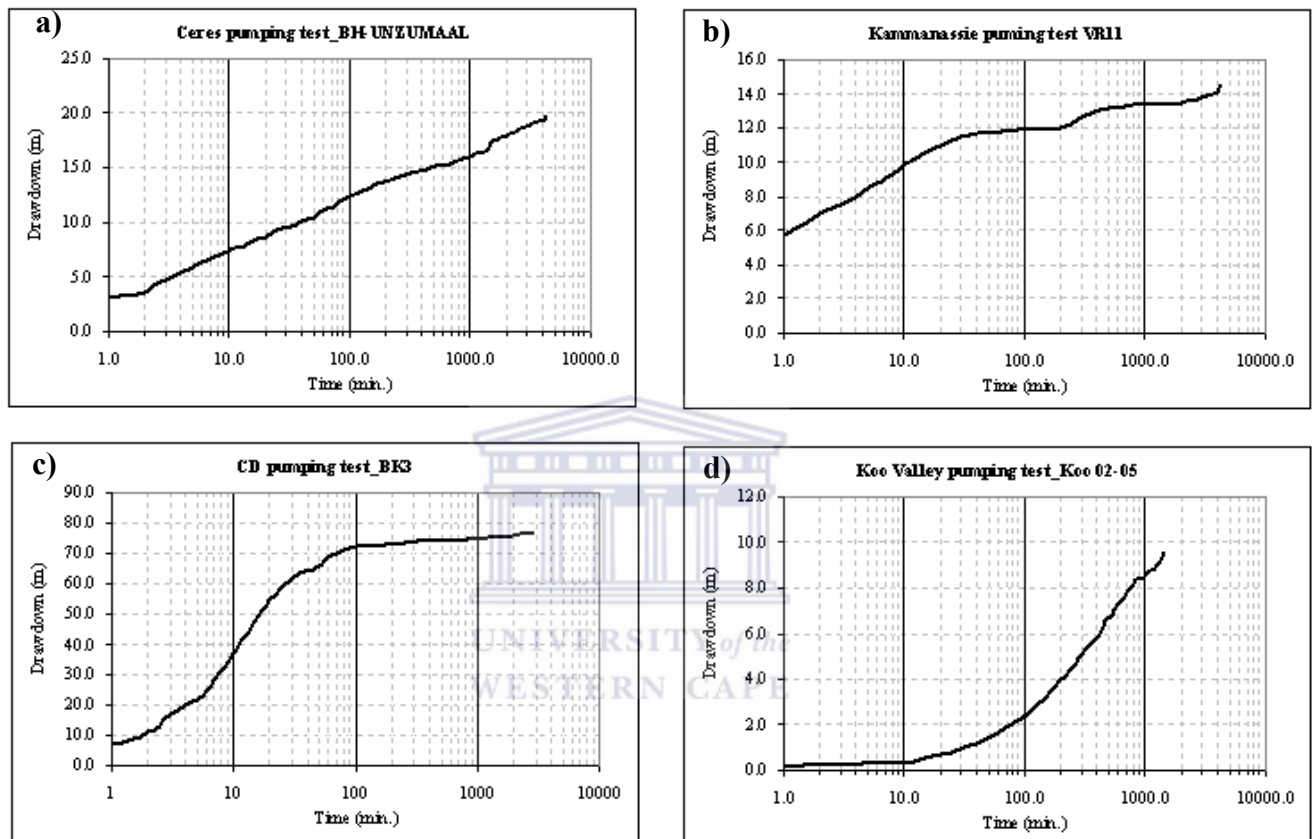


Fig.4-4 General four types of observed drawdowns and log time plot derived from the pumping tests in the TMG (please refer to the text for an explanation of a to d). CD – constant discharge.

4.3.3 Discussion on hydraulic test

The mechanism of aquifer response to pumping test remains unknown in previous studies of the TMG in which the estimation and explanation of aquifer's hydraulic properties are largely based on the analysis of drawdown curves. As discussed above (Fig.4-4), a drawdown curve of type-a can be regarded as a drawdown behavior in a relatively homogeneous aquifer with a sharp response to the external stress, being similar to that of pumping test in porous media. Drawdown curves of type-b and type-c commonly show the massive aquifer response to well water abstraction is tens of minutes lagged behind the commencement of the test. According to van Tonder et al (2002), the initial stage in both type-b and type-c is attributed to the well bore storage and skin effects. This means that the hydraulic properties must be estimated with

the data collected at the late time. After these effects, drawdown of type-b and type-c might divert to a “stepwise flow” and a radial flow respectively; at the late stage the latter can be regarded to be similar to that of type-a. The type-d can be conceptualized as flow to the pumping well is from an aquifer with a closed boundary; and in this time scale the aquifer has the least hydrogeological significance in terms of water supply.

As has been discussed in the Section 3.6.2 of Chapter 3, the stepwise type of drawdown is very common in the TMG sandstones and many other fractured rock aquifers in South Africa and is often explained as being set off by multiple boundary effects. It can be assumed that, along with the expansion of depression cone, multiple fracture flow systems with different hydraulic properties tend to provide water to a pumping well due to the change in pressure head, which is schematically illustrated in Fig.4-5. Based on this assumption, it is necessary to take a look at the time-dependent radius of cone of depression contributed by different fracture flow systems at a given time, by rearranging Eq.(4-10).

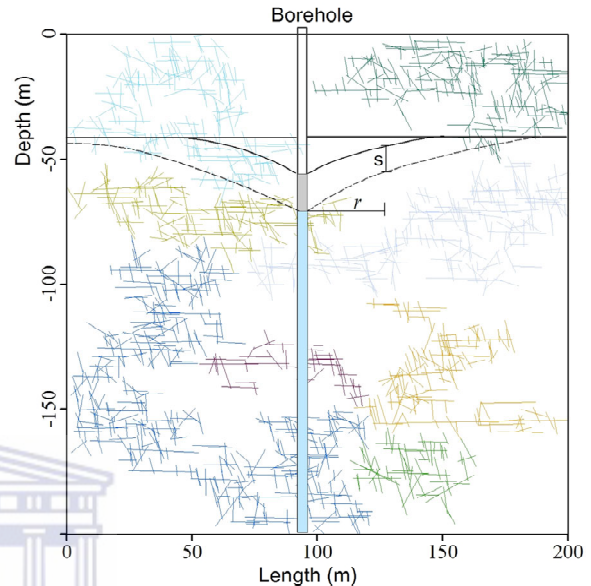


Fig.4-5 Schematic map showing the expansion of depression cone in fracture flow systems

$$s = \frac{Q}{2\pi T} \ln \frac{1.5(T_f \cdot t / S_f)^{1/2}}{r} \quad (4-13),$$

in comparison with the drawdown of the Dupuit Formula, the radius R of the cone at the given time t is:

$$R = 1.5 \left(\frac{T_f t}{S_f} \right)^{1/2} \quad (4-14),$$

in which T_f and S_f is, respectively, equivalent transmissivity and storativity, averaging out of the hydraulic properties of fracture networks involved in the flows to the abstraction well. The expressions of depression cone shed light on the necessity of studying the anisotropic hydraulic properties of TMG fractured aquifers.

On the other hand, analysis of pumping data based on the above solutions should integrate with the field geological observations. As has been discussed in the Section 3.2 of Chapter 3, almost all the wellfields developed in the TMG are fault-related, but very few site-specific studies in the TMG area have mentioned to take such structure into account when using the

Theis or Cooper Jacob solution to estimate both T and S values. In general, when a fault acts as a no-flow boundary, the image well method (Ferris et al, 1962) can be applied by positive superposition of the drawdown of the image well at the pumping well. Using this method, the T and S values have been both estimated for the Gevonden site with the data from pumping test. The result listed in Table 4-3 shows that, in comparison with an infinitely extended aquifer model at this site, the T values estimated from the fault-barricaded aquifer are much higher, but the S values almost go to the lower limit of that of the TMG aquifers.

4.4 Hydraulic conductivity study for the TMG aquifers

In terms of aquifer permeability, as aforementioned, in-situ hydraulic test yields the transmissivity or hydraulic conductivity in a manner of average at the testing scale; for a pumping test this scale can be tens of meters, while the result of a packer test normally represents the scale in meters. As groundwater flow is largely controlled by fractures or fracture network in a fractured rock aquifer, the directional hydraulic conductivity is crucial in the characterization of flow in the anisotropic aquifer. The following study of hydraulic conductivity is based on a published paper of the author (Lin and Xu, 2006).

4.4.1 Problem and objective

Darcy's law is always used to estimate the groundwater flow in both porous and fractured media, depending upon realistic estimates of aquifer hydraulic conductivities (viz. k) and hydraulic gradients (viz. J) at the scale of problem. In the case of fractured rock aquifer, presentation and determination of the hydraulic conductivity proves to be challenging. With respect to a fracture set with a mean aperture of b and a parallel face distance of d , the following classic expression is adopted for flow through the set of conduits (Talobre, 1957; Jaeger, 1972)

$$q = \frac{gb^3}{12\mu d} \cdot J \quad (4-15),$$

where μ is kinetic viscosity of fluid, which is 10^{-6} m²/s for water at 20°C, g the acceleration of gravity and J hydraulic gradient.

Eq. (4-15) represents an idealized type of flow behavior that has been intensively studied, both experimentally and numerically, by many researchers. The term of $gb^3/12\mu d$ in Eq. (4-15) is usually referred to as the hydraulic conductivity K for the set of fractures involved. For the determination of K value, many theories and methods have been developed. A series of

results for one of the intrinsic properties of fractured rock aquifers have been obtained to various extents for more than 30 years. As a summary, there are so far three approaches to the estimation of hydraulic conductivity of fractured rock aquifers, namely:

- 1) K tensor approach based on statistic or stochastic methods of *in-situ* fracture geometry and physical measurements.
- 2) Fracture property field and laboratory tests for the parameter K evaluation.
- 3) Inverse analysis on continuous or discontinuous problems depends on numerical models and parametric calibrations.

The estimation of K values through either pumping or packer test is based on the assumption that the groundwater is flowing through a geological continuum. It is often an expensive exercise to estimate and predict the regional aquifer properties (viz. K and J , etc) from local scale hydraulic tests. Also the large variation of K , both along borehole sections and in between holes, usually makes it difficult to determine the representativeness of the parameters in terms of ground water assessments. Even where a representative elementary volume (*REV*) can be defined, it may not be appropriate to directly apply the local test results to a regional aquifer. In porous media the *REV* can be very small, whereas in fractured media the *REV* may be very large or even does not exist in some cases (Kulatilake and Panda, 2000; Wang et al., 2002).

Statistic methods for determining hydraulic conductivity tensor were developed in 1980s (Hsieh and Neuman, 1985; Oda, 1985; Tian, 1988). The results from these methods can successfully indicate 3-D principle K values and directions by means of coordinate rotation of the incorporation of input data that derived from the surface measurements. The initial assumption of the tensor approach includes:

- 1) groundwater flow is exclusively governed by fractures;
- 2) the fractures through a rock matrix are well-connected, and
- 3) Flows between fracture sets do not interfere, or no deflection flow occurs.

For the ideal flow pattern with M sets of fractures involved in a study area, the hydraulic conductivity of the fracture sets is expressed in the form of matrix which reflects a sort of flow superposition:

$$\begin{cases} \overline{\overline{K}} = \sum_{i=1}^M \frac{gb_i^3}{12\mu d_i} \cdot K_{jl}^i, & j, l = x, y, z \\ K_{jl}^i = [I - \bar{n}^T \cdot \bar{n}] \end{cases} \quad (4-16)$$

where $\overline{\overline{K}}$ is the K tensor matrix accounting for the anisotropic nature of studied media, I is the unit matrix and \bar{n} is the direction cosine vector whose components are expressed in terms of

the dip azimuth β and dip angle α of the fracture sets in the coordinate system where the x, y axes are pointing to the north and east direction, respectively, while z axis is pointing upward. The elements of the matrix are depended on the geometric and physical parameters of fractures, which were studied by many others (Tian, 1989). From Eq. (4-16) two key K parameters, namely principal K values and orientations and their corresponding composite K value can be estimated by employing the techniques of linear algebra.

However the complexity of K in fractured rocks is far beyond what the existing models could handle since there are many geometrical and mechanical factors that impact on the flow through fracture gaps (Snow, 1969; Cook, 2001). Among them, fracture aperture is known to be most critical in controlling the quantity of flow, and the study of the aperture doubtlessly becomes a main focus in this study. The factors affecting the aperture of fractures include geometrical and mechanical properties of the fracture walls such as rigidity, roughness, mineral fillings, and stress level surrounding the fractures, in which the roughness has a crucial impact on the aperture around surface zone (Lomize, 1951; Louis, 1974; Patir and Cheng, 1978). Therefore, an expression of equivalent aperture due to roughness is suggested to calibrate the original K tensor model. Furthermore, by taking into account crustal stress, lithostatic and hydraulic pressures that act on fractures, together with the equivalent aperture, an expression of hydraulic aperture is accordingly developed for model calibration purpose.

4.4.2 Methodology

4.4.2.1 Adaptation of hydraulic conductivity tensor approach

It is well established that the direction of groundwater velocity (V) and hydraulic gradient (J) is usually not coincident with each other over time in fractured rock media. There is an included angle θ between V and J , and the J component on flow direction is

$$J_v = J \cdot \cos\theta \quad (4-17)$$

In an anisotropic medium, the K is not a scalar any more compared with isotropic one. The flow velocity is correspondingly expressed as follows:

$$\left. \begin{aligned} \vec{V}_x &= -(K_{xx} \frac{\partial H}{\partial x} + K_{yx} \frac{\partial H}{\partial y} + K_{zx} \frac{\partial H}{\partial z}) \mathbf{i} \\ \vec{V}_y &= -(K_{xy} \frac{\partial H}{\partial x} + K_{yy} \frac{\partial H}{\partial y} + K_{zy} \frac{\partial H}{\partial z}) \mathbf{j} \\ \vec{V}_z &= -(K_{xz} \frac{\partial H}{\partial x} + K_{yz} \frac{\partial H}{\partial y} + K_{zz} \frac{\partial H}{\partial z}) \mathbf{k} \end{aligned} \right\} \quad (4-18)$$

Where \mathbf{i} , \mathbf{j} , \mathbf{k} are the unit vectors on coordinate x, y, z respectively. Its parameter term is generally presented in the form:

$$\overline{\overline{K}} = \begin{bmatrix} K_{xx} & K_{xy} & K_{xz} \\ K_{yx} & K_{yy} & K_{yz} \\ K_{zx} & K_{zy} & K_{zz} \end{bmatrix} \quad (4-19),$$

Eq.(4-19) is the hydraulic tensor matrix, in which $K_{xy}=K_{yx}$, $K_{yz}=K_{zy}$, and $K_{xz}=K_{zx}$. Note that in Eq.(4-16) the expression of the row matrix \bar{n} is:

$$\bar{n} = [\cos \beta_i \sin \alpha_i \quad \sin \beta_i \sin \alpha_i \quad \cos \alpha_i], \quad i=1, \dots, M. \quad (4-20)$$

The above $\overline{\overline{K}}$ is a symmetric square matrix with three different eigenvalues and corresponding orthogonal eigenvectors satisfying the following relation:

$$(K_{ij} - \lambda_i \delta_{ij})U_i = 0, \quad U_i = [U_{ix} \quad U_{iy} \quad U_{iz}]^T, \quad i=1,2,3. \quad (4-21),$$

where δ_{ij} is Kronecker's symbol, λ_i the eigenvalues and U_i is the corresponding eigenvectors associated to λ_i . Eq. (4-21) is the representative of a homogeneous equation group and the solutions of λ_i and U_i ($i=1, 2, 3$) may be obtained from (4-22) and (4-23) respectively.

$$|K - \lambda I| = 0 \quad (4-22)$$

$$\begin{cases} (k_{xx} - \lambda)U_x + k_{xy}U_y + k_{xz}U_z = 0 \\ k_{yx}U_x + (k_{yy} - \lambda)U_y + k_{yz}U_z = 0 \\ k_{zx}U_x + k_{zy}U_y + (k_{zz} - \lambda)U_z = 0 \\ U_x^2 + U_y^2 + U_z^2 = 1 \end{cases} \quad (4-23).$$

Using U_i ($i=1,2,3$) as the basic vectors, the K tensor reduces to the diagonal matrix:

$$\overline{\overline{K'}} = \text{diag}[\lambda_1, \lambda_2, \lambda_3] \quad (4-24).$$

Hydrogeologically it is easy to understand that the λ_i ($i=1,2,3$) represent three principal K , namely $K_{p1}=\lambda_1$, $K_{p2}=\lambda_2$ and $K_{p3}=\lambda_3$, and the direction of K_{pi} is given by U_i . Whereby, the K value of a given sample site can be repented by the geometric mean of the three principal K :

$$K_{comp} = \sqrt[3]{K_{p1} \cdot K_{p2} \cdot K_{p3}} \quad (4-25).$$

Furthermore, the relationship between K components K_x , K_y and K_z along x, y, and z axes defined above and principal K tensor can be established via U_i

$$\begin{cases} K_x = K_{p1}U_{1x}^2 + K_{p2}U_{2x}^2 + K_{p3}U_{3x}^2 \\ K_y = K_{p1}U_{1y}^2 + K_{p2}U_{2y}^2 + K_{p3}U_{3y}^2 \\ K_z = K_{p1}U_{1z}^2 + K_{p2}U_{2z}^2 + K_{p3}U_{3z}^2. \end{cases} \quad (4-26)$$

Assuming that the flow direction is known (Fig.4-6), using Eqs (4-17) and (4-18) we have the following expression for K along flow direction:

$$K_V = \frac{\overline{\overline{V}} \cdot \overline{\overline{V}}}{\overline{\overline{V}} \cdot \overline{\overline{J}}} = \frac{(K_x \frac{\partial H}{\partial x} \mathbf{i})^2 + (K_y \frac{\partial H}{\partial y} \mathbf{j})^2 + (K_z \frac{\partial H}{\partial z} \mathbf{k})^2}{K_x (\frac{\partial H}{\partial x} \mathbf{i})^2 + K_y (\frac{\partial H}{\partial y} \mathbf{j})^2 + K_z (\frac{\partial H}{\partial z} \mathbf{k})^2} = \frac{1}{\frac{1}{V^2} (\frac{V_x^2}{K_x} + \frac{V_y^2}{K_y} + \frac{V_z^2}{K_z})} \quad (4-27).$$

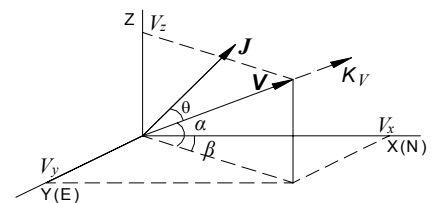


Fig. 4-6 Relationship between flow direction and hydraulic conductivity

Alternatively, using the projective relations of $V_x/V=\cos\beta\cdot\sin\alpha$, $V_y/V=\sin\beta\cdot\sin\alpha$ and $V_z/V=\cos\alpha$ (see Fig.4-6), one may also write that

$$\frac{1}{K_V} = \frac{\cos^2 \beta \sin^2 \alpha}{K_x} + \frac{\sin^2 \beta \sin^2 \alpha}{K_y} + \frac{\cos^2 \alpha}{K_z}. \quad (4-28)$$

The above analyses indicate that the three types of K values, namely geometric mean of K_{pi} ($i=1,2,3$), axial K_j ($j=x,y,z$) and flow direction K_V , are physically different. However, they are related through the K tensors and vector projections. The former (K_{comp}) may be accounting for the K value at a measuring site in the form of scalar that is averaged from three anisotropic principal K_{pi} . The K_i ($i=x,y,z$) are the projections of three principal K_{pi} along original system. Note that the quantity of K_V is not simply the quadratic sum of K_i ($i=x,y,z$) as it used to be because the flow direction K is more physically determined by the components of flow velocity and head gradient than geometrically determined by axial K . There exists a non-linear relationship between K_V and K_i ($i=x,y,z$). Accordingly, if there exist not less than two sets of foregone values of K_V and K_i ($i=x,y,z$) obtained from hydraulic tests and surface measurements respectively, it is possible to deduce the flow direction using the following linear equation:

$$(K_x^{re} - K_y^{re})x_1 + (K_y^{re} - K_z^{re})x_2 = K_V^{re} - K_z^{re} \quad (4-29),$$

where $x_1 = \cos^2 \beta \sin^2 \alpha$, $x_2 = \sin^2 \alpha$, $K_V^{re} = 1/K_V$, $K_i^{re} = 1/K_i$, $i = x, y, z$.

The above-mentioned relations have been programmed in MS Excel Workbook. For the model testing, the basic data were measured at sites of the *TMG* outcrops from which the aperture (b) and distance (d) are geometric mean values and the angles arithmetic ones. The computed results, using the above-mentioned models, are listed in Tab.4-5. The geometric mean of K in Tab.4-5 are ranging from 1 to 21 m/d which are much higher than those of borehole tests mostly ranging from 5×10^{-2} to 1.5×10^{-3} m/d. This is because the inevitable magnification of results when applying the measured data to the smooth plate model. Particularly, the apertures, measured at road cuttings and open quarries where the fractures that have long been undergone disturbance and stress release, tend to be dilated comparing with their original status.

The tensor method provides a tool to estimate K values for well-connected and purely fractured rocks. It is usually applied to the rock formations without relevant hydraulic test data. According to the assumptions of this method, for purely fractured rocks the method may lead to the overestimate of K values when the fractures are not fully connected, whilst it can underestimate the K for fractured porous media with significant permeability in matrix rocks. Although the K from the tensor approach may account for the anisotropic nature of studied

media, it should be noted that the basic data for the K computations are mean values of fracture sets. No matter what types of mean values are taken in the calculation, they are derived from in-situ measurements; so the accuracy of the computed K is dependent on the quality of the measurements. In particular, the aperture usually measured by feeler gauge on a rock exposure is the most sensitive factor in determining K . To minimize the possible influences of weathering or disturbance, multiple readings of aperture value should be taken at a single fracture. Moreover, JRC (joint roughness coefficient) can be sensitive to the K values; thus both the field-scale length profiles and the lab-scale core fractures need to be comparatively scanned to estimate JRC.

Table 4-5 Calculated K values from surface fracture measurements

K Values Site No.	Principal K values (m/d)				Axial K values (m/d)		
	K_{p1}	K_{p2}	K_{p3}	Geometric mean	K_x	K_y	K_z
1-Robertson	2.313	1.880	0.437	1.239	1.940	2.029	0.662
2-Simon's Town	13.816	11.858	2.176	7.091	13.039	12.261	2.550
3-Bot River	38.538	31.257	8.622	21.818	23.741	26.521	28.153
4-Grabouw	13.258	11.804	1.869	6.639	11.121	10.263	5.549
5-Theawaterschloof	6.355	6.007	0.543	2.748	1.554	5.507	5.844

UNIVERSITY of the
WESTERN CAPE

4.4.2.2 Calibration of hydraulic conductivity tensor approach

Equation (4-15) for groundwater flow in fractures is derived from the Navier-stokes differential equation for pressure-induced laminar flow through the gap of two flat parallel plates where the hydraulic aperture is assumed to be uniform. The actual condition of the TMG is quite different, as the rocks including fractures have undergone phases of deformations or even distortions. What can be measured at rock outcrops is the mechanical aperture (Olsson and Barton, 2001) mostly ranging from 1 to 10^{-3} mm. The hydraulic aperture discussed here is regarded as the effective aperture for groundwater flow and can be obtained or inferred from both tracer tests (Charles, 1988) and laboratory experiments. Taking into account the main influencing factors, i.e. roughness and stress condition, Eq. (4-16) can be rewritten by adding the correction coefficients due to fracture roughness and stress condition respectively:

$$\bar{K} = \sum_{i=1}^M \frac{gb_i^3}{12\mu d_i} C_{er} \cdot C_{es} \cdot K_{jl}^i, \quad j, l = x, y, z \quad (4-30)$$

Where C_{er} is the correction coefficient of roughness and C_{es} the correction coefficient of stress condition. From Eq. (4-30), it is easy to understand that the hydraulic aperture is the following:

$$b_h = (C_{er} \cdot C_{es})^{1/3} b. \quad (4-31)$$

Letting $b_{er} = C_{er}^{1/3} b$, the b_{er} may be regarded as the equivalent aperture due to fracture roughness. Correspondingly, letting $b_{es} = C_{es}^{1/3} b_{er}$, the b_{es} is the equivalent aperture due to stresses acting on the rough fracture surface, namely the hydraulic aperture. Therefore, the following sections are focused on the discussion and determination of the C_{er} and C_{es} , respectively, with the intention of the calibration of the tensor model.

1. Fracture roughness

In the TMG rocks, fractures have rough walls and variable apertures and the internal properties of individual fractures that control groundwater flow are still poorly understood. The influence of roughness on fracture apertures has long been discussed and analyzed by many others. Among them the important contributions are those of Lomize (1951), Louis (1974) and Barton et al. (1985).

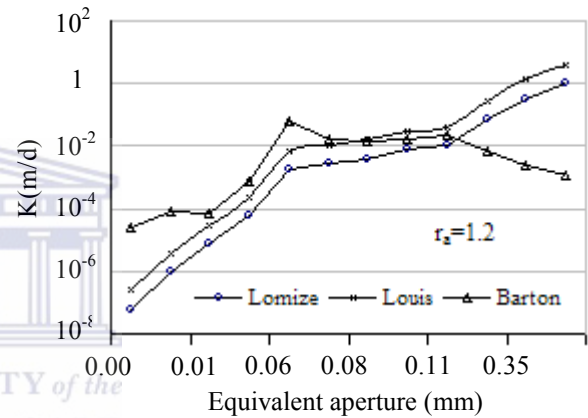


Fig.4-7 K Versus b_{er} by various roughness models using data measured from the TMG sites

Different expression of the aperture

correction coefficient due to roughness listed in Table.4-6 is a compilation of the results from them. A comparison of K values obtained from the different models is plotted in Fig.4-7, where the C_{er} from Lomize and Louis' models shares the same form where the hydraulic radius is $2b$ in Louis' model.

Table 4-6 Mechanical aperture correction coefficient C_{er}

Formula	Source	Remark
$C_{er} = \frac{1}{1.0 + 6.0(r_a)^{1.5}}$	Lomize (1951)	r_a —relative roughness $r_a = \Delta/b$, Δ -asperity
$C_{er} = \frac{1}{1.0 + 8.8(r_a)^{1.5}}$	Louis C (1974)	$r_a = \Delta/D_h$, D_h -hydraulic radius
$C_{er} = \frac{b^3}{(JRC)^{7.5}}$	Barton et al. (1985)	b —mechanical aperture (mm) JRC —joint roughness coefficient

Given the parameter measurements, it seems more practicable to apply Barton's JRC model for macroscopic fracture sets. That is

$$b_{er} = \frac{b^2}{JRC^{2.5}} \quad (4-32),$$

in which b is the mechanical aperture basically measured by feeler gauge and JRC the joint roughness coefficient that can be measured with a profilometer in a field or laboratory scale, and b_{er} is the equivalent aperture calibrated by the roughness other than the hydraulic aperture in this study.

It used to be known that the groundwater flow is dominated more by the bedding fractures within the zone from surface to weakly weathered bedrocks than the structural joints because of the higher mechanical apertures within the bedding fractures. However in most of the *TMG* rocks around the measuring sites, the bedding fractures tend to have a relatively higher JRC value in the range of 2~6. Comparatively, the JRC of the structural or conjugate joints is mainly in the range of 1~3. By applying equivalent aperture b_{er} to the tensor model introduced, the difference of K values between bedding and structural fractures is quite small and the results are listed in Tab.3. Note that the K value for the joint set at site 5 is about one order of magnitude higher as that of bedding fractures. It is attributed to the relatively rougher surfaces in bedding fractures produce more impedance to the inner flow on the surfaces than that of structural joints even though bedding fractures are much longer than structural joints.

Table 4-7 K values for bedding and structural fractures

Index	Bedding Fracture		Structural joint set	
Site No.	Mean JRC	Mean K (m/d)	Mean JRC	Mean K (m/d)
2	3.5	4.35×10^{-4}	1.4	3.88×10^{-4}
4	3	8.21×10^{-4}	1.5	7.13×10^{-4}
5	3.5	9.29×10^{-5}	1.25	2.681×10^{-4}

The comprehensive impact of roughness due to bedding and structural fractures in the *TMG* sites on the K value is listed in Table 4-8. Comparing with the computed results for the 5 sites in Table 4-7, the difference of the average K and axial K values is obvious with three orders of magnitude of K value between smooth and rough fractures. The K results in Table 4-8 can also be roughly consistent with those from pumping tests in the *TMG* aquifers.

Table 4-8 Fracture *JRC* and corresponding *K* values

Index Site No.	Mean <i>JRC</i>	Mean Length (m)	Mean <i>K</i> (m/d)	Axial <i>K</i> (m/d)		
				<i>K_x</i>	<i>K_y</i>	<i>K_z</i>
1	1.7	29.2	1.45×10 ⁻³	6.05×10 ⁻³	5.24×10 ⁻³	9.70×10 ⁻⁴
2	2.4	34.74	2.33×10 ⁻³	3.02×10 ⁻³	2.33×10 ⁻³	2.04×10 ⁻³
3	2.2	9.25	1.623×10 ⁻²	1.88×10 ⁻²	2.18×10 ⁻²	2.13×10 ⁻³
4	2.3	20.50	1.47×10 ⁻³	2.06×10 ⁻³	1.03×10 ⁻³	1.62×10 ⁻³
5	2.4	14.52	1.77×10 ⁻³	2.04×10 ⁻³	1.16×10 ⁻³	2.95×10 ⁻³

2. Combined stress conditions

The properties of a rock mass may change substantially under a certain stress or confined conditions, as opposed to those on the surface. In most cases, crustal stresses or lithostatic pressure acting on a rock mass tends to volumetric reduction. The functional dependency of rock properties with respect to the change in stresses or confined conditions has been studied by many researchers (Goodman, 1974; Bandis et al., 1983). In terms of hydromechanical coupling in fractured rocks, Rutqvist and Stephansson (2003) give a full review that can be traced back to Jacob's storativity

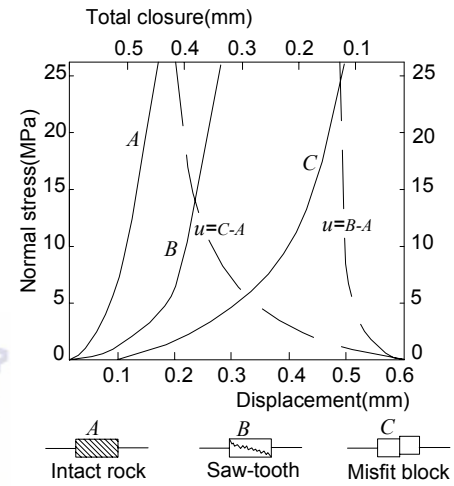


Fig.4-8 Rock mass displacement and fracture closure under normal stress (after Goodman, 1974)

expression in 1940s. Bandis et al. (1983) establishes an expression for fracture displacement under a normal stress condition:

$$u_n = \frac{\sigma_N u_{max}}{K_{ni} u_{max} + \sigma_N} \quad (4-33).$$

In this expression, u_n is the displacement under the normal stress σ_N acting on the fracture surface, K_{ni} the initial normal stiffness of fracture and u_{max} is the maximum closure (Fig.4-8). For shear tests of fractures, Barton et al. (1985) also develops an empirical formula to express the relationship between normal and shear displacements:

$$du_{ns} = du_s \tan d_m \quad (4-34),$$

where d_m is the mobilized dilatation angle and it can be determined as follow (Olsson and Barton, 2001):

$$d_m = \frac{1}{M} JRC_m \log_{10}(JCS/\sigma_N) \quad (4-35)$$

where M is the damage coefficient, JRC_m the mobilized joint roughness coefficient, and JCS the compressive strength of the joint wall.

It is assumed that an arbitrary fracture surface, with a dip azimuth of β and dip angle of α , is subject to a combined three dimension stresses $[\sigma_x, \sigma_y, \sigma_z, \tau_{xy}, \tau_{yz}, \tau_{zx}]^T$, the normal stress σ_N and shear stress τ_s acting on the surface may be expressed as:

$$\begin{cases} \sigma_N = l^2\sigma_x + m^2\sigma_y + n^2\sigma_z + 2lm\tau_{xy} + 2mn\tau_{yz} + 2nl\tau_{zx} \\ \tau_s = [(l\sigma_x)^2 + (m\sigma_y)^2 + (l\sigma_z)^2 - \sigma_N]^{\frac{1}{2}} \\ l = \cos\beta \sin\alpha, \quad m = \sin\beta \sin\alpha, \quad n = \cos\alpha \end{cases} \quad (4-36).$$

In the present case, because rocks are normally subjected to compression by lithostatic pressure, it is convenient to denote the normal and shear stresses on the oblique fracture surface in the case of $\sigma_x = \sigma_y$.

$$\begin{cases} \sigma_N = \frac{\sigma_z + \sigma_x}{2} + \frac{\sigma_z - \sigma_x}{2} \cos 2\alpha + \tau_{zx} \sin 2\alpha \\ \tau_s = \frac{1}{2}(\sigma_z - \sigma_x) \sin 2\alpha + \tau_{zx} \cos 2\alpha \end{cases} \quad (4-37).$$

Whence, the maximum and minimum values of σ_N and maximum value of τ_s may be obtained with respect to the derivatives of $\partial\sigma_N/\partial\alpha=0$ and $\partial\tau_s/\partial\alpha=0$, these yield:

$$\begin{cases} \sigma_{\max} = \frac{\sigma_z + \sigma_x}{2} + \sqrt{\left(\frac{\sigma_z - \sigma_x}{2}\right)^2 + \tau_{zx}^2} \\ \sigma_{\min} = \frac{\sigma_z + \sigma_x}{2} - \sqrt{\left(\frac{\sigma_z - \sigma_x}{2}\right)^2 + \tau_{zx}^2} \\ \tau_{\max} = \frac{\sigma_{\max} - \sigma_{\min}}{2} \end{cases} \quad (4-38).$$

Fractures mainly control the deformation of a rock mass, and they may response to the change of normal or shear stresses even no failures happen; these can be formulated by the relations between the stress and strain increments:

$$\begin{cases} d\sigma_N = K_n \cdot d\varepsilon \\ d\tau_s = G \cdot d\gamma \end{cases} \quad (4-39),$$

where K_n (kN/m) is the stiffness of fracture walls, approximately, $k_n = E/(\pi L_f)$; G is the fracture rigidity modulus, $G = E/2(1+\nu)$, E the elastic modulus (MPa), L_f the fracture length (m), and ν is the Poisson's ratio. Whence, the increments of strains may be expressed in terms of the increments of displacement:

$$\begin{cases} d\varepsilon = du_n / (b_{er} - u_n) \\ d\gamma = du_s / b_{er} - u_s \end{cases} \quad (4-40)$$

in which b_{er} is the equivalent aperture due to roughness, u_n the normal displacement and u_s shear displacement of the fracture. Using Eqs (4-39) and (4-40) yields:

$$\begin{cases} d\sigma_N = \frac{K_n}{b_{er} - u_n} \cdot du_n \\ d\tau_s = \frac{G}{b_{er} - u_s} \cdot du_s \end{cases} \quad (4-41).$$

The first equation in Eq. (4-41) may be integrated with respect to σ_N and u_n respectively. This yields:

$$u_n = b_{er} [1 - \exp(-\frac{\sigma_N}{K_n})]. \quad (4-42).$$

In the case of shearing displacement in Eq. (4-42), the integral may be performed using Eq. (4-37)~(4-38) and assuming that $d_m \approx \tan d_m$:

$$\int_0^{\tau_s} \frac{d\tau_s}{G} = \int_0^{u_{ns}} \frac{1}{b_{er} d_m - u_{ns}} du_{ns}. \quad (4-43).$$

We obtain

$$u_{ns} = b_{er} \frac{1}{M} JRC_m \log_{10}(JCS / \sigma_N) [1 - \exp(-\frac{\tau_s}{G})] \quad (4-44).$$

Eqs (4-34) and (4-35) give expressions for the fracture displacement under normal stress and shear stress, respectively. Note that in these equations the normal stress term can be applicable to effective stress, i.e. $\sigma_e = \sigma_N - r_w h_w$. Considering the relationship between changed fracture aperture and the displacement under combined stress conditions, we have the hydraulic aperture b_h :

$$b_h = b_{er} - u_n + u_{ns} = b_{er} C_{es}^{1/3} \quad (4-45),$$

$$C_{es} = \left\{ \exp(-\frac{\sigma_e}{K_n}) + \frac{1}{M} JRC_m \log(JCS / \sigma_e) [1 - \exp(-\frac{\tau_s}{G})] \right\}^3. \quad (4-46).$$

Using Eqs (4-31) and (4-32), ultimate hydraulic aperture expression is:

$$b_h = b \cdot \frac{b}{JRC^{2.5}} \cdot \left\{ \exp(-\frac{\sigma_e}{K_n}) + \frac{1}{M} JRC_m \log(JCS / \sigma_e) [1 - \exp(-\frac{\tau_s}{G})] \right\} \quad (4-47)$$

4.4.3 Application to the field data

It is obvious from the above hydraulic aperture expression that the hydraulic aperture is affected by both the physical and the mechanical properties of the fractures, particularly the roughness and the stress level on fracture walls. The importance of this hypothetical model is that most of fractured rocks in the TMG area with a thickness of 900~4500m are untouchable with current investigation tools; and except some wellfields can be used for exploration purpose, the majority of TMG area are uninvestigated. For this purpose the predictive models for hydraulic conductivity and flow behavior are necessary and might become a key tool if validated.

4.4.3.1. Hydraulic conductivity at borehole site

The model of hydraulic aperture that incorporates the roughness and combined stress condition was applied in the Rietfontein, Boschklouf and Gevonden borehole sites, respectively. Using the fracture data as listed in Table 4-9 and the basic properties of rock materials given in Fig.4-9, the computed K results are listed in Table 4-10. The hydraulic conductivity calculated for the Rietfontein site is 6.89×10^{-4} m/d (7.97×10^{-9} m/s), the K for Boschklouf site is 4.00×10^{-3} m/d (4.63×10^{-8} m/s), and Gevonden site 5.45×10^{-4} m/d (6.32×10^{-9} m/s), respectively. Among them, the K of the Boschklouf site is much less than that from pumping test; for example it about one order of magnitude less than the K value estimated with pumping test data at the borehole BK3 from which the K is estimated as 1.9×10^{-7} m/s through FC method (Hartnady and Hey, 2002). In this regard, the hydraulic tensor approach appears to yield the K value lower than that of hydraulic tests. However, in comparison with the packer test results from the borehole BH-1 and BH-2 at the Gevonden site, the average K value through tensor method (6.32×10^{-9} m/s) roughly matches the packer tests result mostly falls in the range of 6.14×10^{-2} to 4.68×10^{-5} m/d (10^{-7} to 10^{-10} m/s) (Fig.4-10). This suggests that the K value estimated by the tensor method probably represents the hydraulic conductivity of fractured rocks at a relatively small scale, scale of meters.

Table 4-9 Data sets of fractures from surface measurements

Site	Statistic mean Item	Dip β ($^{\circ}$)	Dip angle α ($^{\circ}$)	Physical aperture (mm)	Spacing (mm)	Roughness (JRC)	Mean length (m)	
Rietfontein	Basic data set	Set 1	66.80	6.42	0.22	463.30	2.20	12.55
		Set 2	67.43	78.28	0.15	290.00	1.20	8.86
		Set 3	205.30	71.07	0.17	271.10	1.40	6.99
		Set 4	157.25	77.11	0.03	437.20	1.00	5.16
Boschkloof	Basic data set	Set 1	243.88	40.09	0.19	408.10	2.10	16.31
		Set 2	330.48	76.76	0.15	270.00	1.30	7.29
		Set 3	93.89	79.02	0.17	341.43	1.30	5.06
		Set 4	62.41	39.70	0.21	680.00	1.20	13.94
		Set 5	221.33	62.44	0.25	303.57	1.50	4.50
Gevonden	Basic data set	Set 1	95.13	19.73	0.16	854.29	3.0	20.78
		Set 2	212.87	71.43	0.27	520.00	1.5	8.72
		Set 3	145.34	81.88	0.05	421.82	1.5	9.12
		Set 4	274.18	80.82	0.10	529.09	1.2	8.56
Distribution		normal	normal		uniform		log-normal	

4.4.3.2 Hydraulic conductivity at depth

The decrease in hydraulic conductivity with depth perhaps implies that fractures tend to be closed with depth. Fig.4-9 shows the relationship between the calculated hydraulic conductivity and depth at the three sites. It is clear that the reduction of hydraulic conductivity (K) with depth roughly follows a negative exponential law with different exponents. At the Rietfontein site, for example, the K value on the surface is 7×10^{-4} (m/d), but then decreases to 9.4×10^{-6} (m/d), 1.29×10^{-7} (m/d) and 8.2×10^{-11} (m/d) at depths of 200 m, 400 m and 750 m, respectively. Unfortunately, there are no in-situ hydraulic test data available in this area to confirm the model predictions.

In 2006, some packer tests were conducted along with the core drilling in boreholes BH1 (from 19.2 m to 113 m) and BH2 (from 7 m to 200 m) at the Gevonden site (see Fig.5-1) where a network of five holes, which penetrate Peninsula formation and the bottom of the Nardouw subgroup of the TMG, has been established for the study of aquifer properties and groundwater monitoring. Fig.4-10 presents the results of the single-packer tests with a test interval of 6 m in the two boreholes. In comparison, the reduction of calculated K value with depth is a bit faster than that of packer tests. Although the K values are different, it is clear that the K generally decreases with depth. The relationship between hydraulic conductivity and depth of the two boreholes have the same pattern.

Table 4-10 Computed K values based on the data set of Table 4-9

Item		i=1	i=2	i=3	
Rietfontein	Principal K (m/d)	K_{pi} (m/d)	1.22×10^{-3}	1.01×10^{-3}	2.65×10^{-4}
		Dip ($^{\circ}$)	312.26	46.77	203.45
		Dip angle ($^{\circ}$)	9.43	25.31	62.75
	Axial K	$K_x = 7.827 \times 10^{-4}$	$K_y = 5.923 \times 10^{-4}$	$K_z = 1.120 \times 10^{-3}$	
	Geometric mean of K_{pi}	6.89×10^{-4}			
Boschkloof	Principal K (m/d)	K_{pi} (m/d)	5.92×10^{-2}	5.74×10^{-2}	3.18×10^{-3}
		Dip ($^{\circ}$)	205.410	135.463	249.662
		Dip angle ($^{\circ}$)	37.742	23.892	42.780
	Axial K	$K_x = 4.53 \times 10^{-3}$	$K_y = 3.77 \times 10^{-3}$	$K_z = 4.17 \times 10^{-3}$	
	Geometric mean of K_{pi}	4.00×10^{-3}			
Gevonden	Principal K (m/d)	K_{pi} (m/d)	2.528×10^{-3}	2.503×10^{-3}	2.567×10^{-5}
		Dip ($^{\circ}$)	32.179	123.115	213.221
		Dip angle ($^{\circ}$)	71.427	0.315	18.570
	Axial K	$K_x = 9.470 \times 10^{-4}$	$K_y = 1.836 \times 10^{-3}$	$K_z = 2.274 \times 10^{-3}$	
	Geometric mean of K_{pi}	5.457×10^{-4}			

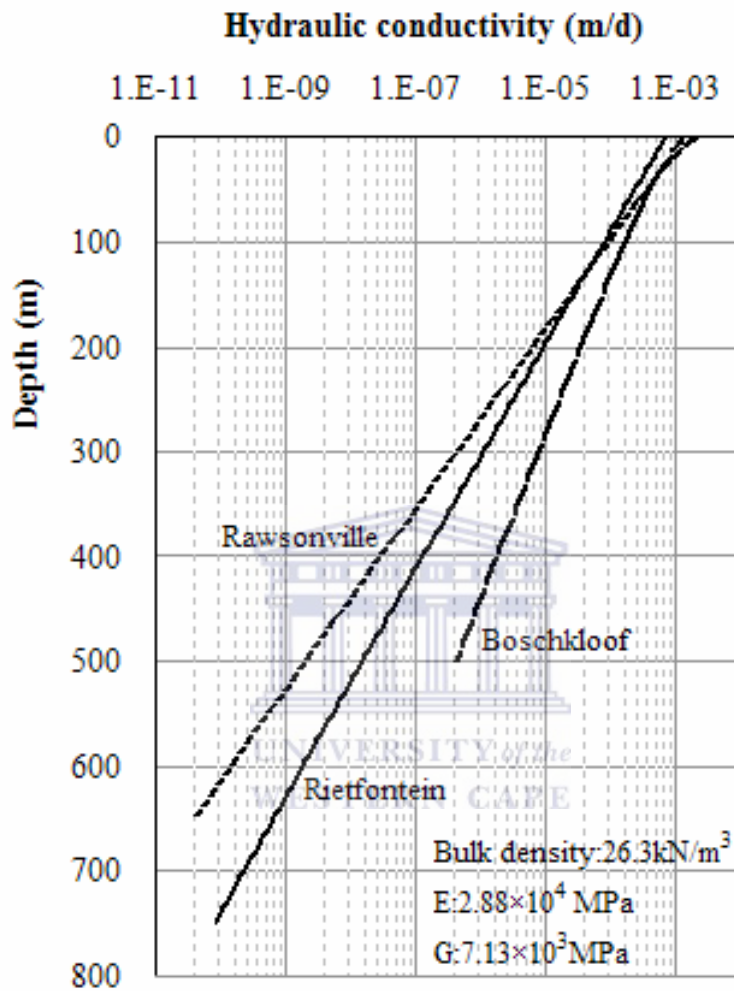


Fig.4-9 Hydraulic conductivity plot against depth of the Rietfontein, Boschkloof and Gevonden sites, using a tensor approach, based on the data measured on the surface and taking into account the impacts of fracture roughness and lithostatic pressure

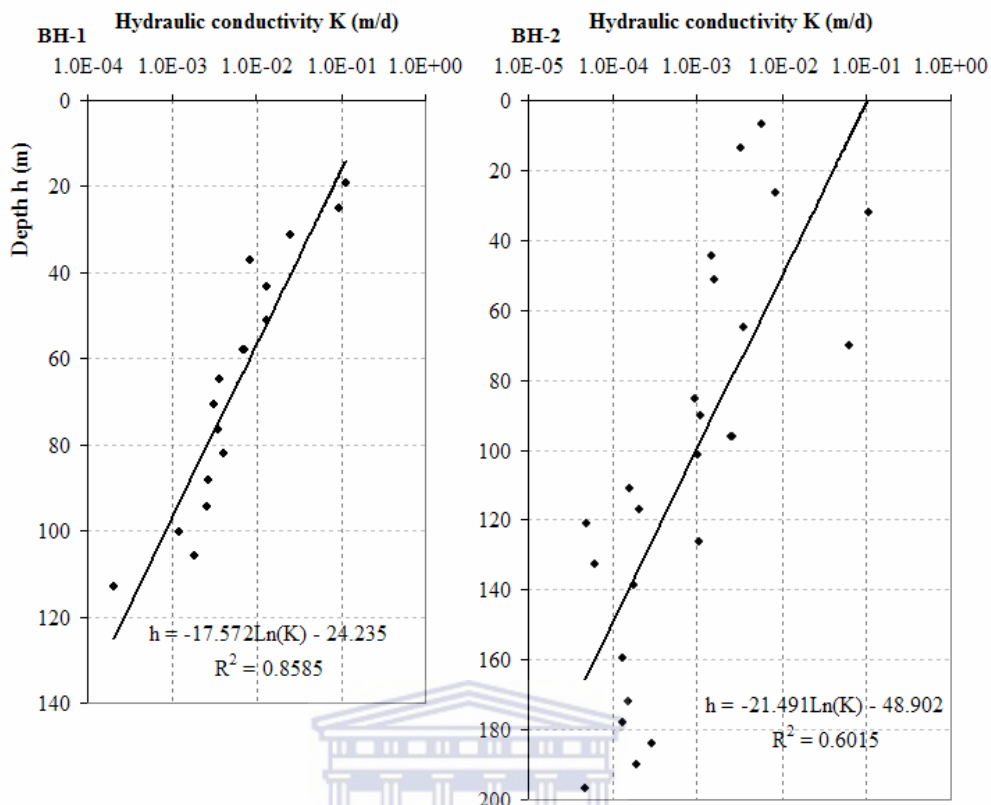


Fig. 4-10 Hydraulic conductivity plot against depth of the TMG sandstone aquifer where the single-packer tests were conducted with an interval of 6 m in boreholes BH1 and BH2 at the Gvonden site. In the trendline equations, h is the depth from the surface and R² the coefficient of confidence

4.5 summary

To characterize storage and flow of groundwater in the TMG aquifers, it is most important to study their hydraulic properties, including porosity and storativity, and transmissivity and hydraulic conductivity, although the estimation uncertainty of these parameters always exists through different approaches.

There are two major ways to determine aquifer storativity, one is through the porosity estimation of rock formation and the other is derived from pumping tests. Laboratory test of rock samples, field measurement of rock blocks, derivation of pumping test data, and the interpretation of geophysical data and remote sensing, yield a wide range of porosity values, from which the scale-dependency of the porosity is revealed and discussed. The conversion of the porosity to aquifer storativity requires a proper estimate of bulk modulus of the rock mass; in this regard, there is tremendous work to be done in the field of hydrogeology in South Africa.

In terms of aquifer permeability, most of transmissivity results of the TMG aquifers have been derived from hydraulic tests, especially the pumping tests have yielded a wide range of the transmissivity values from 9 to 400 m²/d which leads to draw a brief conclusion that the TMG aquifers are highly anisotropic both in regional and local scales. Further more, the applicability of the interpreted results is also discussed through the analysis of four types of familiar drawdown observed in the TMG aquifers. It is observed that both drawdown-based and model-based interpretations of hydraulic tests need to integrate with the geological observations, especially in the TMG aquifers where boreholes are mostly sited to be close to hydrogeological boundaries such as fault structure and lithological contacts.

The hydraulic conductivity of the TMG aquifers is mainly controlled by fractures or fracture network, a new tensor approach is proposed. For the prediction of hydraulic properties of the anisotropic TMG aquifers, fundamental principles of K tensor and some problems with their application to groundwater flow are discussed. It is observed that the K value tends to be higher than that of hydraulic tests because the data sets measured on surface are often overestimated with respect to the fracture apertures even by means of scientific sampling and statistic methods. It is also pointed out that different types of K values derived from K tensor approach have different meanings physically, although they are related. For the use of calibration coefficient of roughness C_{er} , it is recommended that Lomize's model be used for microscopic fractures and Barton's model for relative macroscopic ones.

The results is compared with those from field tests and in turn the tensor model is calibrated to meet the changes in fracture features and fracture setting conditions, from which a depth model of K is accordingly proposed and comparatively studied with the data from hydraulic tests.

The derivation of negative exponential form of hydraulic aperture is based fundamentally on rock mechanics by considering both fracture roughness and stress conditions. Comparing with the results from hydraulic tests at three sites, it is found that the K values estimated through the tensor model may represent that of a relatively small scale in meters; and this scale is dependent on the size of fractures collectively measured. Using this calibrated model it is possible to calculate the hydraulic conductivity at depth, by assuming that the rock masses in an aquifer are subjected to lithostatic pressure. The computed results show that the reduction of K over depths roughly follows a negative exponential law with different exponents. This is also confirmed by the results of packer tests conducted in the Gevonden site and can be compared with that of Snow (1969). The tensor model provides a scientific tool to predict the hydraulic property of the TMG aquifers both on the surface and at depth.

Chapter 5

A site-specific study of hydraulic properties

5.1 Introduction

There are no consistent results that can help to draw a conclusion on the hydraulic properties of the TMG aquifers (Rosewarne, 2002). A common understanding is that the TMG fractured rock aquifers are highly anisotropic at both regional and the local scales. Due to the complexity of geometric and hydraulic properties of these aquifers, the study of site-specific groundwater problems has long been the main target of hydrogeologists involved in relevant researches. So far, the most thorough case study in the field of fractured rock aquifers has concentrated on the Kammanassie wellfields, where carefully designed borehole networks have been developed, and investigations into aquifer properties (Kotze, 2002), groundwater recharge (Wu, 2005), numerical modeling for groundwater storage evaluation (Jia, 2007), and etc carried out. Although discrepancies have arisen from the researches at different study angles, the wealth of data produced is definitely helpful, to a large extent, for the understanding of fractured rock aquifers. On the other hand, because the aquifer types in the TMG area differ one from another, it is important to realize whether the effort is cost-effective to have necessary details for the aquifer characterization that can form the basis of investigations into the related aquifer properties.

In 2005 to 2006, a new groundwater research and monitoring site with a five-borehole network near Rawsonville was established in the TMG fractured aquifer. The study in this chapter is dedicated to the analyses of the field observations through borehole core logging, groundwater observations, hydraulic tests, and the examination of fracture characteristics, with the objective of establishing a site-specific study on aquifer's hydraulic properties, which has rarely been done in the structural syntaxis of the TMG.

5.2 Site hydrogeology

There are 5 boreholes which form a well network located in the Gevonden farm, 6 km west of Rawsonville, Western Cape. A perennial stream runs northwards with the water sourced from a catchment of about 80 km² in which the mountain height mostly reaches 2000 m but is about 290 m on this site. In the area, the majority of the TMG outcrop consists of Peninsula formation. The bottom of Nardouw formations and the Cedarberge formation occur in the

very north of the study area which is bounded by basement rocks in the west and southwest and faults (Brandvlei-Elkenhofdam megafault and Smiths Kraal fault) in the east and southeast (Fig.5-1). The Waterkloof fault northeastwards extends some 15 km cutting through the well site. Controlled by both this fault structure and the NE-trending TMG terranes, geomorphologic features of the area are mainly characterized by the steep bared rock slopes on the Peninsula outcrop, stepwise stream course on which there are three waterfalls with the altitudinal drops of 14 to 40 m, and a 6-m thick pluvial boulder soil covers the site area. Several springs on the stream are identified, but are not linked to one another in a regional flow system because the water head gradient may reach more than 1/20 just by a rough estimation on the 1/50000 topography map. The phenomenon is also familiar in the other adjacent catchments where some more field surveys were initiated to have a better view of the boundary conditions of the study area (please refer to Fig.2-6). This suggests that the observed flow systems on the surface are very local ones that seem to be controlled by fractured blocks. On the other hand, this phenomenon obscures a detailed survey of the regional study.

At the Gevonden site, core drilling of borehole BH-1 and BH-2 commenced in the mid of November 2005 by the drilling teams from the Department of Water Affairs and Forestry (DWAF) and ended in December 2006. Two percussion boreholes (BH-3 and BH-4) were drilled in September 2006 and the BH-5 is an existing borehole (Fig.5-1, Table 5-1). During the drilling and monitoring, some of the borehole details and field observations of groundwater are presented as follows:

- The borehole BH-1 that inclines to the west with a plunge of 60° was drilled to the depth of 250 m (270m in length). This borehole penetrates through the bottom of Nardouw Formation and Cedarberg (shale) Formation, tapping the top of Peninsula Formation. The artesian flow of 0.15-0.3 l/s was identified from three conductive zones at the depth of 67.5m, 95.3, and 213.0m, respectively. In order to conduct a long-term monitoring of the Peninsula groundwater, a 179m long steel casing was installed into the bottom the Cedarberg shale to seal the former two conductive zones, resulting in a remaining flow of about 0.2 l/s.
- The Borehole BH-2 was drilled to a depth 201 m and the casing depth is 65 m. similar to the BH-1, this borehole sited on the fault core zone was initiated to take a look at the rock formations of both fault core and fault fracturing zone. Water level in this borehole is 1.8 m to the top, in comparison, groundwaters of the two borehole were thought to have different origins, and they are both different from the stream water.

- Based on the groundwater observations in the BH-1 and BH-2, the percussion borehole BH-3 was sited in between the BH-2 and the existing borehole BH-5, attempt to link the three as a whole. The BH-3 was drilled in September of 2006 to be an open hole in which the casing was only installed to the depth 16 m to protect to bore collar. During this new percussion drilling, water level and flow rate in the BH-2, BH-5, and the BH-1 are monitored; and it was found that when the air-lift water was pumped out the BH-3 water levels subsequently dropped in both the BH-2 and the BH-3, but now flow changed in artesian borehole BH-1. Eighteen water strikes were reported by the driller in this percussion hole, but this number appeared to be too many according to the later dilution test done by Nel. In order to monitor the link between groundwater presented in the three boreholes and that from the regolith, the 8-m deep BH-4 was made some 45 m away from the BH-3 (Fig.5-1).

Water samples from these boreholes have been aperiodically collected for both in situ and lab analyses since the drilling start. The average water temperature ranges 18.5 to 20°C. In the deep boreholes, water electrical conductivity (EC) has varied between 40 and 60 $\mu\text{S}/\text{m}$ and pH between 5.2 and 6.8, while the EC in the shallow hole ranges from 130 to 160 $\mu\text{S}/\text{m}$. The physical features of groundwater are greatly different from those of stream water that is listed in Table 5-2. Groundwater from the fractured rocks is sodium-chloride dominant, but in the late of 2006 the water type was changed because the overflow of stream water got in from the top (please refer to Appendix I). The major chemical constituents change over time with iron having the most significant changes. This borehole water is ferruginous with a dissolved iron content within 0.15~1.5 mg/l. The presence of iron gives an undesirable reddish color on the borehole surroundings due to the precipitation of $\text{Fe}(\text{OH})_3$ from the hole overflows which can be seen at the BH-1.

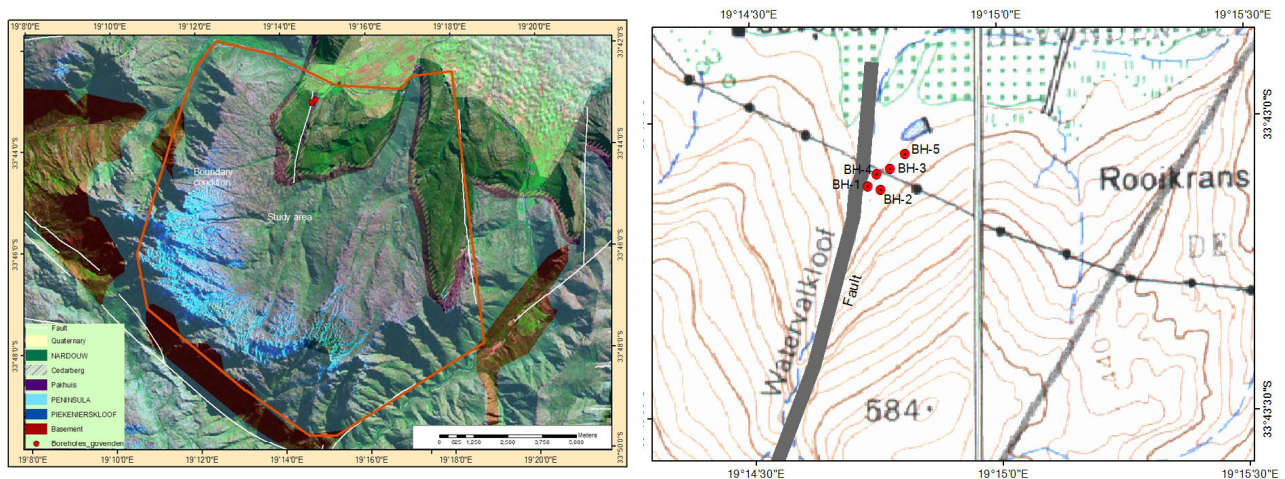


Fig. 5- 1 Study area and boreholes of the Gevonden site, Rawsonvilleonden site

Table 5- 1 Basic information of the boreholes at the Gevonden site

Borehole No	Coordinate (°)		Type	Depth (m)		Inclination	Formations
	E	S		Bore	Casing		
BH-1	19.24615	33.71846	Ø75mm,core drilling	250	156	60°/W	Nardouw to peninsula
BH-2	19.24659	33.71853	Ø75mm,core drilling	201.1	65	Vertical	Peninsula
BH-3	19.24696	33.71790	Percussion	200	16	Vertical	Peninsula
BH-4	19.24654	33.71809	Percussion	8	6	Vertical	Regolith
BH-5	19.24755	33.71749	Percussion	175		Vertical	Peninsula

Table 5- 2 Physical properties of borehole and surface water

Water source item	BH1	BH2	BH3	BH4	BH5	Stream
Ground elevation(m)	273.6	273.06	274.1	274.5	276.9	
T (°)	20.15	19.25	18.5	18.9	20.05	14.50
Water level m to top m	0	1.8	3.05	2.59	5.57	
	273.6	271.26	271.05	271.91	271.33	
pH	6.8	5.5	5.8	5.6	5.2	4.41
EC (uS/m)	50~60	40~70	36~40	130~160	43~50	<10
Formaion	Nardouw	Peninsula	Peninsula	Regolith	Peninsula	Surface water

Note: the ground elevation was measured using a theodolite

5.3 Characterization of fractured aquifer

Like the groundwater in other areas of the TMG, groundwater observed in this site is from the fracture rocks with unknown flow path. This has been evidenced by the field observations through the identification of conductive zones during the core drilling and water level fluctuation during the percussion drilling. Moreover, field observations from the core logs and the site surveys show that the normal fault plays a key role in controlling the occurrence of groundwater. It is observed that the 80m wide fault core, identified to be cemented cataclasites, acts as a groundwater barrier that separates the fractured rock aquifer into the eastern and western parts. In the eastern wall (hanging wall) of the fault, groundwater only occurs with the static water level, but it appear as an artesian flow in the west one (foot wall) (Fig 5-2). It is also observed that the conductive zones intercepted by the boreholes are not at

the fault core but at its fracture zones of the fault. The evidence confirms the conceptual model proposed in Chapter 3 (please refer to Fig.3-1).

With respect to the aquifer in this site, there are three independent flow systems; of these two are fractured rocks on both sides of the fault, and another is the shallow groundwater (the BH-4) flow through the boulder soil. These observations, together with the additional field survey and borehole loggings, not only help to have a better understanding of the TMG aquifers with the involvement of fault structures, but also help to establish a site-specific conceptual model which is partially presented in Fig.5-2.

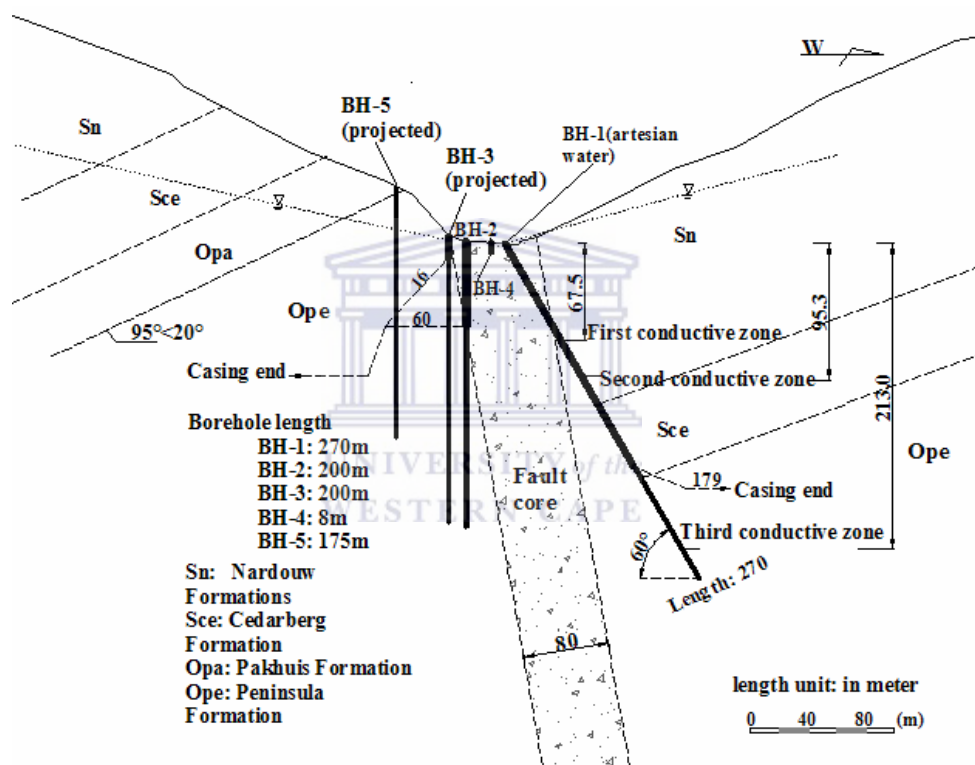


Fig. 5- 2 Schematic hydrogeological cross section, together with the borehole construction

5.3.1 Field logs

5.3.1.1 Core log

The core drilling project was initiated to interpret the geological and hydrogeological significance in the vicinity of the site. Through the establishment of the borehole network, the DWAF was able to develop a new groundwater monitoring station which has long been vacant in this area. The boreholes BH-1 and BH-2 were drilled using diamond coring drilling rigs. The in situ core logs were done along with the drilling progress to avoid the weathering and disturbance of core samples. Lithologies, fractures and associated hydrogeological

information from the core samples were carefully logged, using standard core logging techniques as well as by photographic capturing. Cores were described in terms of the following parameters:

- Rock type
- Colour
- Grain size
- Sorting
- Mineral content
- Sedimentary structures
- Secondary structures

All the core trunks were photographed using a digital camera. The purpose was to have a detailed record of the cores for datum referencing and archiving. The photographs are also used to describe additional features missed during core description, especially with relation to the other interpretations. The core data were transferred from the field notes to standard core

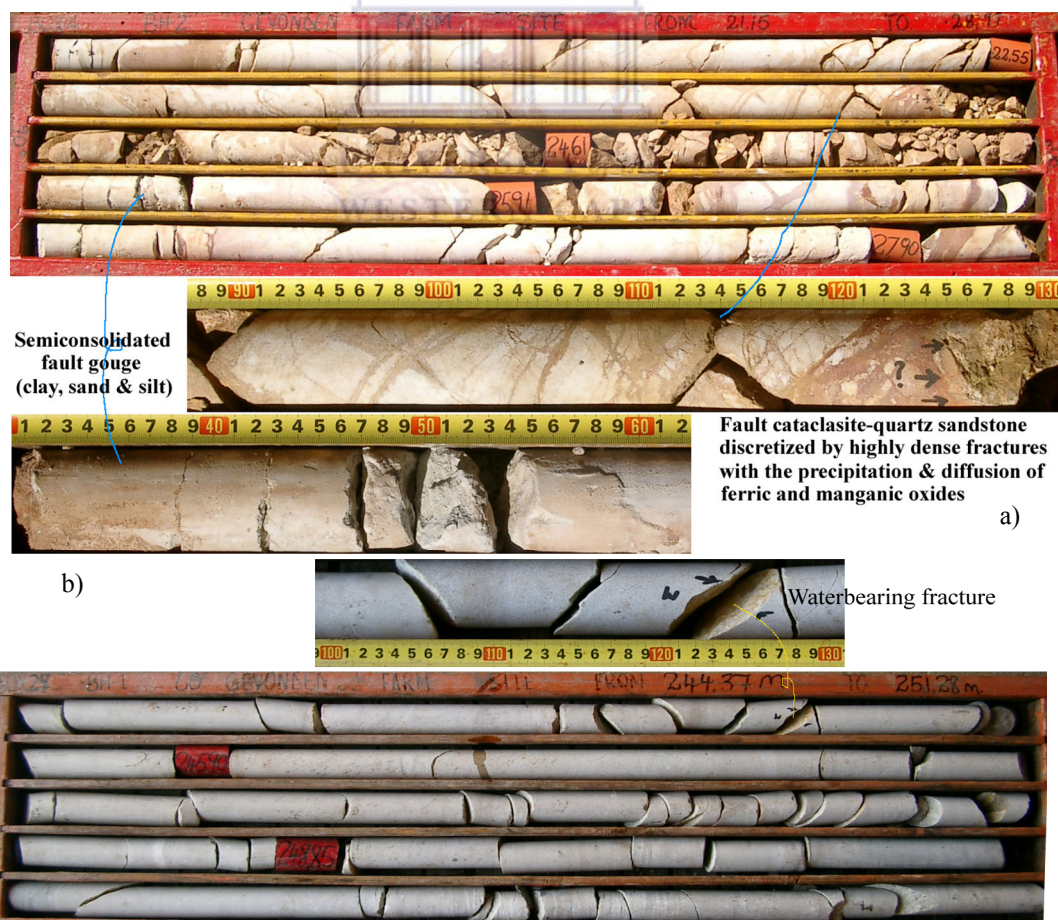


Fig. 5- 3 Core trunks of the BH-1 and BH-2. a) Fault core material at shallow zone of BH-2. b) the Peninsula sandstone and the subvertical conductive single fracture at the BH-1 length of 245m

logging results generated by an Excel-based software developed by the research team (please refer to Appendix B).

In terms of fracture orientation, there are three type of fractures observed in the cores, namely bending fractures with the plunge of $15^{\circ} \sim 25^{\circ}$, substeep fractures ($40^{\circ} \sim 60^{\circ}$), and steep fractures ($>60^{\circ}$). During the core logging for the BH-1 and BH-2, the number of these fractures was counted. The frequency plots of different types of fractures observed in the BH-1 and BH-2 with a logging interval of 1~4 m are shown in Fig. 5-4, in which the top cut-off of the BH-2 is 40 m because it is extremely difficult to capture the fracture data in the highly fractured and weathered fault core at the shallow zone. In general the spatial correlation of fracture density is very weak, especially in the BH-1. In the BH-2, the density of both bedding and sub-steep fractures appears to decrease with depth, especially the fractures below the fault core zone. Contrarily, the steep fractures in both the BH-1 and BH-2 are not substantially depleted with depth; in the BH-2 it shows a uniform spatial distribution of the steep fractures. In same way, these observations are consistent with the results from core sample study on hydraulically active fractures in the Rietfontein deep borehole where the steep fractures become dominant in the relatively deep zone.

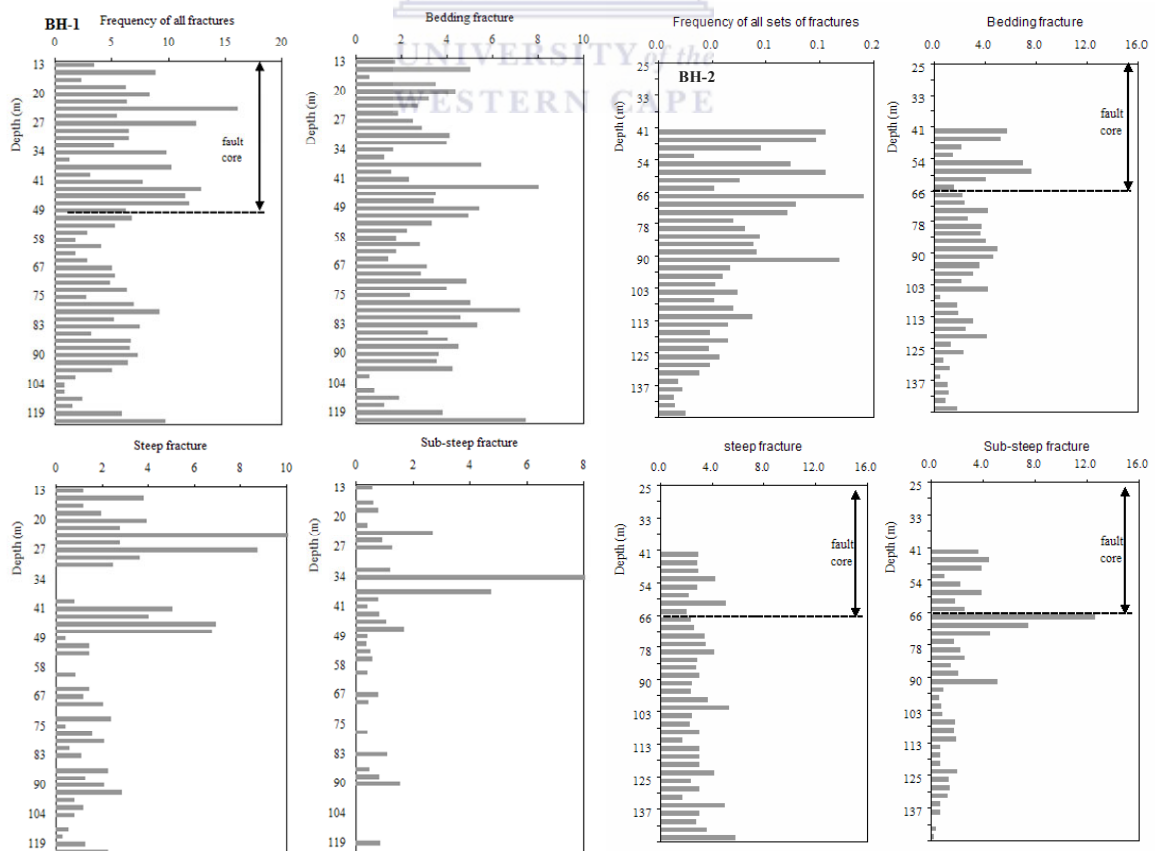


Fig. 5- 4 Fracture frequency plots against depth

5.3.1.2 Surface geophysical log

Among the non-invasive geophysical techniques, the radon emanation method is one of the effective tools to detect the concentration of groundwater (Levin, 2000). This method is based on the nuclear disequilibrium process of the isotopes of uranium family of which the radioactive decay series by alpha recoil process is from ^{234}U through ^{230}Th and ^{226}Ra to ^{222}Rn . Because uranium in groundwater is soluble under oxidizing conditions, water flow in an aquifer may have its isotopic signatures. The distribution and magnitude of the radioactivity of the U family consequently reflects the groundwater concentration in the aquifer. Therefore the radon isotope ^{222}Rn is often employed as a natural groundwater tracer. Particularly it is indicative of open fractures in a fractured rock aquifer.

To ensure the borehole siting and help to establish the conceptual model on a site scale, a series of soil and water ^{222}Rn measurements on the surface was conducted. Using the alpha card instrument, ^{222}Rn was stripped from the air pumped from subsurface soil or the bubble of water and measured in a gas proportional counter. This count is termed pulse number in the alpha card instrument, from which the concentration of the radon gas can be estimated.

$$C_{Rn} = J \cdot N_{RaA} \quad (5-1)$$

in which the C_{Rn} is the concentration of Rn, N_{RaA} the pulse number measured, and J is the coefficient of Rn concentration which is a constant fixed by the measuring equipment.

The in-situ operation procedure of the alpha card equipment has been discussed in detail by Wu et al (2003). In this case, the measurements were conducted in both soil and water. In order to have comparable results, measuring operations are classified into four categories, i.e. soil radon anomaly, soil radon background value, borehole water and stream water radon concentrations (Table 5-3). For the measurement of radon gas in the soils, the measuring probe needs to reach a depth of more than 0.5 m to gain the subsurface air. The operation hence cannot only be proceeded in the bared rocks. Fig.5-6 shows the measuring points of which the coordinates are captured by GPS equipment. At these points, data of pulse number were collected to represent the radon concentration.

Table 5-3 shows that the observed radon pulse number of groundwater ($N_{RaA}=30\sim69$) is much higher than that of stream water ($N_{RaA}=6\sim15$). This also confirms the basis of radon gas concentration for the characterization of groundwater distribution in the fractured rocks. In the soil radon anomaly measurement (Fig.5-5), relative higher pulse numbers mostly fall in the east side of the stream. Especially in the east of the BH-2 and the BH-4 where the Peninsula sandstone is exposed (Fig.5-2), most of the pulse numbers of ^{222}Rn are above 50, in

which the highest ($N_{RaA}=90\sim 107$) occur in between the BH-3 and the BH-5 distributed at the northeast corner of the measuring area. In comparison, the pulse number in the west side of the stream, where the Nardouw sandstone exposed, is much lower with the average of 17.7 out from a pulse number range of 3 to 36. These values are just at the same level of the background values. In the central fault core zone, the majority of the pulse numbers fall in the range of 20 to 40. Perhaps these values represent the radon concentration of the shallow regolith aquifer because the pulse number of the water from the BH-4 is 40.

According to above discussion, ^{222}Rn anomaly data are useful to be indicative of groundwater concentration in the relatively shallow zones such as that of the regolith aquifer and the Peninsula aquifer. In the fractured rock like the Peninsula sandstone, the uneven distribution of pulse number maybe has another indication of the anisotropic feature of open fractures and subsequently the groundwater concentration in this aquifer. In the Nardouw sandstone, the lower pulse number is perhaps attributed to the deep seated artesian flow and the mostly closed fractures in the shallow zone.

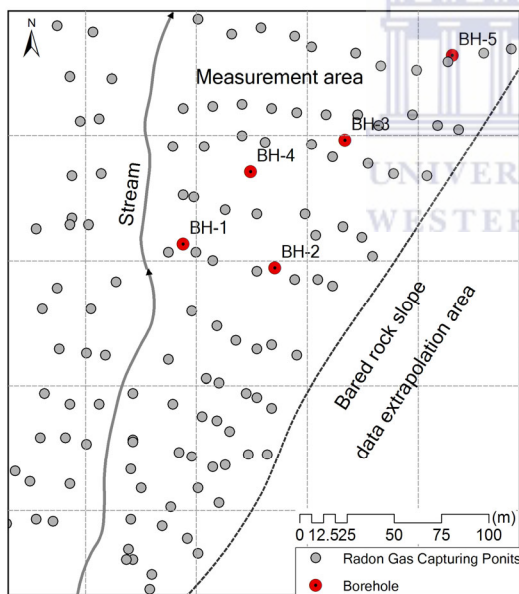


Fig.5- 5 map shows measuring points for the collection of radon (^{222}Rn) gas emanating from subsurface water.

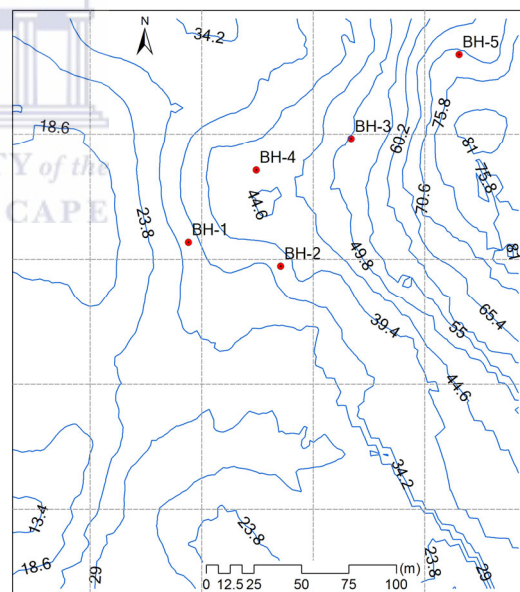


Fig.5- 6 Contour map of pulse number anomaly for radon (^{222}Rn) by Krigin.

Table 5- 3 Statistic of the ^{222}Rn pulse number from different sources

^{222}Rn pulse number	Soil anomaly	Soil background	Groundwater	Stream water
maximum	107	23	69	17
Minimum	3	7	30	6
Average	33.5	12.1	37.8	10.7
Standard deviation	22.6	6.1	19.6	4.5

5.3.1.3 Fracture measurement on the surface

On both the Peninsula and the Nardouw sandstone outcrops fracture data were gathered on orientation, length, spacing, and aperture. The methods of measurement and the data statistics have been discussed in Chapter 3 and Chapter 4, respectively. According to orientation configuration, 334 fractures measured on the sandstone outcrops are put in four categories, of which the statistics of basic elements are list in Table 4-9 and all the measured data are listed in Appendix C. Fig. 5-7 shows the orientation distribution of the fractures,

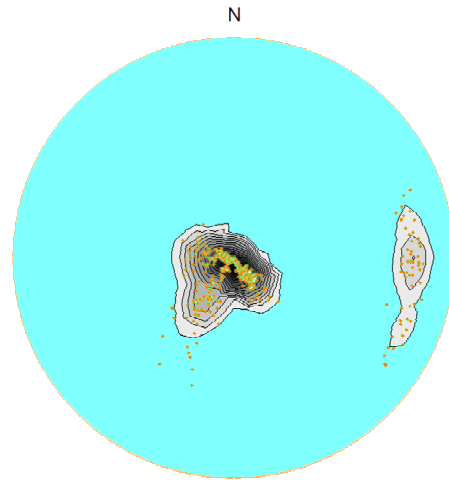


Fig. 5-7 Orientation distribution of fractures measured at the site

in which gently-dipping bedding fractures have a orientation range of $14^{\circ}\sim 28^{\circ}/69^{\circ}\sim 125^{\circ}$ (dip angle/dip azimuth, set 1); and the three others are, respectively, $38^{\circ}\sim 89^{\circ}/192^{\circ}\sim 233^{\circ}$ (set 2), $67^{\circ}\sim 89^{\circ}/123^{\circ}\sim 169^{\circ}$ (set three) and $70^{\circ}\sim 89^{\circ}/235^{\circ}\sim 317^{\circ}$ (set 4). Although the fracture densities are different, the orientation result is apparently comparable with that of the core samples, in which both plunges of bedding fractures are almost identical. Fractures of the set 2 may account for the sub-steep fractures in the core samples, but the other two sets of fractures are mixed in the steep ones.

5.3.2 Fracture network

As aforementioned, the groundwater in the BH-2, BH-3, and BH-4 is connected. In order to have a better understanding of such hydraulic connection in the borehole water, the generated fracture network is used. Based on the fracture data measured on the surface, the method of fracture realization is the same as what has been discussed in Chapter 3 and parts of the results of this site have already been presented there (please refer to Fig.3-23).

Fig. 5-8 shows another two plan views of generated fractures on the profiles of N10E – S190W and N40E – S225W. Fracture networks on the both profiles reveal the similar geometric pattern to the previously discussed. However, in the two generated realities, not only fractures occur in the manner of fracture blocks of interconnected fractures, but also one well-connected fracture cluster at each reality appears to break through both side of the study domain. The former seems to be dominated by bedding and relatively gentle dipping fractures, whereas in the later steep fractures, together with the gentle-dipping ones, control the well connected cluster to extend vertically.

In comparison with Fig.3-20, the rest profiles may be deduced by analogy, from which it is obvious that the fracture reality on the profile trend to the SE-NW may only produce small blocks of interconnected fractures. Thus, if there is a preferential flow path in the fracture rocks, this flow path should have a trend of NE-SW. The distribution of soil radon pulse number seems to support such inference, as the highest pulse numbers are almost concentrated to the northeast.

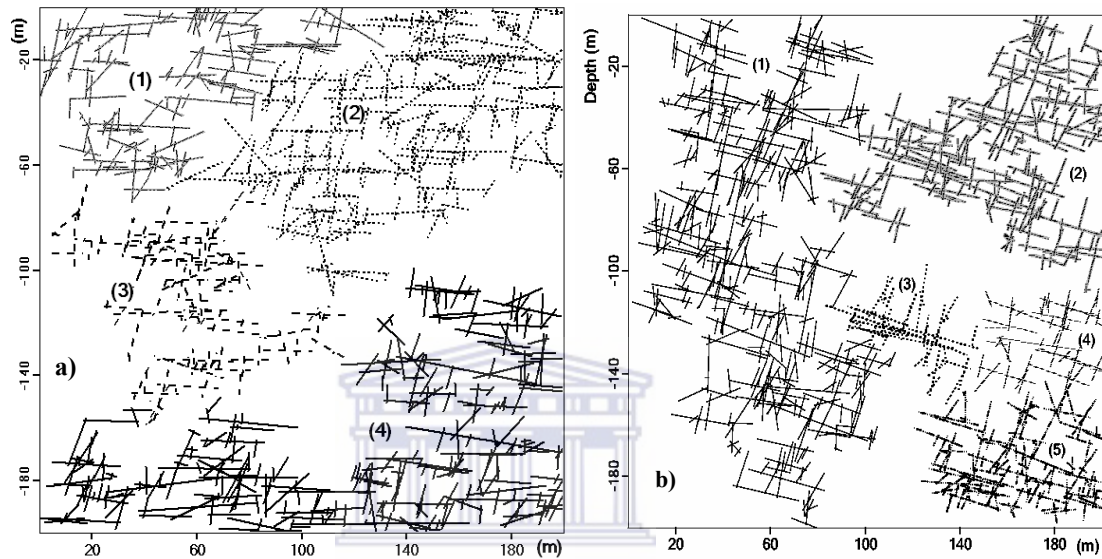


Fig. 5- 8 Plan views of interconnected fracture blocks generated with the data derived from field measurement on profiles: a) profile of N10E-S190W, b) profile N45E-S225W

5.4 Hydraulic properties

To integrate with the other studies of the aquifer properties in this site, the single packer tests with an interval of 6m were done at the BH-1 and the BH-2, respectively, during the process of core drilling. In the mean time, a 24-hour pumping test at the existing borehole BH-5 was carried out in May 2006. After establishment of the groundwater research and monitoring site, another 24-hour pumping test was done at percussion hole BH-3 with

5.4.1 Well bore hydraulic tests

So far, almost all the hydraulic tests conducted in the TMG aquifers are pumping tests. There is no archive file of packer test for hydrogeological exploration in the TMG aquifers can be accessed, except very few from dam foundation investigations (Rowsewarne, 2002). Generally the hydraulic parameters estimated from pumping test represent those of a site scale

in tens of meters, whilst packer test can only be used to estimate such parameters for a limited size of fractured rocks in meters (Nestev et al, 2004).

5.4.1.1 Packer test

In order to evaluate the hydraulic conductivity of the TMG sandstones on a relative small scale (in comparison with pumping test), packer tests in the two coring boreholes were completed using single packer with the interval of 6m. The packer test of whole borehole length could only be conducted in the vertical BH-2. In the inclined BH-1, unfortunately, only a half portion of packer test was done because the normal coring drilling was replaced with wire line drilling after this hole was diverted at a shale band at 140 m below surface.

For the hydraulic tests, the injection pressure in a packer was depth dependent and changed by stepwise as 350-700-1050-700-350 kPa below the depth of 40 m. Hydraulic conductivity (K) was calculated by the following formula suggested by Moye (1967, cited by Park et al, 2002):

$$K = \frac{q}{HL} \left[\frac{1}{2\pi} \left(1 + \ln\left(\frac{1}{r_w}\right) \right) \right] \quad (5-2)$$

where q is flow rate (m^3/s), H is total working pressure (m), L the packer interval (m), and r_w borehole diameter (m).

Because the graphic circles of total working pressure and water take match well during the tests, the mean value of each stepwise test based on equation (5-2) is taken to be the hydraulic conductivity for each interval. Hydraulic conductivity against borehole depth in Fig.4-10 shows that the K value widely ranges from 1.11×10^{-6} to 2.35×10^{-9} m/s (average 2.15×10^{-7} m/s) and 1.25×10^{-6} to 7.25×10^{-10} m/s (average 9.73×10^{-8}) in the BH-1 and the BH-2, respectively. These K values are one to two orders of magnitude less than those from dam investigations (1.97×10^{-6} to 8.1×10^{-7} m/s, Rosewarne, 2002).

In the top portion near the fault zone, the K values vary much and are higher than those at the lower portion of the boreholes. Below the depth of 60 m in the BH-1 and 80 m in the BH-2 the variation of K values becomes stable and the K value gently decreases with depth in both boreholes. The hydraulic conductivity in an order of magnitude of -8 in the BH-1 and -8 ~ -10 in the BH-2 below those depths may represent that of the TMG fractured sandstones in this area. Note that there are many test intervals without water takes from which the $K=0$; this also indicates that hydraulic conductivity from the packer tests depends on both the factors as listed in equation (5-2) but also the local connectivity of fractures in the fractured rocks. Besides, the variation of the conductivity at depth in the both hole reveals a generic trend of

the reduction of hydraulic conductivity as has been discussed in Chapter 4. This suggests that the majority of fractures may tend to be closed in the deeper part of crust (Goodman, 1974).

5.4.1.2 Pumping test

There were two sets of 24-hour pumping tests done respectively at the BH-5 and BH-3. The former was conducted in 23th May 2006 just during the core drilling, whereas the later one was done between 23th~25th Nov 2006.

The observed drawdown of constant discharge rate pumping test at the BH-5 is plotted in Fig.5-9; using Cooper-Jacob method for radial flow, the estimated later-time T value is $7.1 \times 10^{-5} \text{ m}^2/\text{s}$ ($6.1 \text{ m}^2/\text{d}$) and the corresponding K value is $4.2 \times 10^{-7} \text{ m/s}$ ($3.6 \times 10^{-2} \text{ m/d}$).

Similarly, the T value estimated for the BH-3 is $1.7 \times 10^{-4} \text{ m}^2/\text{s}$ ($14.7 \text{ m}^2/\text{d}$) and the K value is $8.8 \times 10^{-7} \text{ m/s}$ ($7.6 \times 10^{-2} \text{ m/d}$); while the T value derived from drawdown recovery is $8.0 \times 10^{-5} \text{ m}^2/\text{s}$ ($6.9 \text{ m}^2/\text{d}$), as twice as that from withdraw drawdown (Fig.5-10).

During the pumping test at the BH-3, the surrounding boreholes BH-1, BH-2, BH-4, and BH-5 were monitored. The artesian flow rate at the BH-1 was manually measured; while the water levels in the pumping hole and the other boreholes were automatically recorded by Diver well pressure loggers. To avoid the turbulence flow that may affect the reading at the pumping hole, the Diver was set to the depth of 20m below the pump inlet. Moreover, water level in

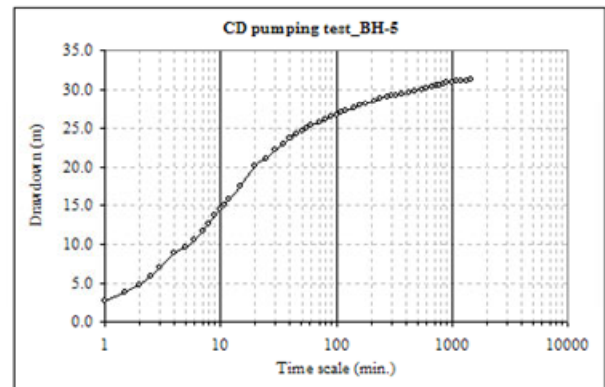


Fig.5- 9 Constant discharge ($q=1.3 \text{ l/s}$) pumping test at BH-5 on 20 May, 2006. The late-time T value is estimated as $7.1 \times 10^{-5} \text{ m}^2/\text{s}$ with corresponding K value of $4.2 \times 10^{-7} \text{ m/s}$, by Cooper-Jacob method

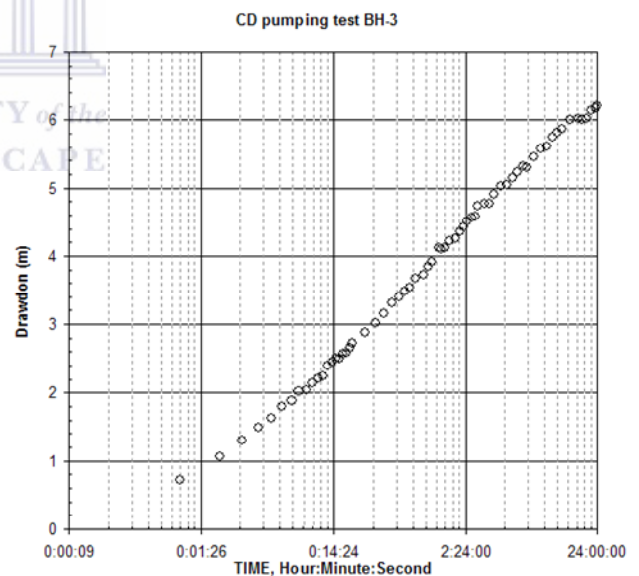


Fig. 5- 10 Constant discharge ($q=1.8 \text{ l/s}$) pumping test at BH-3 on 23 Nov 2006. T value is estimated as $1.7 \times 10^{-4} \text{ m}^2/\text{s}$ and K is $8.8 \times 10^{-7} \text{ m/s}$, by Cooper Jacob method

each borehole was regularly checked after the pumping test commenced; and the drawdown not terminated until recovery was 95% of the initial water levels resumed.

It was interesting to find that only BH-5 had a sharp response to the pumping hole. First retarding drawdown observed at the BH-5 was 3 minutes after the pumping start, whereas it was 5 minutes at the BH-2. Fig.5-11 shows the final drawdown at the pumping and monitoring boreholes, together with the distance between these holes. The maximum drawdown in the BH-2 is merely 0.6 m which seemed to be on the boundary of the depression cone. However, the difference between the distance from the BH-3 to the BH-2 and the BH-3 to the BH-5 is 9 meter, but the drawdown in BH-5 is 4.61m. Monitoring data also show that there is no substantial response of BH-1 and BH-4 to the pump-out water in the BH-3.

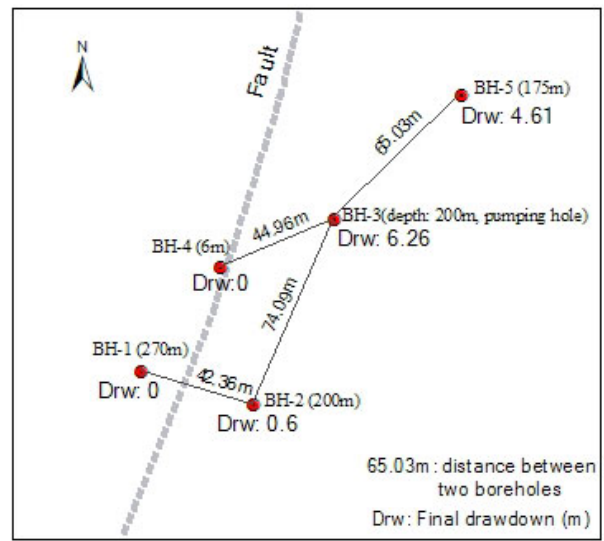


Fig.5- 11 Map shows the final drawdown and distance between boreholes

At the TMG sites, different borehole groundwater responses to the pumping test can be traced if carefully checking the existing testing records gathered from the TMG aquifers. Such aquifer behaviors to external stress reflect a universal anisotropic feature at a site scale in which the uneven drawdown distribution is governed by various-scale fracture networks. In this regard, many of the existing models perhaps have limited applicability to the estimation of the aquifers' hydraulic properties. In this case, for example, the Cooper-Jacob method derived from the Theis theory regarding the aquifer as an isotropic medium is thought unsuitable to interpret the pumping test data gathered from such aquifer that is bounded by the fault as a groundwater barrier. Therefore image well method (Ferris et al, 1962) is introduced to the estimation of the hydraulic properties by positive superposition the drawdown of image well at the pumping hole, which is expressed as:

$$s = \frac{Q}{4\pi T} [W(u_1) + W(u_2)] \quad (5-3),$$

with increase in pumping time the well function in of pumping hole ($W(u_1)$) and image well ($W(u_2)$) both tend to be less than 0.01. The Eq.(5-3) can be presented by Cooper-Jacob formula.

$$s = 0.366 \frac{Q}{T} \log \frac{2.25Tt}{r_w \cdot r_m S} \quad (5-4)$$

in which r_w and r_m is the radius of the pumping well and the distance from the pumping well to the image well respectively, and the other symbol meanings are the same as those of Eq.(4-7). The distance from the BH-3 to the fault is 18 m and that of the BH-5 is 30 m. it is clear that the T and K values is much lower than those estimated by radial flow method (Table 4-5).

Table 5- 4 Hydraulic properties from pumping tests at the Gevonden site

Hydraulic properties	Borehole BH-3 drawdown		Borehole BH-5 drawdown		
	Radial flow		Image well	Radial flow	Image well
	Withdraw	Recovery	Withdraw	Withdraw	Withdraw
T (m ² /s)	1.7×10^{-4}	8.0×10^{-5}	4.5×10^{-4}	7.1×10^{-5}	1.2×10^{-4}
K (m/s)	8.8×10^{-7}	4.0×10^{-7}	1.8×10^{-6}	4.2×10^{-7}	7.9×10^{-7}

5.4.2 Fracture network model (FNM)

As the above discussion, there are many uncertainties in both the estimation and application of hydraulic properties of the fractured rocks, merely due to their spatial anisotropic feature. For this reason, a lot of efforts have been contributed to the study of anisotropic hydraulic properties. Based on the Theis well function, Heilweil and Hsieh (2006) were able to develop a simplified Papadopoulos method to characterize directional transmissivity. Zhang et al (1996) used hydraulic tensor method to estimate the permeability of fracture network with constant aperture. Based on stochastic fracture realization, currently, discrete fracture network (DFN) model is often used to calculated equivalent permeability of fractured rock through percolation theory (Baghbanan and Jing, 2007) or hydraulic conductivity tensor approach (Min et al, 2004). Most of these studies are dealing the 2D groundwater problem from different angles. It should be not that, using stochastic DFN model to study the 2D groundwater problem, there is always a spatial projection of the fracture data. For example, on a 2D plane, all the fractures are assumed to commonly have a vertical plunge because only the fracture strikes can be used to represent the fracture orientations. Thus the estimated hydraulic conductivity K_x and K_y can be representative.

For the calculation of equivalent hydraulic conductivity on the 2D profiles, in this study, the tensor approach as presented Chapter 4 is used. Fractures data with dip direction, dipping angle and length, are extracted from the four interconnected blocks as shown in Fig.5-8a.

Using the central coordinate, the spacing of each fracture is defined as the average distance to its adjacent fractures; and this process can be automatically completed by a VBA subroutine in the ArcGIS software. In this study a constant aperture ($b=0.15\text{mm}$) and constant JRC ($JRC=0.18$) are applied, which are the average of those of four sets of fractures listed in Table 4-9. Therefore it is able to calculate the K values for each fracture block by superposition of each fracture at the block. The computed results listed in Table 5-5 show that the average K value based on Eq.(4-25) is 1.11×10^{-5} m/s that appears to be the higher than the results of hydraulic tests and any K values estimated before are under the same input conditions by the tensor model. This is attributed to the projection of fractures on the profile resulting in the intensification of fracture density and accordingly the spacing between fractures. Therefore, these K values on the 2D plan can only be regarded apparent hydraulic conductivity but not equivalent hydraulic conductivity.

In a fractured rock aquifer, only a few fractures are competent to a flow system (Witherspoon, 2000; Shapiro et al, 2007). This point is supported by the results shown in Fig.5-12 where the major interconnected fractures in the 3D DFN model are presented. Fig.5-12a is the 3D visualization of total fractures generated based on the data listed in Appendix C. The interconnection analysis of these fractures is performed by a 3D face model developed in Microsoft Excel. As a result, Fig.5-12b presents three major blocks comprise interconnected fractures with the fracture number of 2, 18, and 6 from the top to the bottom, in which the block with the most interconnected fractures just accounts for 2.4% of total fractures generated. This suggests that the majority of fractures are not necessary to be involved in a flow system in the fracture rocks. Provide that all of the 18 fractures are open and have the same constant aperture and constant JRC as the above mentioned, using hydraulic tensor model, the calculated directional K values for the 3D problem is listed in Table 5-5. Among them, the average K of 1.22×10^{-8} m/s roughly falls in the range of those from packer and pumping tests.

Table 5- 5 Computed equivalent K values for fracture blocks of interconnected fractures for both 2D and 3D problems

Fracture block		Hydraulic conductivity (m/s)						
		Principle K				Axial K		
		Average	K_{p1}	K_{p2}	K_{p3}	K_x	K_y	K_z
2D problem	Block1	1.57E-05	2.36E-05	1.92E-05	4.46E-06	9.03E-06	1.46E-05	2.36E-05
	Block2	1.33E-05	2.00E-05	1.64E-05	3.62E-06	6.70E-06	1.33E-05	2.00E-05
	Block3	1.03E-05	1.54E-05	1.33E-05	2.19E-06	1.07E-05	1.54E-05	1.41E-06
	Block4	5.01E-06	7.51E-06	7.05E-06	4.58E-07	1.54E-05	1.41E-06	7.51E-06
3D problem	18 fractures in a block	1.22E-08	1.70E-08	1.60E-08	6.65E-09	9.55E-09	3.25E-08	1.65E-08
	Dip direction(°)		210.8	69.1	128.4			
	Dip angle(°)		24.3	60.0	16.4			

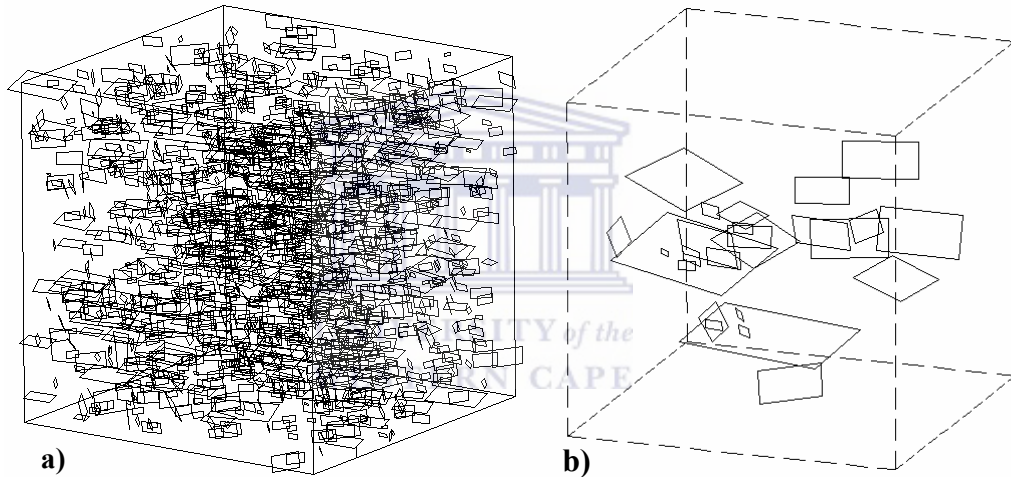


Fig.5- 12 Fracture generated based on the data derived from surface measurements at the Gevonden site (SE views). a) fracture generated with the domain size of $200 \times 200 \times 200 \text{ m}^3$; b) Three major blocks of interconnected fractures are extracted and presented the generated fractures in a cubic box of $100 \times 100 \times 100 \text{ m}^3$. Fracture number of the top is 2, the middle is 18, and the bottom 6.

5.5 Discussion and summary

Due to the complexity of geometric and hydraulic properties of the TMG aquifers, the study of site-specific groundwater problem is of great hydrogeological significance; especially when the study is about aquifer's hydraulic properties. Before commencing a site-specific study, it is important to make sure that the study of a fractured rock aquifer is always an expensive exercise. It is also important to note that if the study of aquifer properties, including hydraulic properties, was merely done without the field observations, the results would have very limited applicability.

In order to have a better understanding of the familiar aquifer type, the fault bounded aquifer in the TMG, together with the study of aquifer properties, a site with a five-borehole network was established. Multidisciplinary approaches to the field observations were employed, including borehole coring and logging, field geophysical survey, field fracture measurement, in-situ identification and examination of groundwater behavior, and hydraulic tests. Associated results from these methods were comparatively analyzed, from which an initial conceptual model was proposed and presented on a plan view. As more understanding is gained from the analytical results, it is realized that the groundwater in the fractured aquifer is actually not flowing through a geological continuum. Large variation of the aquifer responses to hydraulic tests shows difficulty to determine the aquifer's hydraulic properties represented by the T and K . In other words, it is extremely difficult, through hydraulic tests, to give a sound estimate then to tell how much the aquifer's transmissivity is and how much the aquifer's hydraulic conductivity is. This is due to the anisotropic features embedded in the fractured rocks and perhaps can be summarized by the conclusion of scale-dependent aquifer properties which actually implies the uncertainty of problem studied.

Therefore the hydraulic conductivity tensor method is reused to estimate the anisotropic K values. Based on the FDN models, the current problem of a 2D fracture network is discussed. Because groundwater in the fractured rocks is actually a 3D problem, in this study, a 3D FDN model is proposed and shows that only 2.4% of fractures at the measurement scale are probably involved in the flow system, from which the K value for this site is estimated to be in the order of magnitude of 10^{-8} m/s. This is perhaps not the ultimate estimate, but it helps to get an understanding of a 3D reality.

Chapter 6

Summary and recommendation

6.1 Summary

On a regional scale, the TMG Aquifer is both a heterogeneous and anisotropic entity, and a fractured rock aquifer system with unique features as regarding its stratigraphy, structure, and geomorphology. It is compartmentalized into various hydrogeological units, bounded by large faults, lithologies, and topographies. Various-scale TMG aquifers are the fortuitous combination of stratigraphic, tectonic, geomorphologic and climatic features. The establishment of hydrogeological units, associated subunits, and the analysis of aquifer types provide a regional view of the aquifer system and boundary conditions in the vast area, which forms the initial conceptual models for the aquifers in a regional scale. Much more commonly encountered problem in the TMG aquifer is how to conceptualize the aquifer media to meet the understanding of many site-specific problems and from which perform a proper analysis and a sound estimation of the aquifer properties. The discussion of the TMG aquifer types raises the necessity of the aquifer media study, especially the study of fractured media which shows prominence in controlling groundwater in the TMG aquifers. Based on the study and subsequent understanding of fracture networks, it is possible to propose the conceptual model both for fault and relatively small-scale fractured media, which has rarely been done for the TMG aquifers.

Based on previous researches and present study, estimated results of the aquifers' hydraulic properties fall in a wide range of values which reveal big differences between different sites of an area and in different well bores of a site.

Aquifer media

Based on previous studies and current researches, the characterization of the TMG fractured media on regional and local scales has been performed, through the interpretation of existing geological data and remote sensing imagery, the study of core samples, and the analysis of fracture field measurement data, from which an initial conceptual model of fracture network is developed. This model can help to have a better understanding of the TMG fractured rock media and can be applied to the quantification of aquifer properties.

According to the experience of groundwater development in the TMG area, fault structures have attracted much attention in the development of wellfields for water supply. Most of the fault zones developed in the TMG sandstones and siltstones are evidenced to have been recemented and act as aquicludes. Based on the study of fault architecture, a conceptual model of fault is proposed, which stresses that fracture zones at both walls of a fault core may become a particular interest of borehole siting; this suggests that the groundwater occurrence and flow path are dominated by fractures or fracture network.

In the context of hydrogeological setting, it is better to classify fractures in the TMG sandstones into two categories of the open and closed than conventional classification based on the mode of rock deformation. To investigate such types of fractures, a case study on core sample fractures in an 800-m deep borehole at the Rietfontein site is then introduced. Data from fracture field measurement, and fracture core samples and coating scanning are comparatively analyzed, which yield the results in the distribution of orientation, and the variations both fracture density at depth and fracture coating intensity at depth. These results are informative for the characterization of the TMG fracture media; in particular the analysis of fracture coating, which has never been done in the TMG, discloses a mode of hydraulically active fractures at depth.

For the study of a regional problem, remote sensing can be an effective tool, especially when incorporating with GIS technique. For the characterization of fractures on a regional scale, lineaments captured from imagery often provide a crucial clue on the interpretation and analysis of fractured rocks. Using Landsat ETM⁺ imagery, a quantitative analysis is carried out by VBA subroutine developed in the software ArcMap to determine the distributions of lineament orientations and lengths in seven domain areas, from which a universal lognormal distribution of lineament length is established. This distribution pattern can be introduced to the smaller-scale fracture systems, especially where difficulty is encountered on the weathered grounds to have sufficient trace-length data to represent the statistic population.

For the site-specific groundwater problems, because the existing data for characterizing fractured rocks of the TMG are very limited, field measurements on fracture elements are carried out over the sandstone outcrops at selected sites. Based on statistic features and distribution pattern of the fracture elements, fractures on both 2D plan and profiles, and in 3D domains are generated using random processes, from which the connectivity is qualitatively examined. These results commonly show that the interconnected fractures collectively exhibit a mode of separated and anisotropic fracture blocks (networks). Such connectivity pattern is thought to be general in the TMG sandstones, especially where the TMG rocks are exposed

and not confined by overlaying geological formations. Because the basic data is measured at different structural domain and lithologies, the generated results and subsequent fracture connectivity is accordingly representative. In order to verify the validity of the generated model, a case study is briefly carried out in the Boschklouf site, from which some of the field observations of groundwater phenomena can be explained by the models.

Hydraulic properties

To characterize storage and flow of groundwater in the TMG aquifers, it is most important to study their hydraulic properties, including porosity and storativity, and transmissivity and hydraulic conductivity. However, the estimation uncertainty of these parameters always exists through different approaches.

There are two major ways to determine aquifer storativity, one is through the porosity estimation of rock formation and the other is derived from pumping tests. Laboratory test of rock samples, field measurement of rock blocks, derivation of pumping test data, and the interpretation of geophysical data and remote sensing, yield a wide range of porosity values, from which the scale-dependency of the porosity is revealed and discussed. The conversion of the porosity to aquifer storativity requires a proper estimate of bulk modulus of the rock mass; in this regard, there is a large amount of work to be done in the field of hydrogeology in South Africa.

In terms of aquifer permeability, most of transmissivity results of the TMG aquifers have been derived from hydraulic tests, especially the pumping tests have yielded a wide range of the transmissivity values from 9 to 400 m²/d which leads to draw a brief conclusion that the TMG aquifers are highly anisotropic both in regional and local scales. Furthermore, the applicability of the interpreted results is also discussed through the analysis of four types of familiar drawdown observed in the TMG aquifers. It is observed that both drawdown-based and model-based interpretations of hydraulic tests need to integrate with the geological observations, especially in the TMG aquifers where boreholes are mostly sited to be close to hydrogeological boundaries such as fault structure and lithological contacts.

Because the hydraulic conductivity (K) of the TMG aquifers is mainly controlled by fractures or fracture network, a new tensor approach is proposed. For the prediction of hydraulic properties of the anisotropic TMG aquifers, fundamental principles of K tensor and some problems with their application to groundwater flow are discussed. It is observed that the K value tends to be higher than that of hydraulic tests because the data sets measured on surface are often overestimated with respect to the fracture apertures even by means of

scientific sampling and statistical methods. It is also pointed out that different types of K values derived from K tensor approach have different meanings physically, although they are related. For the use of calibration coefficient of roughness C_{er} , it is recommended that Lomize's model be used for microscopic fractures and Barton's model for relative macroscopic ones.

The results are compared with those from field tests and in turn the tensor model is calibrated to meet the changes in fracture features and fracture setting conditions, from which a depth model of K is accordingly proposed and comparatively studied with the data from hydraulic tests.

The derivation of negative exponential form of hydraulic aperture is based fundamentally on rock mechanics by considering both fracture roughness and stress conditions. Comparing with the results from hydraulic tests at three sites, it is found that the K values estimated through the tensor model may represent that of a relatively small scale in meters; and this scale is dependent on the size of fractures collectively measured. Using this calibrated model it is possible to calculate the hydraulic conductivity at depth, by assuming that the rock masses in an aquifer are subjected to lithostatic pressure. The computed results show that the reduction of K over depths roughly follows a negative exponential law with different exponents. This is also confirmed by the results of packer tests conducted in the Gevonden site and can be compared with that of Snow (1969). The tensor model provides a scientific tool to predict the hydraulic property of the TMG aquifers both on the surface and at depth.

Due to the complexity of geometric and hydraulic properties of the TMG aquifers, the study of site-specific groundwater problem is of greatly hydrogeological significance; especially the study is regarding aquifer's hydraulic properties.

In order to have a better understanding of the familiar aquifer type, fault bounded aquifer in the TMG, together with the study of aquifer properties, a site with a five-borehole network was established. Multidisciplinary approaches to the field observations were employed, including borehole coring and logging, field geophysical survey, field fracture measurement, in-situ identification and examination of groundwater behavior, and hydraulic tests. Associated results from these methods were comparatively analyzed, from which an initial conceptual model was proposed and presented on a plan view. As more understanding is gained from the analytical results, it is realized that the groundwater in the fractured aquifer is actually not flowing through a geological continuum. Large variation of the aquifer responses to hydraulic tests shows much difficulty to determine the aquifer's hydraulic properties represented by the T and K . In other word, it is extremely difficult, through hydraulic tests, to

give a sound estimate then to tell how much the aquifer's transmissivity or the aquifer's hydraulic conductivity is. This is due to the anisotropic features embedded in the fractured rocks and perhaps can be summarized by the conclusion of scale-dependent aquifer properties which actually implies the uncertainty of problem studied.

Therefore the hydraulic conductivity tensor method is reused to estimate the anisotropic K values. Based on the FDN models, current problem of 2D fracture network is discussed. Because groundwater in the fractured rocks is actually 3D problem, in this study, a 3D FDN model is proposed which shows that only 2.4% of fractures at the measurement scale are probably involved in the flow system, from which the K value for this site is estimated to be in the order of magnitude of 10^{-8} m/s. This is perhaps not the ultimate estimate, but it help to get the understanding to a 3D reality.

6.2 Recommendations

Based on this study, a number of fields for future and further research on the TMG aquifers are suggested:

1. Because the complexity of geometric and hydraulic properties of the TMG aquifers, and because there is no relevant data to support the large-scale study on the aquifer properties, more research projects focusing on site-specific study need to be launched. Data collected for such study may focus on the consideration of problems of scale-dependency and uncertainty of aquifer properties.
2. In South Africa, lithologic and stratigraphic studies have been completed in great detail. However, for the research and management of groundwater in fractured rock aquifers, tremendous efforts need to be enhanced in the study of geological structure, fault structure in particular.
3. For the estimation of aquifer storage, storativity and porosity are two critical parameters. The former can be estimated from many pumping tests conducted in the area, but the uncertainty of the parameter suggests its limited applicability. Using porosity to estimate storativity, the mechanical properties of rock mass should be predetermined. This requires a lot of laboratory and in situ rock mass tests to be done.
4. So far there yet is not an effective method to perform a sound estimate for the hydraulic properties like T and K of a fractured rock aquifer. This estimation requires a lot of efforts toward the characterization and conceptualization of fracture rocks. For

this reason, a multidisciplinary approach is suggested for the study of hydraulic properties in a fractured rock aquifer.

5. Any model-based or drawdown curve-based studies for pumping test data need to add the field observations on groundwater behavior and geological investigation especially the geological structure.
6. Numerical modeling should be very carefully used in evaluation groundwater problems in the fractured rock aquifers, because it is in most cases very difficult to determine the boundary conditions such as the anisotropic feature of the aquifer body, water body (stream, lake, and so on), and structural and lithologic boundaries.



References

- Andersen NJB and Ainslie LC, 1994, Neotectonic reactivation – an Aid to the Location of Ground Water, *Afr Geo Rev*, 1: 1 – 10.
- Andreoli MAG, Doucoure M, and Van Bever Donker J, 1996, Neotectonics of Southern Africa – a review, *Africa Geoscience Review*, Vol.3, No.1: 1–16.
- Andreoli MAG, Doucoure M, Van Bever Donker J, Faurie JN, and Fouché J, 1995, the Ceres-Prince Fabric (CPEF): an Anomalous Neotectonic Domain in the Southern Sector of the African Plate, in *Centennial Geocongress (1995)-Extended Abstract Vol.I* (Batton JM and Copperthwaite eds.), ISBN: 0-620-19031-0:434 – 437.
- Baghbanan A and Jing L, 2007, Hydraulic properties of fractured rock masses with correlated fracture length and aperture, *International Journal of Rock Mechanics & Mining Sciences*, V44: 704 – 719.
- Bandis SC, Lumsden AC and Barton NR, 1983, Fundamentals of Rock Joint Deformation, *International Journal of Rock Mechanics and Mining Science, Geomechanics*, 20(6): 249-268.
- Barton NR, Bandis SC and Bakhtar K, 1985, Strength, Deformation and Conductivity Coupling of Rock Joints, *International Journal of Rock Mechanics and Mining Sciences*, 22(3): 121-140.
- Bird P, Ben-Avraham Z, Schubert G, Andreoli MAG, and Viola G, 2006, Patterns of stress and strain rate in the southern Africa, *Journal of Geophysical Research* V.111, B08402, doi: 10.1029/2005JB003882, 2006.
- Bradbury KR and Muldoon MA, 1994, Effect of fracture density and anisotropy on delineation of wellhead protection area in fractured-rock aquifers, *Applied Hydrogeology*, 3/94: 17 – 23.
- Bressan, M.A. and Anjos C.D., 2003 Techniques of remote sensing applied to the environmental analysis of part of an aquifer located in the São José Dos Campos region SP, Brazil, *Environmental Monitoring and Assessment*, 84: 99–109.
- Brown SR, 1987, Fluid flow through rock joints: the effects of surface roughness, *Journal of Geophysical Research*, 92B: 1337-1347
- Caine JS, Evans JP and Forster CB, 1996, Fault zone architecture and permeability structure, *Geology* 24:1025–1028.

- Cavrilenko P and GueGuen Y, 1998, Flow in Fractured Media: a Modified Renormalization Method, *Water Resource Research*, Vol.34: 177 – 191.
- Charles EF, 1988, Determination of fracture aperture Multi-tracer Approach, A Report Submitted to the Department of Petroleum Engineering of Stanford University.
- Chevallier, L., 1999, Regional structural geological interpretation and remote sensing Little Karro, WRC Project: K8/324.
- Cook PG, 2001, A Guide to Regional Ground Water Flow in Fracture Rock Aquifers, CSIRO Land and Water, Glen Osmand, Australia: 115pp.
- De Beer, CH, 2002, the Stratigraphy, Lithology and Structure of the Table Mountain Group, In (Petersen K and Parsons R editors eds.): A Synthesis of the Hydrogeology of the Table Mountain Group- Formation of a Research Strategy, WRC Report No. TT 158/01: 9–18.
- Degnan, J.R., Clark, S.F. and Jr., 2002, Fracture-correlated lineaments at Great Bay, Southwestern New Hampshire, USGS open-file report, 02-13, 14pp.
- Department of Water Affairs & Forestry (DWAF), 2002, Utilization and availability of water –Profile of water management in Berg, Breede, Gouritz, Olifants/Doring Water Management Areas, DWAF.
- Domenico PA and Schwartz FW, 1990, Physical and Chemical Hydrogeology, John Wiley & Sons: pp824.
- Dreuzy JR, Davy P, and Bour O, 2000, Percolation parameter and percolation-threshold estimates for three-dimensional random ellipses with widely scattered distributions of eccentricity and size, *Physical Review*, Vol.62, No.5: 5948 – 5952.
- Drury SA, Peart RJ and Deller ME, 2001, Hydrogeological potential of major fractures in Eritrea, *Journal of African Earth Sciences*, 32: 163–177.
- Du Toit AL, 1954, The geology of South Africa (3rd edn.), Oliver and Boyd, London, 611pp.
- Ewer, FK, 1985, Rock Grouting with emphasis on dam sites, Springer-Verlag, PP: 175–188.
- Ferris JG, Knowless DB, Brown RH, and Stallman RW, 1962, Theory of Aquifer Tests, US geological Survey, Water Supply Paper No. 1536E: 174pp.
- Fortuin M, Woodford AC, Rosewarne PN, and Low AB, 2004, Identification and prioritization of type areas for detailed research in terms of the regional variability of the groundwater and ecological characteristics of the Table Mountain Group aquifer systems, SA WRC Report, No.1332/1/04: 13– 18.
- Fouché, K.J., Bate, K.J and van der Merwe, R., 1992, Plate tectonic setting of the Mesozoic Basins, southern offshore, South Africa: A review. In: M.J. De Wit and I.G.D. Ransome

- eds, Inversion tectonics of the Cape Fold Belt, Karoo and Cretaceous Basins of Southern Africa.
- Friese AEW, 2007, Neotectonics of southern Africa: nature, origin and consequence, in Andreoli MAG and Cichowicz A eds., Neotectonics and Mining Seismology- is a Relationship Possible. Seismology Workshop on 8th May 2007, Council for Geoscience, Pretoria: 11– 14.
- Goodman RE, 1974, the Mechanical Properties of Joints, Proc 3rd Int. Congr., Int. Soc. Rock Mechanics, Vol.I:127-140.
- Hälbich IW and Cornell DH, 1983, Metamorphic history of the Cape Fold Belt, in: Sohnge APG and Hälbich IW (eds), Geodynamics of the Cape Fold Belt, Spec. Publ. geol. Soc. S. Afr., 12: 131 – 148.
- Hälbich IW, 1983, A tectogenesis of the Cape Fold Belt, in: Sohnge APG and Hälbich IW (eds), Geodynamics of the Cape Fold Belt, Spec. Publ. geol. Soc. S. Afr., 12: 165 – 175.
- Hälbich IW and Greef GJ, 1995, Final report on a structural analysis of the west plunge nose of the Kammanassie anticline, Technical report to SA DWAF.
- Halihan T, Love A, and Sharp J M, 2005, Identifying Connections in a Fractured Rock Aquifer Using ADFTs, GROUND WATER, Vol.43, No.3: 327–335.
- Hartnady CJH and Hay ER, 2000, Reconnaissance Investigation into the Development and Utilisation of Table Mountain Group Artesian Groundwater, Using the E10 Catchment as a Pilot Study Area. Final Report to Department of Water Affairs and Forestry by Umvoto Africa/SRK Consulting Joint Venture.
- Hartnady CH and Hay ER, 2002a, Fracture system and attribute studies in Table Mountain Group groundwater target generation, A Synthesis of the Hydrogeology of the Table Mountain Group-Formation of a Research Strategy, WRC Report No. TT 158/01, Pretoria: 89–94.
- Hartnady CH and Hay ER, 2002b, Boschklouf Groundwater Discovery, *In (Petersen K and Parsons R eds.): A Synthesis of the hydrogeology of the TMG Formation of a research strategy*, WRC Report No. TT 158/01: 168–177.
- Hartnady CH and Hay ER, 2002c, Experimental deep drilling At Blikhuuis, Oloifant River Valley, Western Cape: Motivation, Setting and current progress, WRC Report No. TT 158/01, Pretoria: 192–197
- Heilweil VM and Hsieh PA, 2006, Determining Anisotropic Transmissivity Using a Simplified Papadopulos Method, Ground Water, V.44, No.5:749 – 753.

- Hill RS, 1988, Quaternary Faulting in the South-eastern Cape Province, Southern Africa
Journal of Geology, 91(3): 399 – 403.
- Horne R, 1995, Modern well test analysis, 2nd edn. Petroway, Inc., Palo Alto.
- Hsieh PA and Neuman SP, 1985, Field Determination of the 3-Dimension Hydraulic
Conductivity Tensor of Anisotropic Media, 1, Theory, Water Resources Research, 21(11):
1655 - 1665.
- Hsieh P, 2000, A Brief Survey of Hydraulic Tests in Fractured Rocks, *in (Faybishenko B,
Witherspoon PA, and Benson SM eds): Dynamics of Fluids in Fractured Rock*, AGU,
Washington DC: 59 – 72.
- Issar AS, 1995, On the regional hydrogeology of South Africa. Unpublished Report No. 3 to
Directorate Geohydrology, DWAF: 39.
- Jaeger C, 1979, Rock Mechanics and Engineering, Cambridge University Press: 161 - 178.
- Jia H, 2007, Groundwater Resource Evaluation in Table Mountain Group Aquifer Systems,
PhD thesis, University of the Western Cape: 75 – 79.
- Jolly JL, 2002, Sustainable use of the TMG aquifer and problems of scheme failure, In
(Petersen K and Parsons R eds.): A Synthesis of the hydrogeology of the TMG Formation
of a research strategy, WRC Report No. TT 158/01: 108~117.
- Karasaki K, Freifeld B., Cohen A., Grossenbacherb K., Cook P., Vasco D., 2000, A
multidisciplinary fractured rock characterization study at Raymond field site, Raymond,
CA, Journal of Hydrology, V236 (2000): 17–34.
- Kresic, N., 1995, Remote sensing of tectonic fabric controlling groundwater flow in Dinaric
Karst, Remote Sensing and Environment, 53: 85–90.
- Kulatilake PHSW and Panda B.B., 2000, Effect of rock block and joint geometry on jointed
rock hydraulics and REV, ASCE J. Engrg. Mech., 126(8): 850–858.
- Kulatilake P, Jeong-gi Um, Wang M, Escandon R and Narvaiz, J, 2003, Stochastic fracture
geometry modeling in 3-D including validations for a part of Arrowhead East Tunnel,
California, USA, Engineering Geology, V.70 (2003): 131–155.
- Kulatilake PHSW and Panda BB, 2000, Effect of Rock Block and Joint Geometry on Jointed
Rock Hydraulics and REV, ASCE J. Engrg. Mech., 126(8): 850 – 858.
- Koch, M. and Mather, P.M., 1997, Lineament mapping for groundwater resource assessment:
a comparison of digital synthetic aperture (SAR) imagery and stereoscopic large format
camera (LFC) photographs in the Red Sea Hills, Sudan, International Journal of Remote
Sensing, 18: 1465–1482.

- Kotze JC, 2002, Towards a management tool for groundwater exploitation in the Table Mountain sandstone fractured aquifer, WRC report No.: 729/1/02.
- Levin M, 2000, the Radon Emanation Technique as a Tool in Ground Water Exploration, *Borehole Water J*, 46: 22-26.
- Lin L and Xu Y, 2006, A tensor approach to the estimation of hydraulic conductivities in Table Mountain Group aquifers of South Africa, *Water SA*, Vol.32, No. 3: 371–378.
- Lin L, Jia H, & Xu Y, 2007, Fracture network characteristics of a deep borehole in the Table Mountain Group (TMG), South Africa, *Hydrogeology Journal*, Vol.15, No7: 1231-1437.
- Lomize GM, 1951, *Filtrasiya v treshinovatykh porodakh (flow in fractured rocks)*, Gosudastvennoe Energeticheskoe Izdatelstvo, Moskva-Leningrad.
- Louis C, 1974, Introduction to Rock Hydraulic, Bureau Recherches Géologiques et minières, Orleans France: III (4): 283– 356.
- Mabee, S.B., Hardcastle, K.C., Wise, D.W., 1994, A method of collecting and analyzing lineaments for regional-scale fractured bedrock aquifer studies, *Ground Water*, 32: 884–894.
- Maclear LGA, 2001, The hydrogeology of the Uitenhage Artesian Basin with reference to the Table Mountain Group Aquifer, *Water SA*, Vol. 27 No. 4: 499–505.
- Margolin G, Berkowitz B, and Scher H, 1998, Structure, Flow, and Generalized Conductivity Scaling in Fracture Networks, *Water Resour Res*, 34:2103–2121.
- McCathy T and Rubidge B, 2005, the Story of Earth and Life, a South African Perspective on a 4.6-billion-year Journey, New Holland Publishing (South Africa): 184–211.
- Meyer PS, 1998, 1999, 2001, An explanation of the 1:500 000 general hydrogeological map of Cape Town 3317, Port Elizabeth 3324, Oudtshoorn 3320, Department of Water Affairs and Forestry.
- Meyer PS, 2002, Springs in the Table Mountain Group, with Special Reference to Fault Controlled Springs, In (Petersen K and Parsons R eds.): A Synthesis of the hydrogeology of the TMG Formation of a research strategy, WRC Report No. TT 158/01: 224–229.
- Min KB, Jing L and Stephansson, 2004, Determining the equivalent permeability tensor for fractured rock masses using a stochastic REV approach: Method and application to the field data from Sellafield, UK, *Hydrogeology Journal*, 12:497 – 510.
- Mourzenko VV, Thovert J-F, and Adler PM, 1998, Percolation and conductivity of self-affine fractures, *Physical Review*, Vol.59, No.4: 4266 – 4284.
- Murray EC, 1996, Guidelines for Assessing Borehole Yields in Secondary Aquifers, Unpublished M.Sc.Thesis, Univ. of Rhodes, Grahamstown.

- National Research Council, 1996, Rock fractures and fluid flow: contemporary understanding and applications, National Academy Press, Washington DC: 29–35.
- Nestev M, Savard MM, Lapcevic P, Lefebvre R, and Martel R, 2004, Hydraulic Properties and Scale Effects Investigation in Regional Rock Aquifers, South-Western Quebec, Canada, *Hydrogeology Journal*, 12:257 – 269.
- Newton AR, Shone RW, and Booth PWK, 2006, the Cape Fold Belt, (in Johnson MR, Anhaeusser CR and Thomas RJ eds.) *the Geology of South Africa*, the Geological Society of South Africa, Pretoria: 521– 530.
- Odling NE, 1997, Scaling and connectivity of joint systems in sandstones from western Norway, *Journal of Structural Geology*, Vol.19, No.10: 1257 – 1271.
- O’Leary, D.W., Friedman, J.D. and Pohn, H.A., 1976, Lineament, linear, lineation: some proposed new word standards for old terms, *Geological Society of American Bulletin*, 87: 1463–1469.
- Olsson R and Barton NR, 2001, An Improved Model for Hydraulic Coupling During Shearing of rock Joints, *International Journal of Rock Mechanics & Mining Science*, 38(2000): 317 – 329.
- Paces JB, Newmark LA, Marshall BD, Whelan JF, and Peterman ZE, 1996, Ages and origins of subsurface secondary minerals in the Exploratory Studies Facility, Milestone Rep. 3GQH450M, USGS, Denver, 1996.
- Park BY, Kim KS, Kwon S, Kim C, Bae DS, Hartley LJ, and Lee HK, 2002, Determination of the hydraulic conductivity components using a three-dimensional fracture network model in volcanic rock, *Engineering Geology*, 66 (2002): 127–141.
- Partridge TC and Maud RR, 1987, Geomorphic evolution of Southern Africa since the Mesozoic, *South African Journal of Geology*, V.90:179 – 208.
- Patir C and Cheng HS, 1978, An Average Flow Model fro Determining Effects of Three-dimension Roughness on Hydrodynamic Lubrication, *ASME J Lobr Techno*, 100(1): 12~17.
- Petersen K and Parsons R, 2002, A Synthesis of the Hydrogeology of the Table Mountain Group- Formation of a Research Strategy, WRC Report No. TT 158/01.
- Pollard DD and Aydin A, 1988, Progress in understanding jointing over the past one hundred years, *Geological Society of America Bulletin*, 100, 1181–1204.
- Pyray-Nolte LJ, Montemango CD, and Nottle DD, 1997, Volumetric Imaging of Aperture Distribution in Connected Fracture Networks, *Geophysical Research Letter*, Vol.24,No.18: 2343 – 2346.

- Ransome IGD and de Wit MJ, 1992, Preliminary Investigation into a Microplate Model for the South Western Cape, in de Wit MJ and Ransome IGD eds: *Inversion Tectonics of the Cape Fold Belt, Karoo, and Cretaceous Basins of Southern Africa*, Balkema, Royyerdam, Holland: 257 – 266.
- Rawewatne PN, 1990, Groundwater Resource Evaluation at St Francis Bay: Project Review, SRK Report No. 171719/5: 35pp.
- Renard P, 2005, The future of hydraulic tests, *Hydrogeology Journal*, 3:259–262.
- Rodell, M. and Famiglietti, J.S., 2002, The potential for satellite-based monitoring of groundwater storage changes using GRACE: the High Land Plains aquifer, Central US, *Journal of Hydrology*, 263: 245–256.
- Rosewarne P, 2002, Hydrogeological Characteristics of the Table Mountain Group Aquifers, In (Petersen K and Parsons R eds.): *A Synthesis of the hydrogeology of the TMG Formation of a research strategy*, WRC Report No. TT 158/01, Water Research Commission, Pretoria: 33~44.
- Rosewarne PN, 1993a, St Francis bay Groundwater Monitoring Final Report, SRK Report No.171719/M6.
- Rosewarne PN, 1993b, Ceres Groundwater Investigation Phase 2: Borehole Siting, SRK Report No.197759/1.
- Rust, IC, 1967. On the sedimentation of the Table Mountain Group in the Western Cape Province: D.Sc. thesis, Geology Department, University of Stellenbosch (unpublished), 110 pp.
- Rust, IC, 1973. The evolution of the Palaeozoic Cape basin, southern margin of Africa in *The Ocean Basins and Margins, Volume 1. The South Atlantic* (A.E.M. Nairn and F.G. Stehli, eds.), Plenum, New York: 247-276.
- Rutqvist J and Stephansson O, 2003, the Role of Hydromechanical Coupling in Fracture Rock Engineering, *Hydrogeology Journal*, 11(2003): 7-40.
- Sander, P., Cheskey, M.M. and Minor, T.B., 1996, Groundwater assessment using remote sensing and GIS in a rural groundwater project in Ghana: lesson learned, *Hydrogeology Journal*, 4(3): 40–49.
- Sander, P., Minor, T.B. and Chesley, M.M., 1997, Groundwater exploration based on lineament analysis and reproducibility tests, *Ground Water*, 35: 888–894.
- Schowengerdt, R., Babock, EM, Ehtridge, L. and Glass, CE, 1979, Correlation of geologic structure inferred from computer enhanced Landsat imagery with underground water supplies in Arizona, *Satellite Hydrology AWRA*: 387–397.

- Serzu MH, Kozak ET, Lodha GS, Everitt RA, Woodcock DR (2004) Use of borehole radar techniques to characterize fractured granitic bedrock at AECL's Underground Research Laboratory, *Journal of Applied Geophysics*, 55 (2004): 137– 150.
- Shapiro AM, Hsieh PA, Burton WC, and Walsh GJ, 2007, Integrated Multi-Scale Characterization of Ground-Water Flow and Chemical Transport in Fractured Crystalline Rock at the Mirror Lake Site, New Hampshire, in *Subsurface Hydrology: data Integration for Properties and Processes*, Geophysical Monograph Series 171: 201 – 225.
- Smart MC and Tredoux G, 2002, Groundwater quality and fitness for use, A Synthesis of the Hydrogeology of the Table Mountain Group-Formation of a Research Strategy, WRC Report No. TT 158/01, Pretoria: 118–123.
- Snow DT, 1968, Hydraulic characteristics of fractured metamorphic rocks of the Front Range and implications to the Rocky Mountain Arsenal well, *Colorado School of Mines Quarterly*, v. 63, no.1.
- Snow DT, 1969, Anisotropic Permeability of fractured media, *Water Resource research*, 5(6): 1273 – 1298.
- Talobre J, 1957, *Rock Mechanics*, Paris.
- Tian K, 1988, An almost developed Technique of karst collapse prevention during mine drainage, *Proceedings of the IAH 21st Congress*, Vol.21, Part 2.
- Thompson ME and Brown SR, 1991, The effect of anisotropic surface roughness on flow and transport in fractures, *Journal of Geophysical Research*, 96B: 21923-21932.
- Titus R, Adams S and Xu Y, 2002, The Sandveld Core, Report prepared for the Department of Water Affairs and Forestry: Directorate Geohydrology, South Africa.
- Umvoto, 2003, Task 1 Report – Hydrogeological Reconnaissance for Table Mountain Group Aquifer Feasibility study and Pilot Project, Report to City of Cape Town: 121pp.
- van Tonder G, Bardenhagen I, Riemann K, Bosch KRJ, Dznanga P, and Xu Y, 2002, Manual on Pumping Test Analysis in Fractured-rock Aquifers, WRC Report No. 1116/1/02: 12 – 27.
- van Tonder GJ, Botha JF and van Bosch J, 2001, A Generalized Solution for Step-drawdown Tests Including Flow Dimension and Elasticity, *Water SA*, Vol. 27 No. 3: 345 – 354.
- Vegter JR, 1995, Groundwater resources of South Africa: An Explanation of a Set of National Groundwater Maps. Water Research Commission (WRC) Report TT74/95, Pretoria.
- Vegter JR, 2001, Groundwater development in South Africa and an Introduction to the Hydrogeology of Groundwater Regions, SA WRC Report, No.TT 134/00: 60–70.

- Velde B, 1984, Electron microprobe analysis for clay minerals, *Clay minerals*, 19(1984): 243–247.
- Wang M, Kulatilake PHSW, Um J and Narvaiz J, 2002, Estimation of REV size and three-dimensional hydraulic conductivity tensor for a fractured rock mass through a single well packer test and discrete fracture fluid flow modelling, *International Journal of Rock Mechanics & Mining Sciences*, 39 (2002): 887–904.
- Waters, P.G., Smart, P.L. and Osmaston, H., 1990, Application of remote sensing to groundwater hydrology, *Remote Sensing Review*, 4: 223–264.
- Weaver JMC, Rosewarne P, Hartnady CJH and Hay ER, 2002, Potential of Table Mountain Group Aquifers and integration into catchment water management, *In* (Petersen K and Parsons R eds.): *A Synthesis of the Hydrogeology of the Table Mountain Group- Formation of a Research Strategy*, WRC Report, No.TT 158/01: 242–248.
- Weaver JMC, Talma AS and Cavé LC, 1999, Geochemistry and Isotopes for Resource Evaluation in the Fractured Rock Aquifers of the Table Mountain Group, WRC Report 481/1/99, Water Research Commission, Pretoria.
- Witherspoon PA, 2000, Investigations at Berkeley on Fracture Flow in Rocks: From the Parallel Model to Chaotic Systems, *in* (Faybishenko B, Witherspoon PA, and Benson SM eds): *Dynamics of Fluids in Fractured Rock*, AGU, Washington DC: 1 – 58.
- Witherspoon PA, Wang JCY, Iway K, and Gale JE, 1980, Validity of the cubic law for fluid flow in a deformable rock fracture. *Water Resources Research*, 16-6: 1016-1024.
- Woodford AC, 2002, Interpretation and Applicability of Pumping-tests in the Table Mountain Group Aquifers, *In* (Petersen K and Parsons R eds.): *A Synthesis of the Hydrogeology of the Table Mountain Group- Formation of a Research Strategy*, WRC Report, No.TT 158/01: 71–84.
- Woodford AC and Chevallier L, 2002, Regional characterization and mapping of Karoo fractured aquifer systems – an integration approach using geographical system and digital image processing, SA WRC technical report, No. 653/1/02: 40–55.
- Wu Y, 2005, Groundwater Recharge estimation in Table Mountain Group Aquifer Systems with a Case Study of Kammanassie Area. PhD Thesis, University of the Western Cape: 52 – 61.
- Wu Y, Wang W, Xu Y, Liu H, Zhou X, Wang L and Titus R, 2003, Radon concentration: A tool for assessing the fracture network at Guanyinyan study area, China, *Water SA*, Vol.29 No.1: 49 – 53.

Xu Y, Wu Y, and Duah A, 2007, Groundwater Recharge Estimation of Table Mountain Group Aquifer Systems with Case Study, WRC Report No. 1329/1/07: 9 –19.

Zhang X, Sanderson DJ, Harkness RM, and Last NC, 1996, Evaluation of the 2-D Permeability Tensor for Fractured Rock Masses, International Journal of Rock Mechanics and Mining Sciences, Vol.33, No.1:17-37.



Appendix A Groundwater chemistry

Report No.: NR6692/2006

ANALYSES REPORT

Lixiang Lin
Universiteit van Weskaapland
Earth Science Dept.

Date received: 12/07/2006
Date tested: 17/07/2006

Reference No.	Lab. No.	Na mg/l	K mg/l	Ca mg/l	Mg mg/l	HCO3 mg/l	CO3 mg/l	SO4 mg/l	Cl mg/l	NH4-N mg/l	NO2-N mg/l	NO3-N mg/l	PO4 mg/l	B mg/l	SiO2 mg/l	As mg/l	Li mg/l	Sr mg/l	Al mg/l	Cr mg/l	Mo mg/l	Mn mg/l
S1 GV-BH 1-3	6692	6.8950	0.7716	3813.687	159.4100	0.0000	2.282	13.200	9.710	0.700	0.000	0.0100	0.0000	0.0000	11.5300	0.0000	0.005	0.077	0.012	0.010	0.000	0.139
S2 GEV-BH 1-6	6693	6.1370	0.5974	9013.075	0.0000	0.0000	1.593	9.710	9.710	1.290	1.030	155.0000	0.0060	0.0000	10.5900	0.0000	0.004	0.111	0.029	0.009	0.000	0.125
S3 Farm Gevonden	6694	6.0740	0.8685	4153.276	0.0000	0.0000	1.684	3.530	3.530	4.560	2.010	296.0000	0.3700	0.0000	8.8600	0.0000	0.005	0.086	0.052	0.007	0.000	0.158
S4 Gev-BH 3	6695	5.3540	0.4371	1.6071	1.366	0.0000	0.0000	4.274	21.190	1.290	0.890	169.0000	0.1100	0.0000	8.1700	0.0000	0.005	0.026	0.033	0.008	0.000	0.022
S5 GV-BH 3-2	6696	5.2390	0.3731	2991.316	0.0000	0.0000	2.986	17.660	17.660	1.010	0.430	69.0000	0.0600	0.0000	8.3200	0.0000	0.004	0.010	0.033	0.003	0.000	0.016
S6 Gev Strm	6697	1.6210	0.0560	1970.236	0.0000	0.0000	0.426	7.950	7.950	1.230	0.870	126.0000	0.0000	0.0000	0.7900	0.0000	0.000	0.003	0.174	0.012	0.000	0.006

Reference No.	Lab. No.	Fe mg/l	Ni mg/l	Cu mg/l	Zn mg/l	Cd mg/l
S1 GV-BH 1-3	6692	0.432	0.029	0.000	0.003	0.001
S2 GEV-BH 1-6	6693	0.298	0.025	0.004	0.007	0.001
S3 Farm Gevonden	6694	1.501	0.008	0.000	0.006	0.002
S4 Gev-BH 3	6695	0.157	0.022	0.002	0.028	0.002
S5 GV-BH 3-2	6696	0.408	0.002	0.006	0.028	0.001
S6 Gev Strm	6697	0.087	0.004	0.021	0.006	0.002

Sample conditions

Samples in good condition.

Statement

The reported results may be applied only to samples received. Any recommendations included with this report are based on the assumption that the samples were representative of the bulk from which they were taken. Opinions and recommendations are not accredited.

Dr. W.A.G. Kotzé (Director)
.....
for BemLab

20-07-2006
.....
Date

Enquiries: Dr. W.A.G. Kotzé
Arrie van Deventer

Report No.: WT3534/2006

ANALYSES REPORT

Lixiang Lin
Universiteit van Weskaaplant
Earth Science Dept.

Date received: 27/11/2006

Date tested: 28/11/2006

Reference No.	Lab. No.	pH	EC mS/m	Na mg/l	K mg/l	Ca mg/l	Mg mg/l	Fe mg/l	Cl mg/l	CO3 mg/l	HCO3 mg/l	SO4 mg/l	B mg/l	Mn mg/l	Cu mg/l	Zn mg/l	P mg/l	NH4-N mg/l	NO3-N mg/l	F mg/l	NO2-N mg/l	PO4 mg/l	Si mg/l	As mg/l
UWC BN01	3534	6.3	11.52	9.55	1.52	7.57	4.00	3.81	8.83	0.00	71.96	1.58	0.01	0.421	0.000	0.000	0.080	1.710	0.590	0.050	0.020	0.240	5.618	0.029
UWC BN02	3535	6.0	3.08	2.70	0.73	1.37	0.69	8.45	7.06	0.00	32.15	0.20	0.01	0.441	0.016	0.015	0.023	1.140	0.590	0.000	0.010	0.069	1.239	0.030
UWC BN03	3536	5.7	5.91	5.36	0.52	2.44	1.38	27.01	11.48	0.00	21.44	5.88	0.02	0.119	0.000	0.015	0.105	1.260	0.700	0.000	0.010	0.330	2.658	0.000
UWC BN04	3537	6.4	10.86	3.78	0.53	17.55	0.60	10.68	6.18	0.00	76.56	0.26	0.01	0.296	0.000	0.002	0.079	1.240	0.490	0.000	0.020	0.237	3.326	0.000
UWC BN05	3538	5.8	5.33	5.37	0.34	1.51	1.22	20.24	9.71	0.00	16.84	1.55	0.01	0.285	0.000	0.008	0.034	1.310	0.000	0.000	0.000	0.100	2.660	0.000
UWC River	3539	5.4	2.12	2.24	0.02	0.30	0.27	0.19	5.30	0.00	15.31	0.45	0.01	0.001	0.002	0.002	0.054	1.260	0.000	0.000	0.000	0.162	1.779	0.000
UWC BH320	3630	5.3	6.19	4.88	0.48	2.21	1.25	3.94	13.24	0.00	16.84	6.86	0.01	0.056	0.000	0.016	0.117	0.170	0.220	0.070	0.020	0.510	4.281	0.047

Reference No.	Lab. No.	Li mg/l	Pb mg/l	Sr mg/l	Ba mg/l	Al mg/l	V mg/l	Cr mg/l	Mo mg/l	Ni mg/l	Cd mg/l	Hg mg/l	Rb mg/l	TDS mg/l	Alkalinity mg/l
UWC BN01	3534	0.000	0.000	0.122	0.000	0.014	0.000	0.006	0.003	0.000	0.000	0.000	0.000	87.400	44.6
UWC BN02	3535	0.000	0.032	0.015	0.001	0.600	0.000	0.009	0.009	0.000	0.000	0.000	0.000	22.730	10.02
UWC BN03	3536	0.000	0.000	0.008	0.002	0.150	0.001	0.009	0.000	0.008	0.000	0.000	0.000	43.900	6.51
UWC BN04	3537	0.000	0.000	0.019	0.000	0.631	0.000	0.010	0.001	0.002	0.000	0.000	0.000	80.200	40.58
UWC BN05	3538	0.000	0.041	0.010	0.001	0.022	0.001	0.011	0.005	0.006	0.000	0.000	0.000	39.600	5.012
UWC River	3539	0.000	0.000	0.003	0.002	0.070	0.000	0.010	0.000	0.012	0.000	0.000	0.000	15.940	7.52
UWCBH320	3630	0.000	0.010	0.005	0.013	0.089	0.000	0.004	0.009	0.009	0.001	0.000	0.010	48.100	5.51

Sample conditions

Samples in good condition.

Statement

The reported results may be applied only to samples received. Any recommendations included with this report are based on the assumption that the samples were representative of the bulk from which they were taken. Opinions and recommendations are not accredited.

Dr. W.A.G. Kotzé (Director)

.....
for BemLab


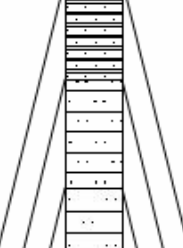
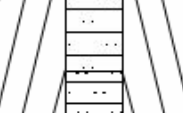


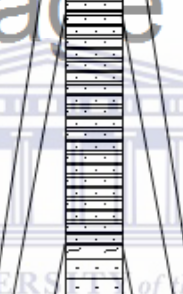

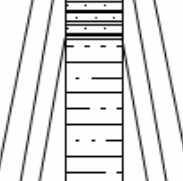
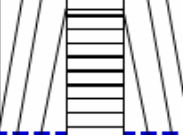
04-12-2006















.....
Date

Enquiries: Dr. W.A.G. Kotzé
Arrie van Deventer


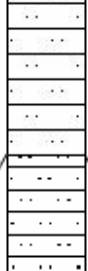
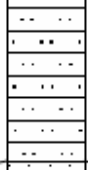
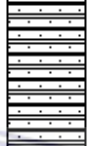
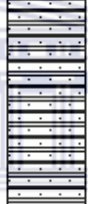

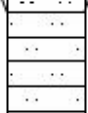
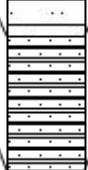
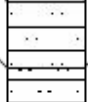
Appendix B Borehole core logging

Well ID	UWC BH-1	Well Log: Lithology and Construction						
Gevoden, Rawsonville								
Drilling method:		Core drilling		Contract No.		none		
Coordinate		X	19.24558333		Scale		H	7
		Y	33.71851666				V	400
Surface Elevation (m)		273.55		Diameter (mm)		75		
Well depth (m)		270.55		Commencing date		20051120		
Casing depth (m)		179		Ending date		20061129		
Layer No.	Strata	Thick (m)	Elev. (m)	Depth (m)	Column map	Lithology	Remark	
1	Q4	7.55	266	7.55		Alluvial & pluvial deposits: Grit, gravel and boulder.	borhole inclination of 60°, dipping to the west.	
2	Nardouw	6.69	259.31	14.24		Brown, reddish, blueish and strongly weathered medium~coarse grained sandstones		
3	Nardouw	2.94	256.37	17.18		Weathered brown~reddish sandstone with a clay band of 80mm in thickness	Packer tests from 16m to 120m with each interval of 6m	
4	Nardouw	13.54	242.83	30.72		Fault zone. highly fractured brown, blueish~reddish sandstones sandwiching shales of 50~80 mm in thickness.		
5	Nardouw	4.88	237.95	35.6		Lightly fractured blueish~reddish litharenites and siltstones.		
6	Nardouw	10.62	227.33	46.22		Dark grey~reddish, medium grained litharenites, lightly fractured, with shale bands of 50~100mm in thickness.	Borehole diverted at 41.82m, the followings are loggings with redrilled hole at the same position	
7	Nardouw	7.78	219.55	54		highly fractured brown~reddish medium~coarse grained sandstone with minor shales.	Wire drilling	
8	Nardouw	12.16	207.39	66.16		Lightly~moderately fractured grey blueish~grey reddish sandstones with extensive iron diffusion and veins in fractures.		

9	Nardouw	10	197.39	76.16		Grey~blueish medium grained quartz sandstone, lightly fractured.	
10	Nardouw	9.01	188.38	85.17		Grey~blueish thickbedded medium grained quartz sandstone and mica-feldspar sandstone, lightly fractured.	First conductive zone at 77.5~78.8m, artesian flow Q=0.083 l/s from a steep fracture.
11	Nardouw	5.96	182.42	91.13		Dark grey sandstones interbedding with silty shales.	
12	Nardouw	6.44	175.98	97.57		Grey ~ blueish thickbedded medium grained quartz sandstones.	
13	Nardouw	7.68	168.3	105.25		Highly fractured dark grey midbedded sandstone and siltstone.	
14	Nardouw	6.27	162.03	111.52		Grey - dark grey, thin to midbedded sandstones and siltstones, lightly-moderately fractured.	Second conductive zone at 106m, total artesian flow Q=0.15 l/s, from a subvertical fracture
15	Nardouw	10.51	151.52	122.03		Grey~dark grey, medium- to thickbedded litharenites with minor shaly siltstones.	
16	Nardouw	13.62	137.9	135.65		Lightly fractured grey~dark grey, medium- to thickbedded litharenite, quartz sandstone with minor shaly siltstone and silty shale.	
17	Cedarberg	5.46	132.44	141.11		Dark grey, thinbedded to medium-bedded sandstone and siltstone with minor silty shales.	

18	Cedarberg	6.39	126.05	147.5		Grey~dark grey, litharenite and siltstone with minor shales and silty shales.	
19	Cedarberg	8.85	117.2	156.35		Dark grey~ grey interbedded shaly siltstone, siltstone and shales.	
20	Cedarberg	14.74	102.46	171.09		Dark grey midbedded silty shales with minor sandwiched shaly siltstones	
21	Cedarberg	18.44	84.02	189.53		Dark grey thinbedded silty shales sandwiched shaly siltstone and siltstone	
22	Peninsula	3	81.02	192.53		Dark grey medium- to thickbedded coarse grained pebble-supported sandstone with minor siltstones.	
23	Peninsula	3	78.02	195.53		Dark grey medium- to thickbedded quartz sandstone, with minor pebble-supported litharenites.	
24	Peninsula	8.95	69.07	204.48		Highly fractured light grey thin- to mid-bedded quartz sandstone	
25	Peninsula	9.01	60.06	213.49		Highly fractured grey fine-mid grained quartz sandstone	
26	Peninsula	9.11	50.95	222.6		Grey mid-bedded fine-grained quartz sandstone	
27	Peninsula	8.2	42.75	230.8		Grey thin- to mid-bedded fine-grained quartz sandstone with minor grey shale bands, a magnetite concretion at 228.5m.	
28	Peninsula	15.1	27.65	245.9		Moderately fractured grey fine to medium grained quartz sandstone.	Third conductive zone at 245.5m total flow Q=0.25 l/s, from a steep fracture.
29	Peninsula	2.95	24.7	248.85		Grey fine-grain quartz sandstone	
30	Peninsula	8.9	15.8	257.75		Grey~ dark grey mid- to thick-bedded, mid- to coarse-grained quartz sandstone with minor litharenites	
31	Peninsula	12.8	3	270.55		Grey thickbedded, mid- to coarse-grained quartz sandstone	

Well ID	UWC BH-2	Well Log: Lithology and Construction					
		Gevoden, Rawsonville					
Drilling method:		Core drilling		Contract No.		none	
Coordinate		X	19.24601667		Scale	H	7
		Y	33.71863333			V	500
Surface Elevation (m)		273.06		Diameter (mm)		75	
Well depth (m)		201.06		Commencing date		20060305	
Casing depth (m)		65		Ending date		20060915	
Layer No.	Strata	Thick (m)	Elev. (m)	Depth (m)	Column map	Lithology	Remark
1	Q4	5.51	267.55	5.51		Brown-reddish grit and gravel	Rest water level: 1.61m to surface
2	Q4	4.29	263.26	9.8		Brown-reddish grit, gravel, and boulder	
3	TMG	5.81	257.45	15.61		Fault zone. Jointed mottled cataclastite with extensive iron diffusion in fractures, highly weathered.	
4	TMG	5.34	252.11	20.95		Fault zone. Extensively weathered, jointed, greyish, reddish sandstones.	
5	TMG	18.95	233.16	39.9		Fault zone. Weathered, iron cemented fault cataclasite with minor sandstones.	
6	TMG	17.5	215.66	57.4		Fult zone. Brown-reddish, medium grained quartz sandstone, highly fractured, with iron and manganese diffusions in fractures	Packer tests from 3.8m to bottom with each interval of 6m
7	TMG	7	208.66	64.4		Fault zone. Grey, blueish-grey quartz sandstones with minor cataclasite.	
8	Penisula	8.2	200.46	72.6		Grey, Grey-brown medium grained quartz sandtone, iron diffusion along major fractures	
9	Penisula	15.97	184.49	88.57		Grey- dark grey medium-coarse grained quartz sandtone with minor shale bands of 5~15cm in thickness. slight iron diffusion along fractures.	

10	Peninsula	2.38	182.11	90.95		Brown medium grained sandstone, extensively jointed with strong iron diffusion along fractures.	
11	Peninsula	29.05	153.06	120		Grey - dark grey, medium- to thick-bedded, medium-coarse grained quartz sandstones and litharenites with slight iron and manganese diffusion along fractures.	
12	Peninsula	18.77	134.29	138.77		Greyish medium- to thick-bedded quartz sandstone with minor siltstone and shales.	
13	Peninsula	26.53	107.76	165.3		Dark grey, mediumbedded shaly siltstones and sandstones.	
14	Peninsula	9.79	97.97	175.09		Grey - dark grey, medium- to thick-bedded, medium-coarse grained quartz sandstone with minor shaly siltstones.	
15	Peninsula	9.32	88.65	184.41		Dark grey, medium- to thick-bedded, coarse-grained sandstone and minor shaly siltstones.	
16	Peninsula	9.1	79.55	193.51		Dark grey shaly siltstones and sandstones	
17	Peninsula	4.55	75	198.06		Dark grey, medium- to thick-bedded, cross-bedding coarse-grained sandstones with minor shaly siltstones.	
18	Peninsula	3	72	201.06		Dark grey, thickbedded quartz sandstone.	

Appendix C Fracture data from field measurement

Dip	Direction	Strike	Dip angle	Spacing (mm)	Aperture (mm)
85		175	20	890	
90		180	18	900	0.11
110		20	16	760	0.15
115		25	17	630	
82		172	19	780	
96		6	21	920	0.26
95		5	25	1100	
92		2	17	860	0.22
80		170	22	790	
99		9	19	900	
112		22	20		0.18
111		21	21	590	0.16
117		27	15	1000	
69		159	16		
93		3	20	590	
110		20	18	866	
83		173	21	895	
88		178	22		
75		165	19	946	
73		163	22	970	
84		174	17	855	
87		177	16	770	0.22
70		160	19		
89		179	21	880	
91		1	21		
98		8	16		0.15
92		2	18		
92		2	15		0.2
92		2	21		0.19
113		23	17		
95		5	22		
94		4	17		0.22
90		180	18	860	
120		30	20		
107		17	22		0.18
125		35	17	750	0.2
88		178	21		
117		27	21		0.19
76		166	22		
103		13	14	1002	
107		17	28		
120		30	18		
95		5	24	1005	
90		180	25		
104		14	17		
91		1	22		
105		15	19		
78		168	18	850	
86		176	17		
77		167	23		

92	2	20		
96	6	20		
96	6	23		
92	2	25		
123	33	20		
75	165	25		
205	115	88	350	
210	120	89	500	0.3
220	130	85	550	0.26
216	126	82		0.21
225	135	84	400	
223	133	78	650	0.17
200	110	45	350	
211	121	65	460	0.25
215	125	88	470	
212	122	72		0.33
203	113	55	450	
217	127	77		0.35
198	108	39	590	
214	124	65		0.29
220	130	84	660	
205	115	51		0.3
222	132	68	670	
214	124	66		
221	131	87	450	
209	119	72	433	
227	137	71	500	
217	127	72		
199	109	67	900	
230	140	61		
208	118	70		
218	128	62	460	
223	133	68		
224	134	65	520	
199	109	88		
215	125	79	490	
194	104	85		0.29
213	123	73		
217	127	84	530	
213	123	75		
216	126	76		
207	117	58		
207	117	80		
218	128	68	550	
207	117	79		0.22
212	122	62		
211	121	71		
226	136	79		
215	125	74		
230	140	60		
216	126	67		0.26
221	131	69		
220	130	71		
203	113	49		

219	129	86		0.35
208	118	62		
211	121	81		
204	114	86		0.27
216	126	70		
192	102	65		
212	122	73	505	
225	135	59		
218	128	70		
200	110	73		
207	117	52		0.22
214	124	41		
198	108	70	540	
208	118	71		0.19
233	143	73		
205	115	78		
213	123	87		
206	116	70		
203	113	68		
216	126	75		
211	121	72		
217	127	66		
219	129	77		
206	116	82	520	
211	121	67		
207	117	74		
210	120	84		
227	137	76		
208	118	67		
197	107	73		
222	132	50		
212	122	89		
222	132	75		
140	50	88	250	
145	55	89	400	0.12
150	60	85		
150	60	86	350	
155	65	87		
135	45	78	600	0.01
130	40	79		
161	71	81		
135	45	83	300	0.02
150	60	76	330	
152	62	73	350	
159	69	73		0.08
146	56	74		
140	50	86		0.1
138	48	70	330	
153	63	81		
147	57	84		0.01
147	57	83		0.09
138	48	81	510	0.04
156	66	77		
148	58	84	600	0.03

131	41	84		
153	63	82	640	0.02
162	72	87		
157	67	84	400	
164	74	83		
158	68	87	470	
148	58	79		
138	48	80	495	
144	54	89		
150	60	87	390	
132	42	80		
138	48	73		
139	49	87	330	
140	50	82		
159	69	87		
162	72	79		
129	39	90	335	
152	62	76	390	
144	54	77		
145	55	81	400	
153	63	89		
144	54	87	410	
148	58	74		
145	55	79		
165	75	89	488	
146	56	89		
148	58	80		
138	48	80	520	
152	62	82		
134	44	75		
152	62	85		
144	54	85		
153	63	83		
145	55	82		
128	38	80		
158	68	83		
139	49	89		
155	65	82		0.09
141	51	83		
141	51	85		
145	55	79		0.05
148	58	86		
145	55	77		0.03
157	67	83		
141	51	90		
133	43	81	500	
150	60	87		
145	55	78		
157	67	84		
150	60	85		
152	62	78	420	
161	71	81		
142	52	82		
147	57	80		

139	49	80		0.03
126	36	77		
127	37	84		
135	45	74		
140	50	80		
145	55	79		
144	54	87		
156	66	85		
142	52	80		
147	57	76		
145	55	78		
152	62	86		
141	51	70		
142	52	78		
127	37	79	440	0.01
153	63	89		
140	50	81	400	0.08
123	33	84		
133	43	90		
148	58	78		
147	57	86	470	0.06
141	51	86		
146	56	88		
143	53	80		
139	49	89		
148	58	72	355	
150	60	84		
131	41	84		
152	62	80		
126	36	82		
123	33	78	380	
148	58	88		
150	60	82	400	
135	45	67		
157	67	83		
169	79	85		
145	55	82		
250	160	88		
270	0	89		
265	175	85	600	
260	170	83	650	0.15
289	19	84		0.05
300	30	75	350	
275	5	76	450	
255	165	72		
268	178	81	605	
290	20	83		
295	25	85	510	
272	2	76		0.11
255	165	80	400	0.15
263	173	81		0.04
270	0	87		
280	10	81		
276	6	85		

276	6	84		
267	177	82		
254	164	86	670	
255	165	80		
268	178	74		
278	8	85		
271	1	76	650	0.05
249	159	82	460	0.17
297	27	83	500	
277	7	87		
271	1	88		
292	22	87		
268	178	83	380	0.06
276	6	80	390	
282	12	87		
273	3	84		
258	168	78	390	0.05
250	160	87	410	
296	26	88		
280	10	86		
288	18	70		
286	16	81		
264	174	87	620	
290	20	80	540	
274	4	83		
259	169	78	600	
268	178	78		
292	22	84	570	
292	22	83		
255	165	89		
281	11	79		
294	24	78	585	
284	14	74	615	
265	175	83		
289	19	84		
276	6	84		
260	170	75		
252	162	79		
248	158	71		
242	152	86		
265	175	81	670	
249	159	80	600	
265	175	77		
289	19	76		
243	153	78		
277	7	79		
235	145	75		
305	35	76		
272	2	89		
317	47	74	390	
293	23	76	590	
282	12	76		
267	177	81		
270	180	74		

294	24	85	540	
298	28	87	610	
268	178	74		
283	13	90		
292	22	86		
286	16	77		
251	161	74	500	0.15
271	1	80	600	
278	8	73		
276	6	74		
280	10	80		
295	25	76	430	
306	36	85		
266	176	72		

